Torsional Vibration Attenuation in V-Type Locomotive Diesel Engine Crankshaft using Centrifugal Pendulum Absorber

SeyedMohammad Shojaalsadati

A Thesis

In

The Department Of Mechanical and Industrial Engineering

Presented in Partial Fulfillment of the Requirements

For the Degree of Master of Applied Science (Mechanical Engineering) at

Concordia University

Montreal, Quebec, Canada

2014

CONCORDIA UNIVERSITY
School of Graduate Studies

This is to certify that the thesis prepared

By: **SeyedMohammad Shojaalsadati**

Entitled: **"Torsional Vibration Attenuation in V-Type Locomotive Diesel Engine Crankshaft using Centrifugal Pendulum Absorber"**

and submitted in partial fulfillment of the requirements for the degree of

Master of Applied Science (Mechanical Engineering)

Complies with the regulations of this University and meets the accepted standards with respect to originality and quality.

Signed by the Final Examining Committee:

_____ Chair
Dr. S.V. Hoa

_____ Examiner
Dr. M. Packirisamy

_____ Examiner External
Dr. K. Galal

_____ Co-Supervisor
Dr. R. Sedaghati

_____ Co-Supervisor
Dr. R. Bhat

Approved by: _____
Dr. S. Narayanswamy, MASc Program Director
Department of Mechanical and Industrial Enginering

_____
Dean Christopher Trueman
Faculty of Engineering & Computer Science

Date: _____

Abstract

Torsional Vibration Attenuation in V-Type Locomotive Diesel Engine Crankshaft using Centrifugal Pendulum Absorber

SeyedMohammad Shojaalsadati

The torque fluctuation due to the intermittent combustion pressure and inertia effect of the reciprocating parts generates torsional excitation on the crankshaft of all internal combustion engines. This excitation imposes considerable amount of torsional vibration on the crankshaft. Therefore the torsional vibration modeling and design of an auxiliary absorbing mechanism are very crucial, especially in locomotive diesel engines where the crankshaft is under excitation with high amplitude coupled with large inertia forces due to generators, compressors or fans.

In this research, the capability of centrifugal pendulum vibration absorbers (CPVA) commonly used in rotating machinery to attenuate the torsional vibration in a Locomotive V-type diesel engine crankshaft is investigated. First, an advanced torsional modeling of the locomotive crankshaft has been carried out. This is followed by the development of an accurate excitation torque of a real locomotive engine to the 8^{th} order. The torsional response of the crankshaft under the derived excitation torque has then been investigated.

Finally, the model of the crankshaft incorporating the CPVA (auxiliary system) has been developed and then capability of CPVA to attenuate the torsional vibration of the crankshaft (main system) at resonance frequencies has been investigated. Moreover, the

effect of pendulum parameters such as length and mass on the torsional vibration response of the crankshaft in both time and frequency domains has been studied.

Acknowledgement

I would like to take this opportunity to express my appreciation to the CN company, who provided funding for this study during my M.A.Sc education through the Fellowship of Railway Engineering Dynamics, which helped me to keep my concentration focused on the research.

I would like to take this opportunity to express my gratitude to my thesis supervisors, Prof. Rama Bhat and Prof. Ramin Sedaghati, for their support, help, encouragement, and guidance through my graduate studies at Concordia University.

I would also like to express my deepest gratitude to my lovely wife, Rezvan Saber, for her limitless patience, understanding and encouragement during the period of my thesis preparation.

Last but not the least; I am extremely appreciative of my parents and family, for their continuous and endless love and support. I should thanks all of my friends who were beside me during the time of my master education and wish them success and happiness in their life.

Table of Contents

Lists of Figures

List of tables

Nomenclature

CPVA	Centrifugal Pendulum Vibration Absorber
DOF	Degrees-Of-Freedom
DVA	Dynamic Vibration Absorber
FFT	Fast Fourier Transform
RoHR	Rate of Heat Released
RPM	Round per Minute
A	Area of piston section
a	Radius of the rolling circle
c_p	Heat capacity of the fluid at constant pressure
c_v	Heat capacity of the fluid at constant volume
I_{rec}	Polar mass moment of inertia of reciprocating part
J	Polar mass moment of inertia of the disk
K	Stiffness of the shaft
Le	Effective length
m	Pendulum mass
P	In-cylinder pressure

Q	Heat
V	Volume
V_m	Pendulum velocity
$\mathrm{m_{rec}}$	Mass of the reciprocating part
m_{rot}	Mass of the rotating part
M_{eff}	Effective mass
$\mathrm{M_T(t)}$	Excitation torque
n	Speed ratio of gear
r	Pendulum length
R	Radius of the pendulum implemented point
$\bar{X}$	Connecting rod centre of gravity
x	Horizontal coordinate system
y	Vertical coordinate system
ω	Excitation frequency
ω_n	Natural frequency
Ω	Angular velocity of the rotor
μ	Fluid viscosity

θ	Rotation of the shaft
Φ	Angle of twist of the rotor
φ	Relative rotation of pendulum to the shaft
ψ	Vibration disturbance part of rotating shaft

Chapter 1. Introduction

1.1 Motivation and objectives

Controlling torsional vibrations in rotating systems such as reciprocating engines, turbines, compressors etc. is still subject of research and investigation. A steady rotational speed is desirable in rotating machinery. This helps to extend the fatigue life of components and to reduce vibration and noise which also enhance the riding quality in vehicles. However, it is generally impossible to maintain a precisely constant rotational speed. The unsteady nature of the external loads, cycle-to-cycle variations (such as those which occur in internal combustion engines), inertial loads from connecting linkages, gas pressure effects, and so forth, all tend to induce torsional vibrations in rotating components during operation.

Generally vibration reduction methods are classified into three distinct categories:

1. *Active Control*: This method has been widely developed in the past several years, and the underlying principle is quite simple [1] . The approach lies in reducing an undesirable perturbation by generating an out-of-phase motion so that destructive interferences generated completely eliminate the vibrations. Active control generally gives the best vibration reduction performance, but it is not widely used due to its high cost, complex hardware, the necessity to have an external energy supply and its lack of robustness and reliability in an industrial environment.
2. *Semi-Active Control*: This method is a kind of active systems for which the external energy requirements are lower than those required for typical active

control. For example, the battery power is sufficient for their operation. Semi-active devices can not add or remove energy to the structural system. They basically control structural parameters such as spring stiffness or coefficient of viscous damping to generate the desired resisting forces to suppress vibration. As semi-active devices utilize the motion of the structure to develop the control forces, no instability can occur. Among semi-active devices electro and magneto rheological fluids (ER and MR) based devices have recently received appropriate attention [2], [3]. The effectiveness of these fluids lies in their ability to change the apparent viscosity instantly with respect to the applied electric or magnetic field. The ER/MR dampers are fail-safe devices and require minimal power to operate. However, the modeling of the fluid behavior as well as the development of the controller still represents major challenges for real-life applications.

3. *Passive Control*: In this method vibration attenuation is accomplished by implementing a structural modification by adding either a dissipative material (e.g., viscoelastic material such as viscous dampers [4]) or a dynamic vibration absorber (DVA) [5], [6]. Passive control strategies represent a very interesting and cost-effective alternative to the aforementioned methods as their performance is acceptable without requiring external energy supply.

In general, the reduction of torsional vibrations in a rotating shaft such as automotive crank shaft is achieved using different classes of dampers or absorbers [7], [8]. Often torsional vibration dampers are applied at one end of the crankshaft, such as a flywheel, which can have a wide variety of geometric configurations. The flywheel is connected to the shaft by suitable elastic and damping elements.

Between different kinds of dampers, viscous dampers (Houdaille type) are very common in reciprocating engines to help limit torsional vibrations and crankshaft stresses [9], [10], [11]. These dampers are normally designed to protect the engine crankshaft and not necessarily the driven machinery. To be effective, dampers need to be located at a point with high torsional, usually near the anti-node of the crankshaft mode, because their dissipative force has direct relationship with the response at the point they are connected.

A viscous damper as shown in Figure 1.1 consists of a flywheel that rotates inside the housing, which contains a viscous fluid such as silicon oil. An un-tuned damper does not contain an internal torsional spring [12].

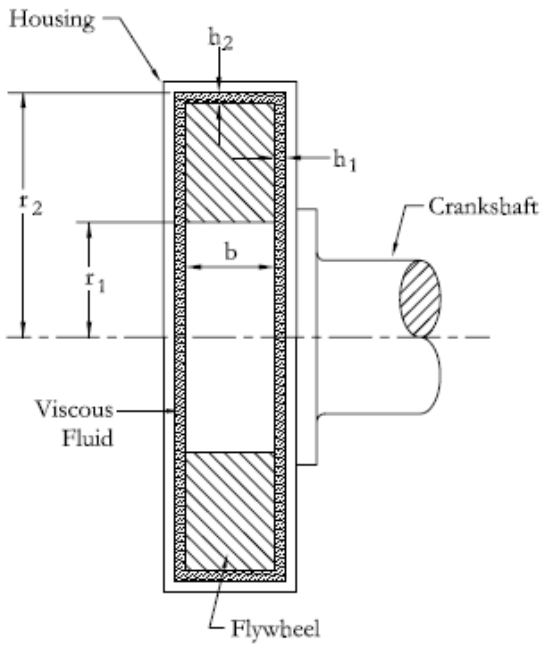

Figure 1.1: An un-tuned viscous vibration damper [12]

The shearing motion of the fluid between the flywheel and housing surfaces dissipates vibration energy as heat. The damping characteristics can be adjusted by changing the internal clearances between the housing and flywheel, h1 and h2, and/or the fluid

viscosity (μ). From the Shock and Vibration Handbook [11], an approximate damping constant can be calculated from the following equation:

$$c = 2\pi\mu\left[\frac{r_2^4}{h_2} + \frac{r_1^4}{2h_1}\right] \tag{1.1}$$

However, viscous dampers have their own problem in real applications. All dissipative dampers are subject to heating, even overheating, because they convert mechanical energy into heat. Overheating is not desirable as it causes the damping capacity of the material to decrease and, consequently, the amplitude of the vibration to grow with increased heating. This can easily result in complete destruction of the damper and consequently severe fatigue problems in the whole system. Therefore, viscous dampers have a limited service life and require periodic checks and maintenance and their life cycle is limited. For example, according to Simpson Industries, the recommended time for the change of dampers is after approximately 25,000 to 30,000 hours of service [13]. Superior Ltd. recommends replacement of dampers every 24,000 to 35,000 hours depending on the engine model [14].

All of these issues make it more attractive to use the dynamic passive vibration absorbers for attenuating the vibration in systems as they are cost-effective and need minimum supervision without requirement of external power supply.

One of the more popular DVAs, especially in rotary systems, is the centrifugal pendulum vibration absorber (CPVA). It is essentially a tuned absorber whose natural frequency varies in direct proportion to the rotational speed of the crankshaft. Hence it works to attenuate vibration at different orders of excitation which normally exist in reciprocating

engines. It also does not introduce additional weight to the design of the system and hence can be used in many applications. This makes the CPVA an attractive alternative for the reduction of torsional vibrations in engines justifying a detailed study of its dynamic performance worthwhile.

Locomotive diesel engine is one of the most high power capacity engines in the transportation industry. Due to the required power output, the reciprocating parts and connections are under large dynamic forces and stresses which make the vibration control very crucial for acceptable operation. One of the most important parts of this mechanism is the crankshaft which has many coupled elements. Defects in crankshafts due to excessive torsional vibration are very common in railway industry and are troublesome during operation.

In one of the field tests, which is reported in [12], the defect caused by operating an engine at its natural frequency can be seen clearly in Figure 1.2. It can be seen that the shaft of the motor has spiral cracks. It should be noted that the cracks occurred at 45 degree angle to the shaft axis that indicates a torsional vibration problem.

Figure 1.2: Sample failed engine crankshaft (in 45° due to torsional vibration) [12]

This defect occurred within two years of operation and twice in a diesel engine driving a 6 MW synchronous generator at 450 RPM. Both failures were at journal 8 (between throws 7 and 8) due to coincidence of the resonance frequency on the fourth order of the excitation due to the engine in-cylinder pressure. This shows that knowing the critical points of vibration on the crankshaft is also very important when approaching the problems of its torsional failure.

Normally locomotive diesel engines connected to an alternator do not have a flywheel, and hence the design and use of CPVA as a passive absorber on the locomotive crankshaft and at the critical location, which can attenuate the fluctuation amplitude at all orders of desired frequency, would be of paramount importance.

For this purpose, this study aims at torsional modeling of the locomotive crankshaft considering all effective coupled parts and investigating the dynamic effects of CPVA in attenuating the torsional vibration.

1.2 State-of-The-Art (Literature Review)

Here the relevant studies addressing torsional vibration of the crankshaft and also centrifugal pendulum vibration absorber (CPVA) as an effective device to attenuate torsional vibration has been systematically reviewed.

1.2.1 Torsional vibration of crankshaft

Torsional vibrations occur in crankshafts due to the torque variations during transforming reciprocating motion into the rotary motion. The excessive torsional vibrations can lead to the fatigue failure of crankshaft. Therefore, study of the torsional vibrations in rotary systems is very crucial. Moreover, riding quality requirements limit the amount of noise, vibration and harshness from the engine as discussed in [15], [16] and [17]. Hence the dynamic analysis of the crankshaft assembly plays an important role in crankshaft design to understand these issues.

There are numerous classic books such as [18], [19] or more recent books such as [20] and [21] on torsional vibration. In some early works on torsional vibrations [22], [23], [24], [25] crankshaft models were developed in an isolated manner. In this procedure, the engine was basically modeled as a rigid block and the natural frequencies and responses of the crankshaft were calculated using either the Holzer method, or the transfer matrix method and finite element method. Most research works considered small four or six-cylinder engines [26], [27] and [28]. Few research works have investigated larger engines [29] and [30]. It should be noted that a large number of cylinders involve higher inertias, overlapping combustions and torsional vibration modes which severely complicate the analysis.

Some studies deal with experimental measurements of the vibration considering the variation in the angular velocity of the crankshaft as in [31] or defining a new polar coordinate system for measuring instantaneous angular speed in [32].

There are many approaches used for torsional modeling of crankshaft in the literature considering different parameters. In [33] the authors verified an engine crankshaft torsional model as subsystem of the powertrain, which lead to the rotational multi body system. The effect of change in the geometry on torsional vibration due to crank angle has been discussed in [34]. Some works on parametric analysis of torsional vibration in non-uniform force transmission using Lagrange's equations has been carried out in [35]. In [36] the forced vibration response of a diesel engine crankshaft assembly, which takes into account the non-constant inertia, is studied using numerical integral method. The simulation results are compared with a lumped mass model and a detailed model using the system matrix method.

The engine excitation torque is the main source of excitation considered in most of the theoretical and experimental studies [37], [38], [39], [40] and [41]. In these studies, the model is represented by sets of inertia disks linked together by linear springs with torsional stiffnesses such as in [42]. For example, Figure 1.3 shows the sample discrete model of the crankshaft with coupled inertia disks in a 50-degree V-20 engine which develops 4 MW at a speed of 1500 rpm.

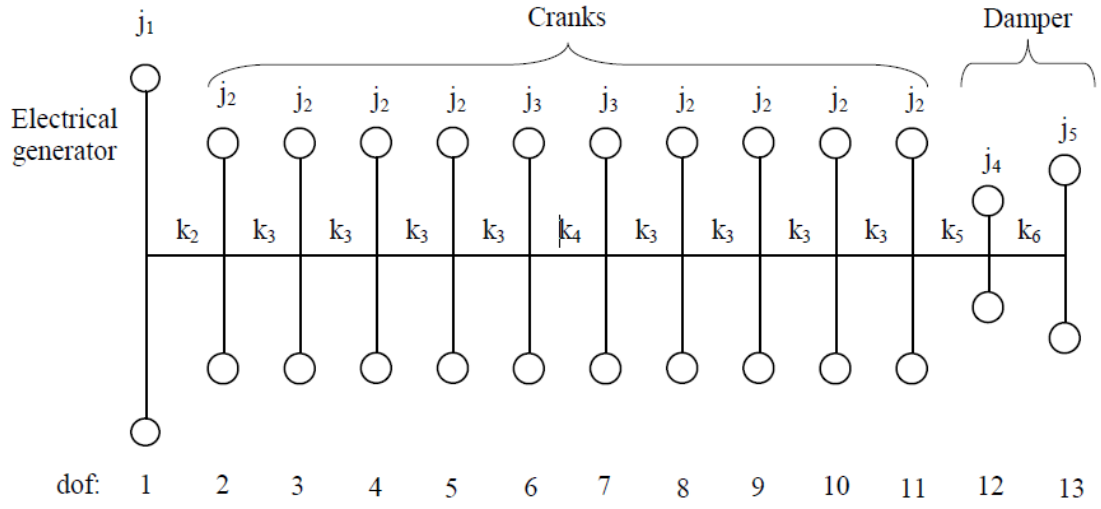

Figure 1.3: Sample discrete model of crankshaft with inertia disk-shaft [43]

In this model each crank has its own polar mass moment of inertia (j), and are connected to each other by shafts with various stiffnesses (k). In [44] the vibration isolation of engine mount system in the entire frequency range has been studied using a coupled three degrees of freedom engine model with both elastomeric and hydraulic mount under engine excitation force.

1.2.2 Centrifugal Pendulum Vibration Absorber (CPVA)

The CPVA is comprised of a simple pendulum mounted on a vibrating carrier, as shown in Figure 1.4. The pendulum suppresses the effects of torsional disturbances in the linear range. In the linear range, i.e., small angular displacements of the pendulum absorber, the pendulum can be tuned to reduce the effects of disturbances which are at a frequency proportional to the rotational speed of the crankshaft. Furthermore, the pendulum adds only a small amount of mass to the system and hence does not increase the rotating inertia. Additionally, it dissipates an insignificant amount of energy in the form of heat.

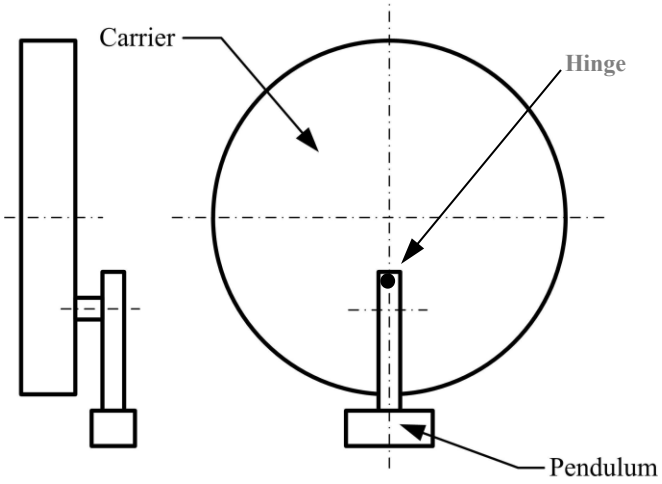

Figure 1.4: Centrifugal pendulum vibration absorber (CPVA)

The CPVA absorber was first introduced in 1929 [18] and has since been widely applied to eliminate torsional vibrations in geared radial aircraft-engine propeller systems [45]. Formerly, Den Hartog in his book [6] and a paper [46], Newland [47] and Bailey [48] and more recently Wei (et al) [49] and Jose et al. [50] conducted a linear analysis of the dynamic response of the CPVA and discussed the characteristics of its large amplitude nonlinear motion. Sharif-Bakhtiar and Shaw [51] studied the effects of damping on a CPVA with moderate amplitude motion and motion-limiting stops. Sharif-Bakhitar and Shaw [52] reported on the effects of nonlinearities and damping on the dynamic response of a centrifugal pendulum vibration absorber. Cronin [53] considered the problem of shake reduction in automobile engines using a CPVA.

Typical cases of application include helicopter rotors [54], [55] and more recently [56], radial aircraft engines [45] and combustion engines [57]. Some literature discussed the different possible path design for CPVAs for decreasing the undesirable nonlinear effects, such as circular [58], [59] noncircular (cycloids [60] , epicycloid [61], [62]). In one study

[63], different CPVAs have been modeled through a fully customizable element, with computer-aided programming. Special attention has been given to modeling CPVAs with cycloidal paths and epicycloidal paths.

Among the interesting properties of these systems are the possibilities of instabilities arising from multiple absorbers [64], [65] and [66], impact responses on the flexible structures [67], and super harmonic resonances [68].

Implementing CPVAs in different positions on the cam shaft was also discussed in some studies [69] in addition to the use of multiple absorbers on rotating shaft [70].

Some experimental tests also have been carried out for testing dynamic response and different paths of CPVA on a rotating shaft [71] or on V-type engine [72].

Finally, in very recent studies, some experiments were carried out on new model Planetary CPVAs used in downsized hybrid combustion engines [73] and on new non-bifilar tautochronic paths for CPVA investigated in [74]. Besides that there were efforts to study the application of CPVAs in active control [75].

1.3 Scope of the present research

Based on the literature review, the torsional modeling of crankshaft in automotive engine and rotary machines such as compressors and turbines has been well studied. However, very few studies have been done on the locomotive diesel engines, which are limited to only considering the reciprocating cylinder-piston mechanism connected to flywheel or dampers. Also in most of the cases the in-line cylinder for reciprocating mechanism has been assumed. However, rarely they have considered the behavior of the V-type locomotive engines either from the theoretical or experimental point of view.

Considering the above, the main scope of this research is to conduct thorough investigation on the locomotive crankshaft torsional modeling, considering all the coupled parts such as main and auxiliary generators, air compressor and radiator fans with respect to the effect of gear connection in all of them if necessary and the inertia effect of reciprocating parts. It should be noted that dynamic simulation is performed for a real freight locomotive V-type engine to extract all applicable torsional vibration characteristics such as natural frequencies and mode shapes. In addition, in-cylinder pressure equivalent harmonic excitation has been derived for an actual engine.

The dynamical formulation for a simple tuned centrifugal pendulum absorber connected to one inertia disk mounted on a shaft has been well studied in the literature. There are some studies that have been done for the effect of tuned CPVA in reducing the vibration amplitude. However, the effect of changing the pendulum parameters such as pendulum length and mass on the amplitude of vibration and frequency response is rarely discussed in the literature. Most of the studies approximated the analysis approach to linearized model for finding response of pendulum absorber mechanism. Very few studies were carried out on the application of the pendulum absorber on multi-degrees of freedom system. There is no study on application of pendulum absorber on a V-type locomotive diesel engine.

Here, we have formulated the system simulation using Matlab/Simulink based on the Runge-Kutta (Ode-45) method to find the nonlinear response of the CPVA mechanism. After verifying the model on simple CPVA mechanism, we studied the application of tuned and un-tuned CPVA with circular path on the real freight locomotive. Torsional model of a real freight locomotive combined with CPVA has been used to investigate the

attenuation of undesired vibration due to the critical speed caused by in-cylinder fluctuating torque. Finally, the importance of adjusting pendulum parameters such as their length and mass in a tuned manner and their effects on the time domain and frequency response has been investigated.

1.4 Thesis organization

This thesis contains six chapters. In chapter one the importance of torsional vibration control to avoid the crankshaft failure has been discussed and the motivation for the use of passive CPVA as absorber for attenuating the vibration in reciprocating engines is presented. Then the literature review about torsional modeling of crankshaft and the application of CPVAs have been conducted in order to highlight the scope of this study.

In chapter two, after a brief presentation of the different kinds of CPVAs, the modeling of a simple 2-DOF torsional system with a circular path CPVA has been done. After finding the equations of motions using Lagrange's equations, the model has been simulated in Matlab /Simulink software for extracting the numerical response in time and frequency domain. Then the effects of tuned and un-tuned absorber in attenuating the vibration at the natural frequency of the model when subjected to a simple harmonic excitation have been presented.

In chapter three, the approach for finding linear torsional vibration modeling of V-type locomotive diesel engines in the form of lumped inertia disks and shafts for different parts of the locomotive has been presented. By considering a sample freight locomotive (U25B-GE), the equivalent torsional modeling has been formulated in order to extract the resonance frequencies and different mode shapes.

Chapter four carries out the derivation of in-cylinder pressure harmonic excitation for the locomotive diesel engine using the curve fitting procedure in Matlab which uses the Fourier series to find the orders of the excitation. The final fluctuating torque due to combustion calculated using the well-known handbook has also been presented.

In Chapter five, we used the results of chapter three and four as input for torsional vibration analysis of the locomotive crankshaft. In this chapter the model of the crankshaft considering the implementation of CPVA has been derived in nonlinear format using Lagrange's equations. Then by observing the response of the system under the excitation forces derived in chapter four and with/without absorber at the critical point, the effect of different pendulum parameters on reduction of the vibration amplitude and shift of resonance frequencies are discussed.

In chapter six, conclusions are listed and explained. The major contributions during this research have been presented. Finally some topics for future research are suggested for controlling the torsional vibration using CPVAs.

Chapter 2. Modeling and Application of CPVA on a Simple 2-DOF Torsional System

2.1 Introduction

This chapter is devoted to the theory and modeling of the centrifugal pendulum vibration absorber. Using the Lagrangian Formulation, the equations of motion for pendulum absorber connected to a simple disk have been derived. Matlab/Simulink software is employed to obtain the response of the system in different situations. In section 2.2 a brief description of different kinds of the pendulum absorbers and their application are given. Section 2.3 is devoted to modeling a simple type pendulum absorber with discretized mass moving in a circular path. The derivation of equations of motion using Lagrange's equation has been done in section 2.4. In section 2.5 Matlab simulation of the time domain response of modeled system with and without CPVA has been obtained. Finally in section 2.6 the frequency domain responses of the system with and without CPVA are obtained for confirmation of previous results.

2.2 Description of different centrifugal pendulum absorbers

Different kinds of pendulum absorbers have been grouped together from two points of view. One would be related to the mechanism and mechanical implementation of the absorber and the other related to the path of the pendulum movement during rotation of the shaft or disk on which it has been connected.

Since 1980's most of the implementation of CPVAs is based on circular path design considering the linear theory. Some slight adjustments have been considered to avoid certain undesirable nonlinear behaviors that can occur in absorbers [76]. The main

problem is that the natural frequency of the pendulum with circular path will change with pendulum amplitude. It has nonlinear effects and an increase of the pendulum amplitude reduces its natural frequency. This mistuning causes the CPVA not to properly operate at large amplitudes. To avoid this shortcoming, one of the first solutions ways offered by Madden [77] was to replace the non-circular path with a *cycloidal* path for implementing in the helicopter rotors for vibration attenuation.

When a circle is rolling on a straight line the path of one node on the circumference would be a cycloid, see Figure 2.1.

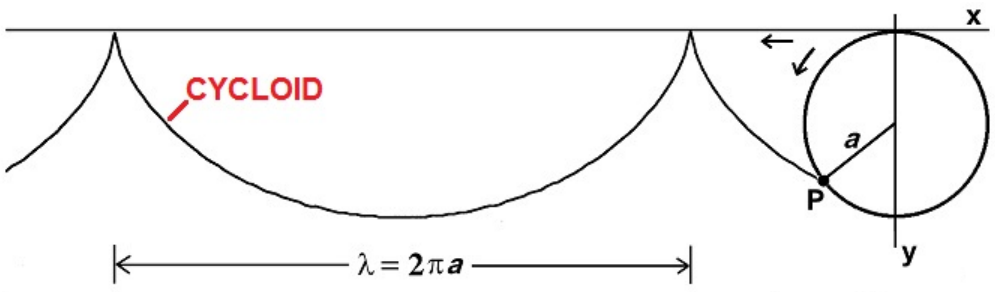

Figure 2.1: The cycloid path created by arbitrary circle with radius a, the length of each cycle is $2\pi a$ [60]

The cycloid path can be expressed using the *x* and *y* as coordinate system as:

$$x = a(t - \sin t)$$
$$y = a(1 - cost) \tag{2.1}$$

where a is the radius of the rolling circle, and the equation covers one cycloid for every $t = 2\pi$. The reason for this design was to decrease the oscillation frequency of the pendulum in different range of its amplitudes of vibration.

An *epicycloid* path offered by Denman [61] forms a better solution for stabilizing the frequency of the CPVA at all amplitudes of absorber motion. There was also an experimental study done at Ford Motor Company for this kind of path line where the results are available in a paper of Borowski et al [78].

The epicycloid motion is similar to the cycloid curve, however, the path is obtained by rolling of a circle around the circumference of another circle, see Figure 2.2.

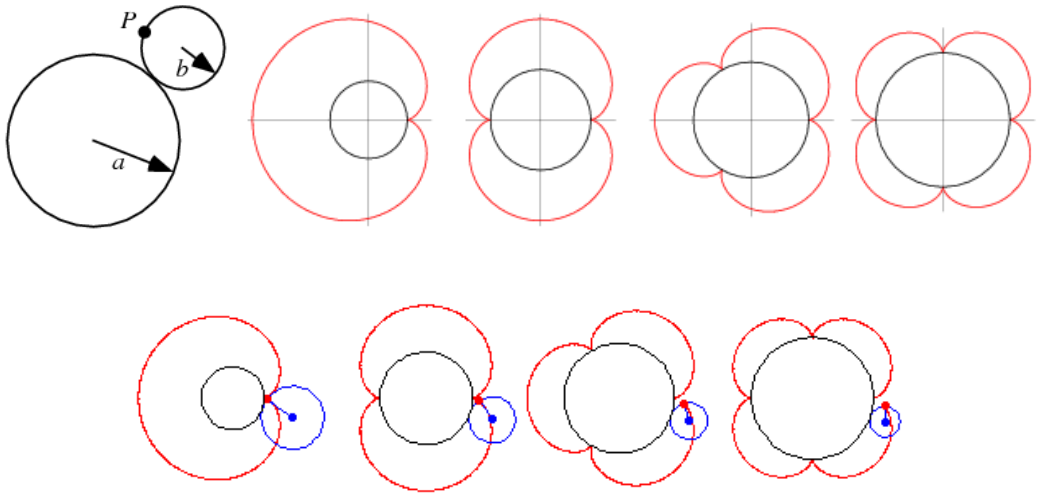

Figure 2.2: The different kinds of epicycloid path regarding different values for a and b [78]

In this figure from left to right the ratio of the (a/b) is equal to 1, 2, 3 and 4. As it can be seen, the ratio of inner over rolling circle, $k=a/b$, defines the number of the epicycloids produced in one revolution.

The parametric representation of the epicycloid path considering the x and y as coordinate system is given by:

$$x = (a+b)\cos\theta - bcos(\frac{a+b}{b}\theta)$$
$$y = (a+b)\sin\theta - bsin(\frac{a+b}{b}\theta) \quad (2.2)$$

where *a* and *b* are radii of the fixed inner circle and the rolling circle, respectively.

Considering CPVAs from the mechanism and mechanical implementation point of view, the simple type with circular path would be a suitable type for a preliminary investigation. As shown in Figure 2.3, it consists of a mass with known center of gravity connecting to a point on a rotor with distance R from the centroid of the rotor. The pendulum is constrained to move in the *x*-*y* plane.

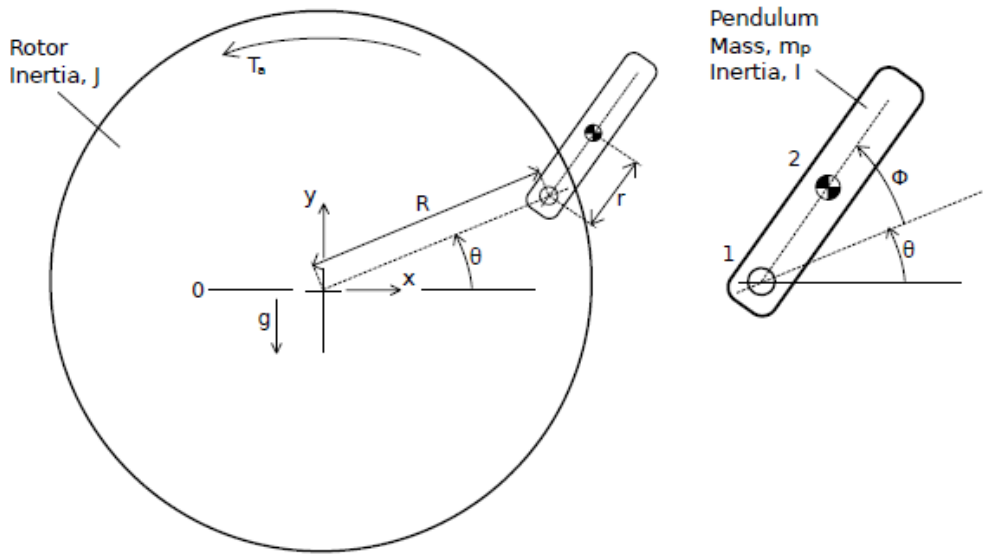

Figure 2.3: Geometrical modeling of the simple type CPVA with circular path. R is the distance between centroid of rotor and connecting point to CPVA. r is the distance between C.G of pendulum mass and the connecting point. [63]

This kind of implementation for pendulum is not common any more as the effective mass of pendulum during rotation of the rotor will change. This happens due to inconsistency between the absolute angular velocity of the pendulum ($\dot{\varphi}$) and the angular velocity of the rotor ($\dot{\theta}$). Dynamic behavior of this simple implementation causes difficulty in tuning the absorber at a specific frequency.

For solving the instability of the pendulum, the Bifilar type CPVAs as shown in Figure 2.4 may be used. These absorbers are very similar to the simple type absorbers. The only difference is that the pendulum mass is suspended at two points instead of one.

Bifilar CPVA is more practical in implementation because it has many advantages. First of all, due to bifilar suspensions the absolute angular velocity of the pendulum ($\dot{\alpha}$) is same as the angular velocity of the rotor ($\dot{\Omega}$). This will allow us to consider the pendulum mass as a point mass moving along a circular path resulting in stability of the CPVA performance. Secondly in cases where the length of absorber has to be very short - for example when tuning higher-order harmonics are desired - the bifilar approach provides us the possibility of having large pendulum mass in comparison with the total mass of the unit without the necessity of having large pendulum length [8]. Therefore options for the shape and size of the pendulum are more flexible and can be chosen to fit the mechanism intrinsically.

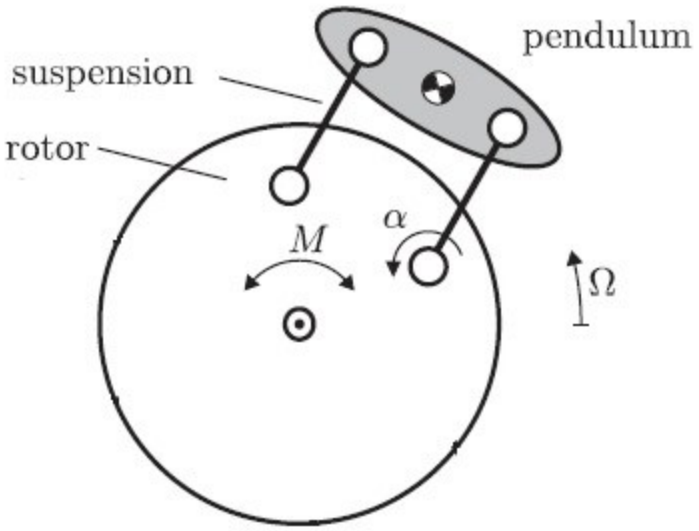

Figure 2.4: Schematic of bifilar type CPVA unit, the pendulum and rotor angels are α and Ω respectively, M is the applied torque on the rotor. [74]

Sometimes there may be some limitation of space in the engine or the instruments where it is desired to connect the absorbers. In these cases another implementation called the *Roller CPVA* would be used. In such pendulums a hole at an appropriate location of the rotor is implemented and a mass which acts as the pendulum mass can roll around a circular or semi-circular path. This type of implementation is very common in the flywheels or gearwheels as shown in Figure 2.5. Sometimes it can also be implemented on the crank web on the existing balance weights [79]. The advantage of internal roller CPVA is that we can use the application of the absorber without occupying any extra space on the machine or the desired mechanism. They are also very useful when we want to provide very short pendulum length (L) in order to absorb vibrations at higher harmonics.

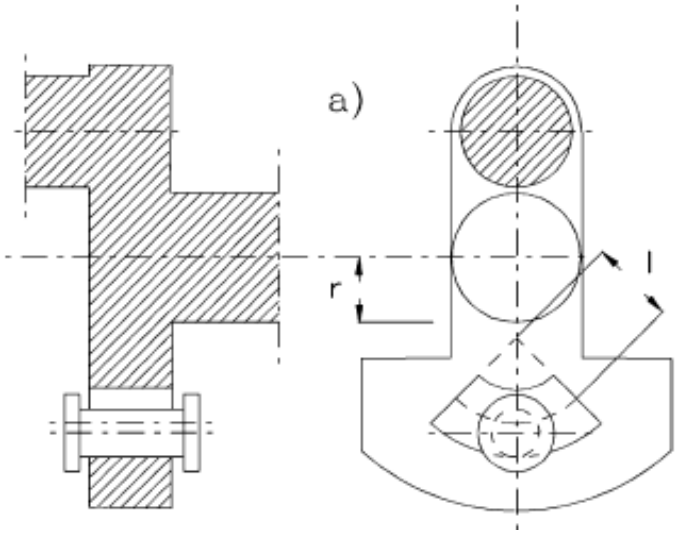

Figure 2.5: Internal roller-type CPVA, in this case r is the radius of hinged point and l is the length of pendulum [8]

2.3 Centrifugal Pendulum Vibration Absorber modeling

In order to describe the application of CPVA, it is very important to formulate a dynamic model of the mechanism. A reasonable and simple model of the pendulum can be done by considering a lumped mass (m) pivoted to a point (O') on the rotational shaft with radius R and inertia J_0 through a rod with negligible mass and length r (as illustrated in Figure 2.6) in such a way that it remains always in-plane with the shaft.

For dynamic analysis of this mechanism, finding the absolute velocity terms of the CPVA mass in the direction of unit vectors e_1 and e_2 around point O as shown in Figure 2.6 is important. If we consider the unit vector of e_1' and e_2' fixed to the rotary system on point O', the angle θ as rotation of the shaft around point O and angle φ as the relative rotation of the pendulum with respect to the rotating shaft; the velocity of the pendulum (V_m) can be found by vectorial addition of velocity of pendulum mass itself with respect to O' and the velocity of O'. Hence, $V_m = V_{m/O'} + V_{O'}$

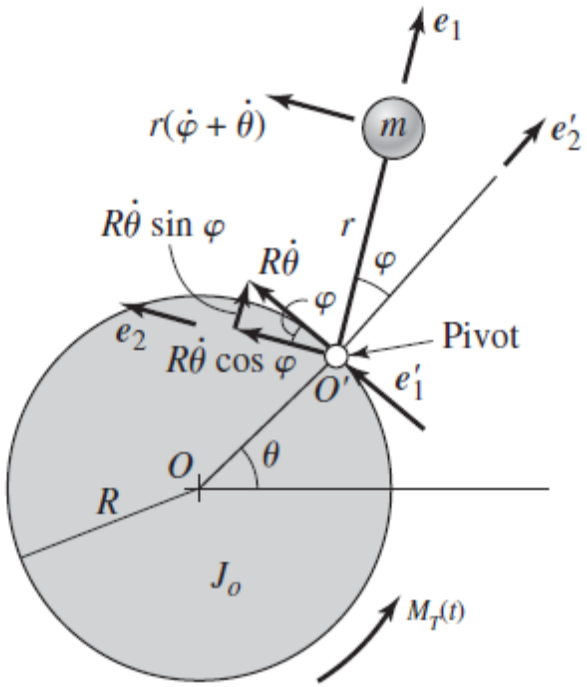

Figure 2.6: Dynamic body diagram of centrifugal pendulum absorber, $M_T(t)$ is an external moment applying on the rotating shaft. [80]

Hence, the velocity of the pendulum mass with respect to fixed point O can be described as:

$$V_m = R\dot{\theta}e_1' + r(\dot{\theta}+\dot{\varphi})e_2 = (R\dot{\theta}sin\varphi)e_1 + (R\dot{\theta}cos\varphi + r(\dot{\theta}+\dot{\varphi}))e_2 \qquad (2.3)$$

The velocity of the pendulum will be used in the following section for deriving equations of motion using the energy method.

2.4 Application of tuned CPVA on a simple 2-DOF torsional system

The effectiveness of the 2-DOF spring-mass absorber discussed in detail in reference [81], is limited to a narrow frequency range. This is because of creating two new

resonance frequencies after tuning the absorber at the natural frequency of the main system.

For a rotating system such as an automobile engine, the exciting torque is proportional to the rotational speed (Ω), which can vary over a wide range. Therefore an effective absorber should have its natural frequency proportional to the speed. Centrifugal vibration absorber pendulum (CPVA) has this unique nature and thus can be an effective vibration absorbing system in rotary machines such as reciprocating engines and turbines.

However, tuning of CPVA based on their characteristic parameters is very important for optimum and stable vibration absorbing application. We have derived the governing equations of motion for pendulum absorber in 2-DOF case to investigate the effect of tuning parameters and their optimal values.

2.4.1 Derivation of equations of motion using Lagrange's equation

The velocity of the pendulum with respect to the centre of the rotating disk has been calculated in previous section. If we consider that our disk which is under moment M(t) has been connected to the rotating shaft with rotating speed Ω and stiffness K (see Figure 2.7), a torsional vibrating model with two degrees of freedom system can be considered. To derive, the equations of motion using Lagrangian method, the kinetic energy (T) and potential energy (U) of the system should be calculated.

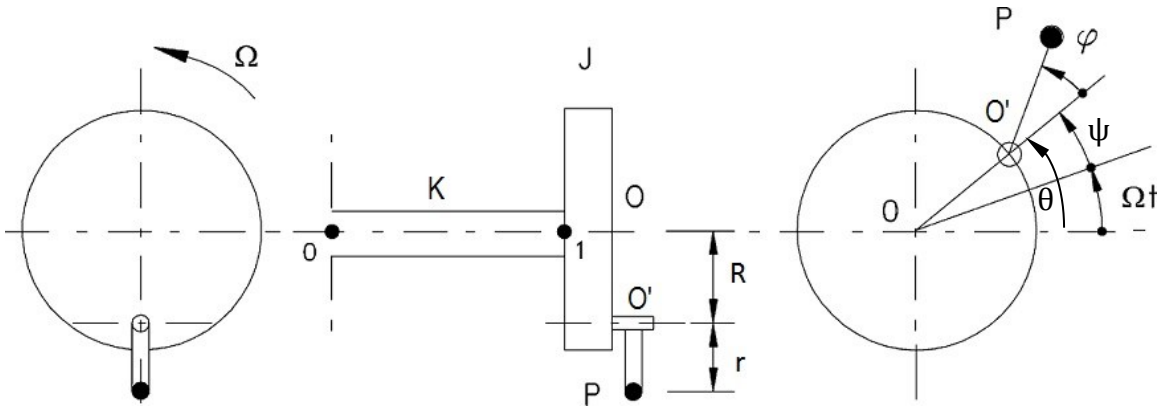

Figure 2.7: Pendulum absorber connected to the rotating disk (with moment of inertia J) and shaft (with stiffness K) [8]

For kinetic energy we need the angular velocity of the disk ($\dot{\theta}$) and the linear velocity of the pendulum (V_m). In a rotary system, the rotation θ consists of two parts. One is a steady-state rotation Ωt (due to rotation at a constant angular velocity Ω), and other part $\psi(t)$ is due to vibration disturbance superimposed over this rotation. Thus, we can mathematically write:

$$\theta(t) = \Omega t + \psi(t) \tag{2.4}$$

Therefore $\dot{\theta}(t)$ would be

$$\dot{\theta}(t) = \Omega + \dot{\psi} \tag{2.5}$$

The kinetic energy of the system can be calculated as follows:

$$T = \frac{1}{2}J\dot{\theta}^2 + \frac{1}{2}m(V_m.V_m)$$

$$= \frac{1}{2}J(\dot{\theta}^2) + \frac{1}{2}m\left[(R\dot{\theta}\sin\varphi)^2 + (R\dot{\theta}\cos\varphi + r(\dot{\theta}+\dot{\varphi}))^2\right]$$

$$= \frac{1}{2}[J + m(R^2 + r^2 + 2rRcos\,\varphi)]\dot{\theta}^2 + \frac{1}{2}mr^2\dot{\varphi}^2 + mr(r + R\cos\varphi)\dot{\varphi}\dot{\theta} \qquad (2.6)$$

$$= \frac{1}{2}[J + m(R^2 + r^2 + 2rRcos\,\varphi)](\Omega + \dot{\psi})^2 + \frac{1}{2}mr^2\dot{\varphi}^2$$

$$+ mr(r + R\cos\varphi)\dot{\varphi}(\Omega + \dot{\psi})$$

For potential energy, stiffness of the shaft and the gravity effect come into picture. However, normally the rotational speed of system is considerably high especially in reciprocating engines, thus generating large centrifugal force ($mR\,\Omega^2$) which dominates the gravitational force. As a result the gravity effect can be ignored with reasonable accuracy.

Considering this, the potential energy term can be described as:

$$U = \frac{1}{2}K\psi^2 \qquad (2.7)$$

Considering the potential and kinetic energy terms and external moment $M_T(t)$ acting on the disk, we can find the equations of motion for vibrating disk and pendulum. However, as there is no damping element in our system, the Lagrange equations reduce to the following:

$$\begin{cases} \dfrac{d}{dt}\left(\dfrac{\partial T}{\partial \dot{\psi}}\right) - \dfrac{\partial T}{\partial \psi} + \dfrac{\partial U}{\partial \psi} = \mathrm{M_T(t)} \\ \dfrac{d}{dt}\left(\dfrac{\partial T}{\partial \dot{\varphi}}\right) - \dfrac{\partial T}{\partial \varphi} + \dfrac{\partial U}{\partial \varphi} = 0 \end{cases} \tag{2.8}$$

After substituting Eqs. (2.6) and (2.7) into Eq. (2.8), we obtain:

$$(J + mR^2 + mr^2 + 2mRr\cos\varphi)\ddot{\psi} + (mr^2 + mRr\cos\varphi)\ddot{\varphi}$$
$$-2mRr\dot{\varphi}\sin\varphi\left(\Omega + \dot{\psi}\right) - mRr\dot{\varphi}^2\sin\varphi + K\psi = \mathrm{M_T(t)} \tag{2.9}[1]$$

$$(r + R\cos\varphi)\ddot{\psi} + r\ddot{\varphi} + +R\sin\varphi\,(\Omega + \dot{\psi})^2 = 0$$

Considering small amplitude of oscillations for the pendulum and disk, we can use the linearization of trigonometric terms by the approximation of sin φ ≈ φ and cos φ ≈ 1. This results in the following linear equations:

$$(J + mR^2 + mr^2 + 2mRr)\ddot{\psi} + (mr^2 + mRr)\ddot{\varphi} + K\psi = \mathrm{M_T(t)}$$

(2.10)

$$(r + R)\ddot{\psi} + r\ddot{\varphi} + R\Omega^2\varphi = 0$$

Assuming that the rotor has the steady rotational speed of Ω and the sinusoidal vibratory term with amplitude ϕ and fluctuating frequency of ω, the pendulum differential equation is derived from the second equation in Eq. (2.10) as:

$$r\ddot{\varphi} + R\Omega^2\varphi = (r + R)\psi\omega^2\sin(\omega t) \tag{2.11}$$

From this equation the natural frequency of the pendulum (ω_n) can be calculated as:

[1] To be sure that the calculation and driving the equations of the motion were done in a correct way, the Matlab parametric codes of Lagrange equation have been written. Given the kinetic energy and potential energy of any mechanism as input, the final equation of motions is derived as the output of the program. The developed Matlab code and the results are provided in Appendix I.

$$\omega_n = \sqrt{\frac{R\Omega^2}{r}} = \Omega\sqrt{\frac{R}{r}} \tag{2.12}$$

From Eq. (2.12) we can see that there is a linear relationship between the natural frequency of pendulum and the rotational speed (Ω).

2.4.2 Response of the system with/without CPVA using Matlab/Simulink modeling

Based on the Eq. (2.12), the parameters that can be determined by the designer for tuning of the pendulum are the length of pendulum (*r*), and the pendulum hinge location (*R*). To reach the desired infinite effective inertia of the pendulum we should tune the natural frequency of the pendulum exactly at the forcing frequency of the external torque on the rotor (ω). There is a relationship between the rotational speed (Ω) and the forcing frequency, ω.

The reciprocating systems use the crank piston mechanism for providing the necessary rotational power for rotary machines such as wheel sets, generators, turbines, etc.

Regardless of the number of cylinders in a reciprocating engine, we have 2-stroke and 4-stroke combustion mechanism for firing, which relates the firing torque cycle and rotational speed (Ω). In reciprocating engines, crankshaft plays the role of changing the reciprocating mechanism to rotational motion. It can be modeled as a rotating shaft connected to the inertia disks.

Here we would like to initially investigate the effect of a CPVA on the reduction of vibration in simple shaft and disk with arbitrary stiffness and inertia under sinusoidal torsional excitation. The modeling of the mechanism has been done in Matlab/Simulink software considering the derived governing equations of motion given in Eq. (2.10).

Let us assume a simple undamped system without CPVA as shown in Figure 2.8 with arbitrary shaft stiffness of $K = 1000^{(N/M)}$ and inertia of $J = 0.1^{(N.S^2/Rad)}$ under harmonic excitation of $M_T(t) = 50\sin(\omega t)$. The natural frequency of the system can be calculated as follows:

$$0.1\ddot{\theta} + 1000\theta = 50\sin(\omega t)$$

$$\omega_n = \sqrt{\frac{K}{J}} = \sqrt{\frac{1000}{0.1}} = 100^{rad/s} \tag{2.13}$$

$$= 954.93^{rpm}$$

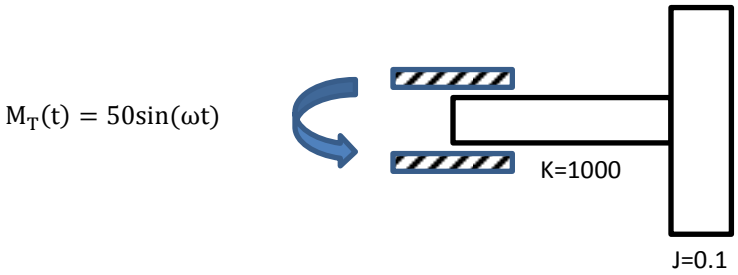

Figure 2.8: Simple single degree of freedom system (θ) torsional system without absorber

If we excite the system exactly at the natural frequency (ω=$100^{rad/s} = 15.9\,Hz$) the resonance behaviour is expected. Figure 2.9 shows the time domain response of the system for this case. As it can be seen, the disk amplitude of vibration increases steadily due to the resonance, which is not desirable as it causes high dynamic stress and eventual failure of the rotating system.

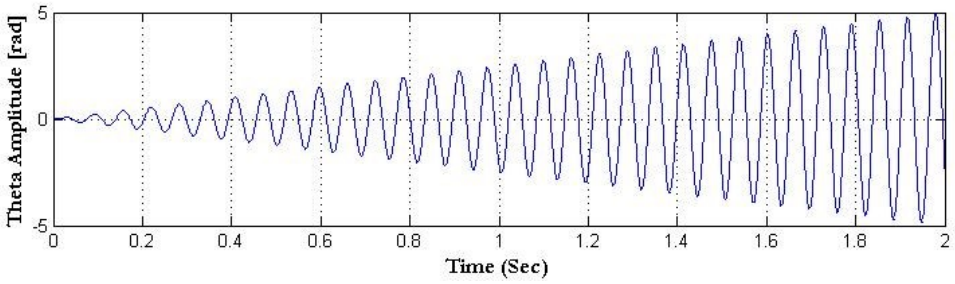

Figure 2.9: Time domain response of single DOF torsional system without CPVA excited on its natural frequency.[1]

Now let us consider the same system combined with the CPVA on the inertia disk as shown in Figure 2.10. It is simple model of the rotary system with CPVA where the pendulum is modeled with a mass (m) and pendulum length (r) attached to the inertia disk. The governing equations of motion are the same as Eq. (2.9) where ψ is the vibration of disk, φ is vibration of the pendulum and $M_T(t) = 50\sin(\omega t)$ (same as the exciation of the single DOF system)

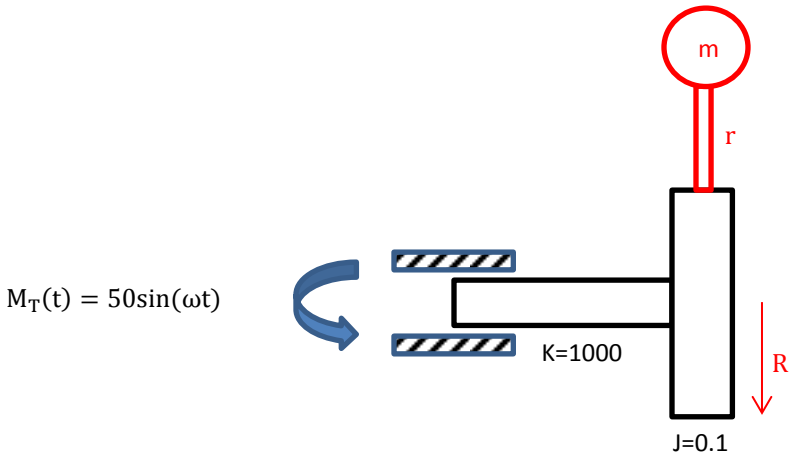

Figure 2.10: Two single degree of freedom system (ψ & φ) torsional system with absorber

[1] This system has been modeled in Matlab/Simulink software and the responses have been extracted by application of the ODE4 solver which is based on the 4th order Runge-Kutta method. The modeling block diagram and the Matlab code are provided in Appendix II.

It should be noted that in this case the forcing frequency ω is the same as rotational speed Ω. To have the optimum effect of the CPVA, its natural frequency should be tuned to the forcing frequency to reach the maximum inertia effect of CPVA causing reduction of vibration in the main inertia mass of the rotor. If we assume the radius of the inertia disk as 0.15 (m), then using Eq. (2.12), we obtain the length of the pendulum, r as:

$$\omega_n = \Omega \sqrt{\frac{R}{r}} \quad , \quad \omega = \Omega = \omega_n \qquad (2.14)$$
$$r = R = 0.15\, m$$

It means that the pendulum length should be set equal to the radius of the position that it will be connected to (in this case because it is attached to the outer surface of the disk it would be equal to the 0.15 m).

The two DOFs system with tuned vibration absorber has been modeled in Matlab/Simulink (The Code and simulation block diagram are provided in Appendix II). The mass of disk and pendulum are considered to be 11 kg and 2 kg, respectively. The vibration response of both disk and pendulum in time-domain at resonance condition is shown in Figure 2.11.

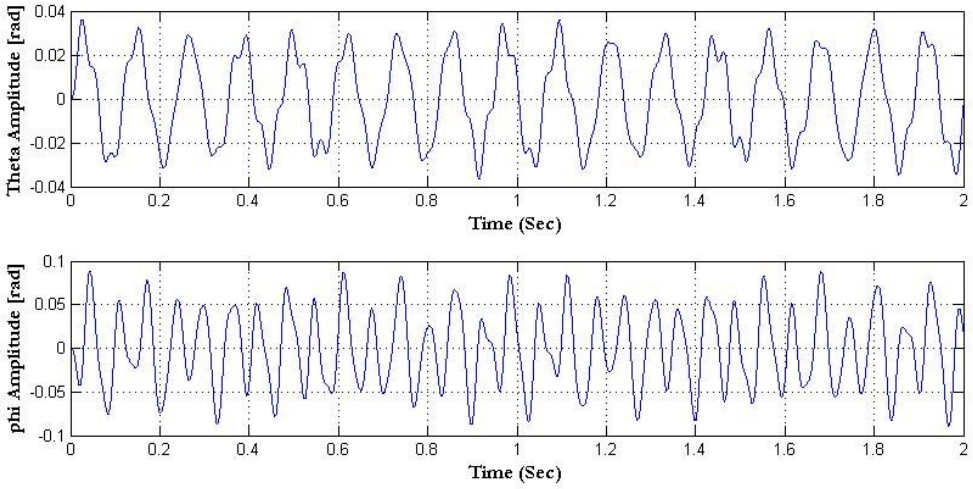

Figure 2.11: Time domain response of two DOF torsional system with CPVA tuned (r=R) excited on its natural frequency

It can be seen that the CPVA does not allow the amplitude of vibration of the disk to go to infinity in comparison to the without CPVA case shown in Figure 2.9. For this case, the amplitude of the disk (theta) is approximately limited to maximum amount of 0.03 rad.

To better realize the importance of tuning, let us consider the pendulum length as r=2R (un-tuned condition). The result is shown in Figure 2.12. As can be seen, although the amplitude of vibration for the pendulum is reduced, the maximum vibration amplitude of the main rotary system has increased to almost 0.04 rad.

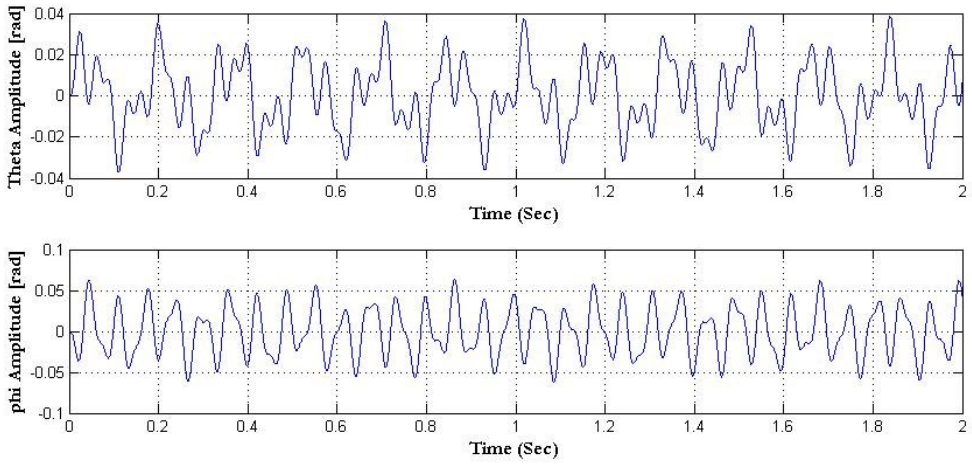

Figure 2.12: Time domain response of two DOF torsional system with CPVA un-tuned ($r=2R$) excited on its natural frequency

Similarly, for the un-tuned case of $r=0.5R$, as shown in Figure 2.13, the vibration response of the main rotary system has significantly increased with maximum value of almost 0.07 (rad). The amplitude of vibration for pendulum has also increased in this case as the effective pendulum length is reduced.

Considering the above, the importance of tuning of the most effective application of the pendulum absorber can be realized. It can be seen that by a small amount of un-tuning, the reduction in attenuation of vibration is considerable.

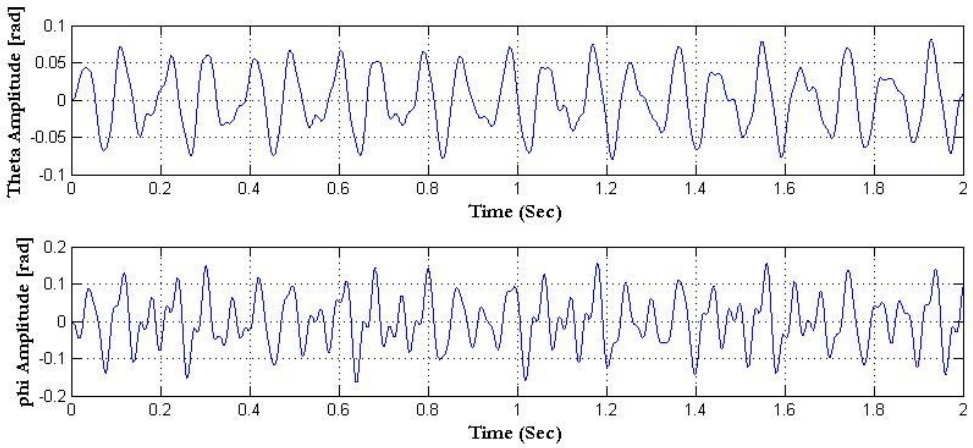

Figure 2.13: Time domain response of two DOF torsional system with CPVA un-tuned (r=0.5R) excited on its natural frequency

2.4.3 Frequency response of the system with/without tuned CPVA

Here the frequency response of the main rotary system with and without tuned CPVA has been studied.

Utilizing the FFT function in Matlab software, the frequency spectrum of the time domain response can be obtained. By examining the frequency spectrum, one can easily identify the natural frequencies of the system. Now for the simple rotating system discussed in previous section, by applying FFT on the time domain response (Figure 2.9), the frequency spectrum can be obtained as shown in Figure 2.14 (Matlab code for FFT analysis is provided in Appendix III). It can be seen that the frequency analysis exactly shows the natural frequency of the system at $\omega_n = 15.9^{(Hz)}$

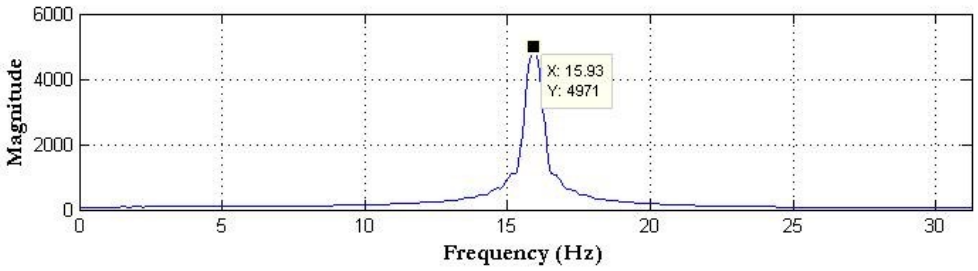

Figure 2.14: Frequency response simple (1-DOF) rotary system, without CPVA

After applying the CPVA and tuning it based on Eq. (2.14) r=R, as expected the frequency spectrum of the system (two DOFs system) would show two frequencies as shown in Figure 2.15.

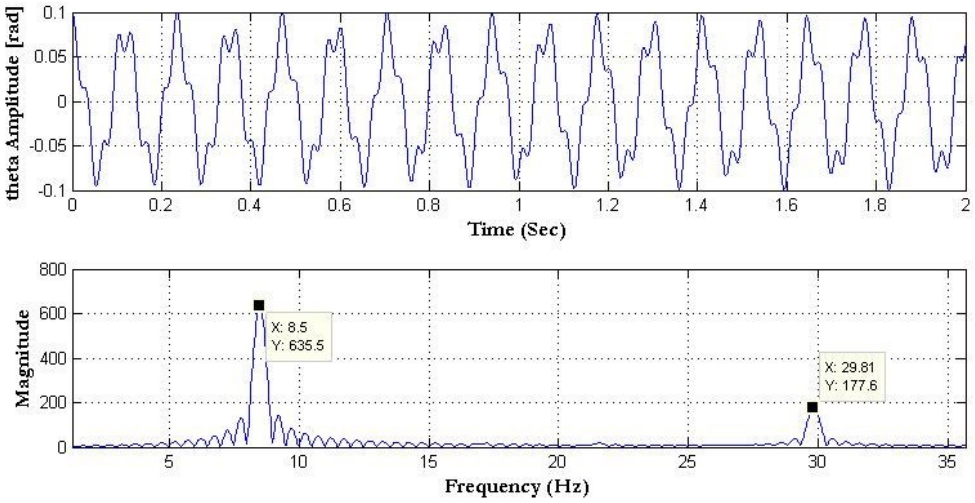

Figure 2.15: Frequency response of the simple (2-DOF) rotary system, with CPVA, tuned (r=R)

It can be seen that after applying the CPVA and tuning it in a proper way based on the characteristic of the rotating system, the natural frequency of the system (w_n=15.9 Hz) will be shifted to two new natural frequencies of w_{n1}=8.5 (Hz) and w_{n2}=29.8 (Hz) which

is far enough from the natural frequency of the main system. Thus exciting the main system at its natural frequency, will not cause undesirable resonance.

It should be noted that tuning of absorber most of the time depends on the working speed of the rotating system. The worst case happens when the working speed is exactly at the natural frequency of the system as discussed before. Sometimes the working frequency does not coincide with the natural frequency of the system. However, we may desire to also attenuate the vibration at that particular working frequency. For these cases, CPVA is quite suitable as it synchronises itself automatically based on the rotational speed of the shaft to which it has been connected. Therefore by considering the Eq. (2.12) and designing the pendulum length (r) for tuning based on the value of ω_n and Ω, the desired attenuation can be achieved.

2.5 Conclusions

In this chapter, the application of centrifugal pendulum vibration absorber for suppressing the vibration in rotating systems has been discussed. The simple case of one shaft and one inertia disk has been studied, and the modeling has been done with Matlab/Simulink software. The results show that by properly using the tuned CPVA, a considerable amount of attenuation in magnitude of vibration can be achieved. CPVA plays the role of passive damper capable of covering different rotating speed range. The importance of tuning is studied by varying the pendulum length to different values than the tuned length (un-tuned conditions). The vibration suppression capability of the CPVA has been significantly decreased in the un-tuned conditions.

Chapter 3. Torsional Vibration Modeling of the Reciprocating Locomotive V-type Engine

3.1 Introduction

In diesel locomotives, the traction force is produced by a main alternator, which subsequently feeds the traction motors driving the axles. The controlling procedure is handled electronically. Auxiliary systems such as cooling, heating, braking, lighting and accommodation power are mainly similar in both electric and diesel locomotives. The only difference between these two kinds of locomotives is that diesel locomotives carry power generating source around with it, instead of connecting to the overhead wires or a third rail which are feeding from generating station. In diesel locomotives the diesel engine coupled to an alternator produces the required electricity. Normally a fuel tank is also provided to feed the diesel engine.

Statistics shows that a modern diesel locomotive with the same weight of an electric locomotive produces about one third of the power in comparison [82]. However, the construction of electric railway track imposed substantial cost due to the necessity of providing power supply network such as overhead line or third rail to feed the locomotive.

In this chapter we want to formulate the torsional model of a locomotive crankshaft considering all the parts and instruments coupled to it during operation.

A diesel locomotive by itself is a complex structure. However some main parts are common in most of the diesel locomotives designed by different manufacturers around

the world. For example, Figure 3.1 shows the main parts of a US-built diesel-electric locomotive.

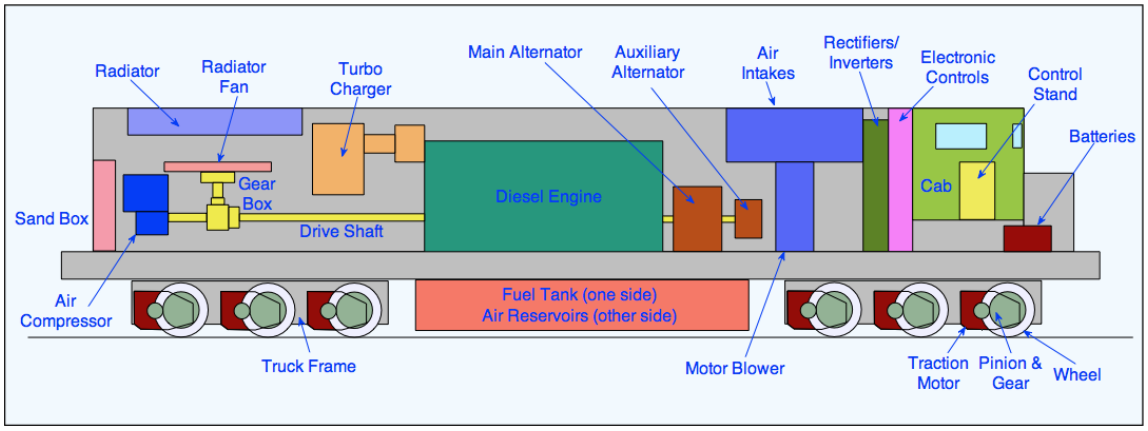

Figure 3.1: Ordinary diesel-electric locomotive parts [83]

Some parts play an important role in the torsional vibration analysis of locomotive crankshaft and thus having general information about these parts and their application are important before evaluating their inertia effect in vibration. Here in the following, some general information regarding important parts in Diesel Locomotive Engine has been summarized from references [82], [84], [85] and [86].

Diesel Engine:

The main power source of the locomotive is diesel engine. It can have 'in line' or in 'V-type' arrangement. It contains a large block for cylinder. The engine rotates the crankshaft at up to 2,000 rpm and this drives the various main and auxiliary parts needed to power the locomotive. The engine produced power is used for rotating the AC or DC main alternator or generator.

Main Alternator:

Main alternator is driven by diesel engine which provides traction to move the train. The output AC electricity provides power for the traction motors mounted on the trucks (bogies). In older locomotives, the alternator was a DC machine, called a generator. It produced direct current which was used to provide power for DC traction motors. Many of these machines are still in regular use. The next development was the replacement of the generator by the alternator which still use DC traction motors. The AC output is changed to DC required for the traction motors using rectifiers.

Auxiliary Alternator:

Passenger train locomotives are equipped with an auxiliary alternator. This provides AC power for lighting, heating, air conditioning, dining facilities etc. on the train. The output is transmitted along the train through an auxiliary power line. In the US, it is known as "head end power" or "hotel power". In the UK, the auxiliary alternator is used to supply the air condition equipment of the cars which is called Electric Train Supply (ETS).

Traction Motor:

Traction motors are provided on the axles to give the final drive since the diesel-electric locomotive uses electric transmission. These motors were traditionally DC but the development of modern power and control electronics has led to the introduction of 3-phase AC motors. Depending on the number of the locomotive axle, there are between four and six motors on most diesel-electric locomotives. A modern AC traction motor with air blowing can provide up to 1,000 hp.

Crankshaft:

The crankshaft (drive shaft) transmits the main output from the diesel engine to the radiator fans and compressor at one end and the alternators at the other end.

Radiator and Radiator Fan:

The mechanism of radiator in the locomotives is the same as in an automobile. Water is distributed around the engine block to keep the temperature within the most efficient range for the engine. The fans driven by the diesel engine cool down the water passing through it.

Gear Box:

The radiator and its cooling fan are often settled in the roof of the locomotive. Diesel engine drives the fan through a gearbox because it is necessary to change the direction of the drive upwards.

Diesel Engine Types:

Diesel engines are categorized into two main types, the two-stroke engine and the four-stroke engine. As the names show, they differ in the number of movements of the piston required to complete each cycle of operation. The simplest is the two-stroke engine. It has no valves. The exhaust from the combustion and the air for the new stroke is drawn in through openings in the cylinder wall as the piston reaches the bottom of the down stroke. Compression and combustion occurs on the upstroke. The revolutions cycle in two-stroke engines is twice that of a four-stroke engine with similar power.

The four-stroke engine cycle is as follows: Down stroke 1 – air intake, upstroke 1 – compression, down stroke 2 – power, upstroke 2 – exhaust. Valves are required for air intake and exhaust, usually two for each. In this respect it is more similar to the modern petrol engine than the 2-stroke design.

The preference of two-stroke over four-stroke or vice versa is depending on the application. However, it can be said that the 2-stroke design is simpler than the 4-stroke and can obtain greater power than a 4-stroke engine from a block of equal size. But the two-cycle design is less efficient and causes significantly greater stress on engine components which can lead to increase in wear and maintenance works [87]. Also the 4-stroke engine is more fuel efficient.

V-Type cylinders:

Diesel engines can be designed with the cylinders "in-line", "double banked" or in a "V". The double banked engine has two rows of cylinders in line. Most diesel locomotives now have V form engines. This means that the cylinders are split into two sets, with half forming one side of the V. For Example, V8 engine has 4 cylinders set at an angle forming one side of the V with the other set of four forming the other side. The crankshaft is at the base of the V. The V12 was a popular design used in the UK. In the US, V16 is usual for freight locomotives and there are some designs with V20 engines.

3.2 Importance of modeling and torsional analysis

A multi-cylinder reciprocating machine contains many reciprocating and rotating parts such as pistons, connecting rod, crankshaft, flywheel, damper and auxiliary drives. The system is so complex that it is difficult, if not impossible, to undertake an exact analysis

of its vibrational characteristics. The information that one can obtain from such a rigorous analysis, is also of doubtful value for the present-day speeds of reciprocating machinery. The actual system is characterised by the presence of unpredictable effects such as variable inertia, internal damping, misalignment in the transmission units, uneven firing intervals etc. The analysis can be best carried out, by putting the inertias of rotating and reciprocating parts at discrete points on the main shaft. The problem then reduces to the forced vibration study of an N rotor system subjected to varying torques at different cylinder points [19].

Following the transmission of the torque in the regular engines with reciprocating mechanism such as internal combustion engines in different vehicles, the harmonic components of different orders will act on the system. If any of these harmonic orders coincide with one of the torsional critical speeds of the system, the resonance and high dynamic stress occurs in the system. This phenomenon, obviously, are not desired due to the defects and failure which they will cause in the system which is discussed widely in the Chapter one (Introduction).

Therefore knowing the vibration behavior of the reciprocating engines can help to detect and prevent those effects by considering them at the design stage.

3.3 General locomotive parts modeling approach

To obtain an acceptable torsional modeling for locomotive engine based on the parts which are mounted on the crankshaft, after observation and as it has been shown in Figure 3.1, we found that these parts play an important role in vibration behavior of crankshaft in usual locomotives:

- V-type piston and connecting rod
- Main generator
- Auxiliary generator
- Radiator fans
- Air compressor
- Torsional stiffness of crankshaft

Each of these components should be modeled as an inertia disk in our final inertia disk-shaft modeling. Considering them as inertia disks in the model categorized separately is explained below.

3.3.1 V-type piston and connecting rod

Determination of polar mass moments of inertia is a straightforward procedure for rotating parts [19]. However, it is not quite simple in the case of reciprocating parts. For a piston connected to the crankshaft, we should consider two different inertias caused by two different rotating and reciprocating mass of piston and connecting rod all together.

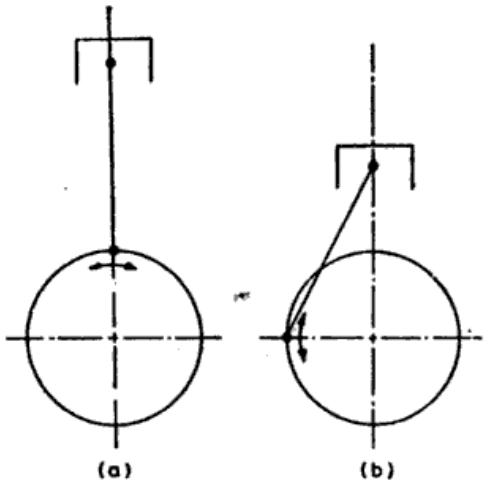

Figure 3.2: Different position of equivalent mass moment of inertia for a piston [19]

Assuming the mechanism such as the one shown in the Figure 3.2, we can see from Figure 3.2 (a) that with small oscillations of the crank, there is no vertical motion for the piston in this position, and hence the equivalent inertia of the piston is zero. Whereas in Figure 3.2 (b) position, the piston has practically the same acceleration as that of the crank pin and the equivalent inertia is $m_{rec}r^2$, where m_{rec} is the mass of the reciprocating parts and r is the crank throw. Hence, the total polar mass moment of inertia varies from I_{rec} to $I_{rec} + m_{rec}r^2$, when the crankshaft is rotating. This modeling is verified also by other references such as [19], [88]. As in one rotation of the shaft there are two positions with zero inertia and two positions with $m_{rec}r^2$additional inertia, we consider as an approximation, the system to have an average inertia given by:

$$I = I_{rot} + \frac{1}{2} m_{rec} r^2 \tag{3.1}$$

There is no considerable difference between the inline cylinder engine and v-type cylinders in case of mass moment of inertia calculations; Figure 3.3 shows a sketch of ordinary V-type connecting rod.

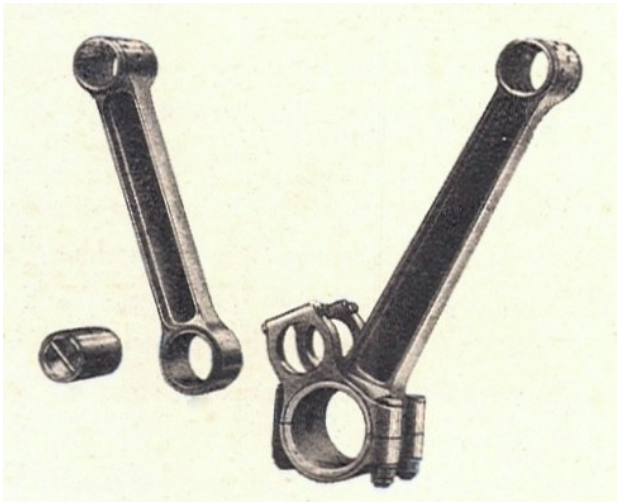

Figure 3.3: Sketch of ordinary master rod and connecting rod in V-type mechanism [84]

In V-type engine there would be a master rod and a connecting rod connected by a pin to the master rod. As the shape shows, the pin plays a role in balancing the weight difference of the master and connecting rod. So for modeling the V-type connecting rod and piston, first of all we should find the center of the gravity of the rod and dividing the whole mass of the connecting rod into lump mass at each end. Finally m_{rec} and m_{rot} should be considered based on the following formulas for calculating the mass moment of inertia of whole body from equation (3.1):

$$m_{rec} = m_{piston} + m_{rod,rec} \quad , \quad m_{rot} = m_{pin} + m_{web} + m_{rod,rot} \tag{3.2}$$

where m_{piston} is the mass of piston head, $m_{rod,rec}$ is the mass of portion of the connecting rod considered as reciprocating part from center of gravity, m_{pin} is the mass of crank pin on each bank, m_{web} is the mass of crank web in each bank and $m_{rod,rot}$ is the mass of connecting rod considered as rotating part from center of gravity formula.

For v-type engines as we have two cylinder piston mechanisms in each bank all the masses should be multiplied by two for calculating the effective mass moment of inertia.

3.3.2 Main generator

In most diesel-electric locomotives the highest inertia in torsional modeling would be related to the main generator as it is the heaviest part which is connected to the crankshaft. In addition to that in locomotive engines there is no flywheel. The generator armature is coupled directly to the crankshaft and it will play the role of the flywheel for maintaining the torque continuous and smooth.

In generators, about one third of the mass is that of the armature and this mass should be considered in calculating the mass moment of inertia of the main generator in locomotive engine [89].

For calculating the inertia of the rotating parts an effective mass (M_{eff}) corresponding to the rotating parts is assumed to obtain:

$$\mathrm{J} = \frac{1}{2} M_{eff} R^2 \tag{3.3}$$

3.3.3 Auxiliary generator

The method for considering the mass of the auxiliary generator is also same as that of the main generator but there is some difference in coupling to the crankshaft. This generator connects to the crankshaft indirectly via a geared system in most of the time. For modeling the inertia disk connecting to each other via geared system we should consider the gear ratio (speed ratio) of the mechanism which affects the amount of the mass moment of inertia and stiffness of connecting shafts in the mechanism. We should multiply the mass moment of inertia (J) and connecting shaft stiffness (K) of one side by the square of the speed ratio.

Figure 3.4 shows the method more clearly:

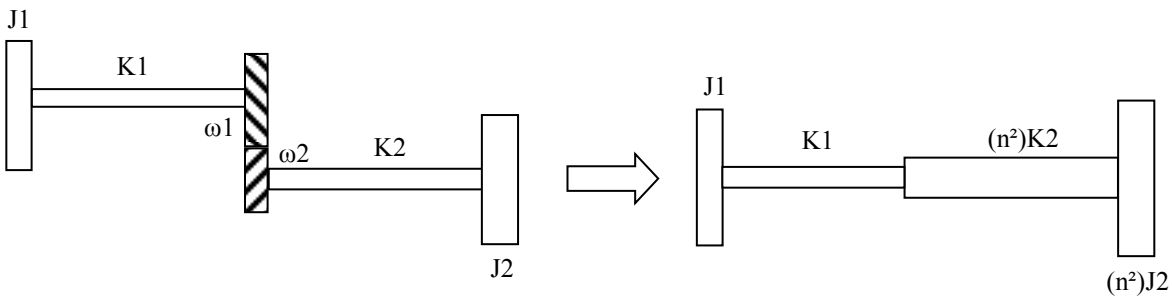

Figure 3.4: Geared system equivalency method

If the speed ratio is considered to be ω2/ω1=n for the straight rotor we should then multiply the mass moment of inertia of disk and stiffness of second shaft by n² as shown in Figure 3.4 [19], [88].

3.3.4 Radiator fans

The radiator fans which in most cases are more than one in locomotives structure are also coupled through geared system to the crankshaft. We should consider their masses for calculating the mass moment of inertia and the geared equivalency is also same as that of the auxiliary generator.

3.3.5 Air compressor

The air compressors are used for producing the compressed air required for application of blowers in the locomotive or the braking systems. They also are coupled directly to the crankshaft and take their power from the diesel engine. In most cases the compressors are connected to the end of the shaft. Their moment of inertia are also important in vibration modeling of the locomotive crankshaft.

3.3.6 Torsional stiffness of crankshaft

In determining the torsional stiffness of shafts connecting the rotors, the main complexity arises from the crank webs. This is due to the bending of crank webs and twisting of crank pin. Several experiments have been carried out on a number of crank shafts of large slow engines, which have shown that the equivalent length (L_e) of crankshaft as shown in Figure 3.5 is nearly equal to the actual length, if the diameter of main shaft is equal to the crank pin diameter [19].

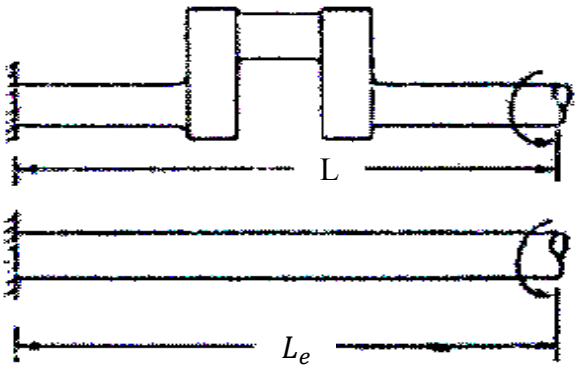

Figure 3.5: Equivalent length of a crank [19]

In general the procedure that is adopted to reduce the reciprocating machine system to a mathematical model is to use a basic diameter, which corresponds to the journal diameter of the crankshaft.

3.4 Case study of engine's crankshaft torsional modeling (U25B-GE freight locomotive)

3.4.1 Locomotive description and specification

For this study, the diesel-electric locomotive which is normally used in railway industry is considered. The chosen locomotive is a GE locomotive model U25B which is

commonly used in railway freight transportation throughout the North American continent and the whole world. Here some general information required to develop the simplified torsional vibration model of this locomotive crankshaft has been presented.

The locomotive is powered by a 16-cylinder four stroke cycle, turbo-charged diesel engine with 9 inch by 10 ½ inch cylinders in a 45 degree V-arrangement. The engine has an integral head and cylinder arrangement which can be removed easily. It is equipped with cast-iron pistons, valve seat inserts and the Bendix fuel system. The cylinder liner is chrome plated and 3/16 inches thick.

Each connecting rod assembly consists of a master connecting rod and slave connecting rod. These rods are made of forged alloy steel. The slave rod bolts to a pin fitted in the master connecting rod and the master connecting rod is bolted to the crankshaft. This design provides for a maximum of bearing surface area.

The engine crankshaft is directly connected to the traction generator armature. When the generator is electrically energized (from batteries) through its start field, the generator acts as a motor to rotate the crankshaft to start the engine.

Some important information which is necessary for deriving the torsional modeling of this locomotive has been given in Table 3.1. The detailed specifications are provided in Appendix IV.

Table 3.1: U25B-GE freight locomotive engine technical specifications

ENGINE SPECIFICATIONS	Model	7FDL16
	Gross Horsepower	2750
	Number of Cylinders	16
	Stroke Cycle	4
	Cylinder Arrangement	450V
	Bore	0.229 m
	Stroke	0.267 m
	Compression Ratio	12.7-1
	Idle Speed	400 RPM
	Maximum Governed Speed	2000 RPM
	Firing Order	1R–11, 3R-3L, 7R -7L, 4R–4L, 8R-8L, 6R-6L, 2R-2L, 5R-5L
	Turbocharger	Single
ENGINE DIMENSIONS	Height (Overall Including Stack)	2.711 m
	Length (Overall Including Generator)	6.615 m
	Width (Overall)	1.734 m
	Weight (Including Generator)	25855 kg

Other data required for modeling:

Piston mass: 10 (kg)

Crank throw: 0.133 (m)

Crankshaft diameter: 0.203 (m)

Connecting rod length: 0.6 (m), Mass: 63 (kg), thickness: 0.09 (m)

Width varying from 0.1 to 0.2 (m)-narrow end connected to piston

Crank web cross section: 0.15 x 0.09 (m)

Crank pin diameter: 0.203 (m)

Engine mounted to the crankshaft at 0.146 (m) interval

Auxiliary generator gear ratio: (3:1)

Radiator fans geared ratio: (2.5:1)

3.4.2 Equivalent torsional modeling

Having the necessary data we can start the locomotive part by part based on material in section 3.2 to find the inertia-disk-shaft model of entire locomotive engine.

First of all the calculation of the center of gravity and equivalent reciprocating mass and rotational mass of connecting rod in each bank will be considered as follows. Figure 3.6 shows the sketch of the connecting rod for each piston.

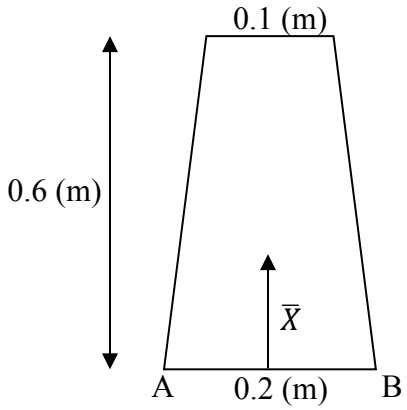

Figure 3.6: Connecting rod simplified sketch

First of all based on the Figure 3.6, the trapezoid shape can be devided to two triangle and one rectangular. Considering the superposition, by finding the centres of gravity of each shape with respect to the line AB, the centre of gravity for the connecting rod can be calculated as:

$$\bar{X} = \frac{2\left(0.05 \times 0.3 \times \frac{0.6}{3}\right) + (0.1 \times 0.6 \times 0.3)}{2(0.05 \times 0.3) + (0.1 \times 0.6)} \quad \Rightarrow \quad \bar{X} = 0.27\ (m) \qquad (3.4)$$

Having this value we can find $m_{rod,rec}$ and $m_{rod,rot}$ considering that the mass of connecting rod is 63 kg:

$$\begin{cases} m_{rod,rec} + m_{rod,rot} = 63 \\ \dfrac{0.6 \times m_{rod,rec}}{m_{rod,rec} + m_{rod,rot}} = 0.27 \end{cases} \rightarrow \begin{matrix} m_{rod,rot} = 34.65\ (kg) \\ m_{rod,rec} = 28.35\ (kg) \end{matrix} \quad (3.5)$$

Finally having the reciprocating and rotary part mass of the connecting rod we can find the whole reciprocating mass and rotating mass as follows:

$$m_{rec} = m_{piston} + 2m_{rod,rec} = 66.7$$
$$m_{rot} = m_{pin} + m_{web} + 2m_{rod,rot} = 94.25 \quad (3.6)$$

Therefore: In each bank $\begin{cases} m_{rec} = 66.7\ (kg) \\ m_{rot} = 94.25\ (kg) \end{cases}$

Finally:

$$J_{rec} = \frac{1}{2} m_{rec} \times R^2 = 0.59$$
$$J_{rot} = \frac{1}{2} m_{rot} \times R^2 = 0.83 \quad (3.7)$$

After the calculation, it can be found that J in each bank is equal to 1.42 (kg.m²). Therefore considering 8 banks in this locomotive engine, there should be 8 inertia disks

with mass moment of inertia of 1.42 in the model as representative of reciprocating cylinder-piston mechanism.

Having the weight of the other parts such as generators and compressor etc. we can calculate their mass moment of inertia and their correct location that we should attach them to our model. It should be noted that for auxiliary generator and radiator fans, based on the rule of geared system mentioned in section (3.3.3) we should multiply their inertia and their shaft stiffness in correction coefficient. For straight rotor modeling, the coefficient is 9 for auxiliary generator and 6.25 for radiator fans. Figure 3.7.b shows the final disk-shaft torsional vibration model of the U25B locomotive shown in Figure 3.7.a.

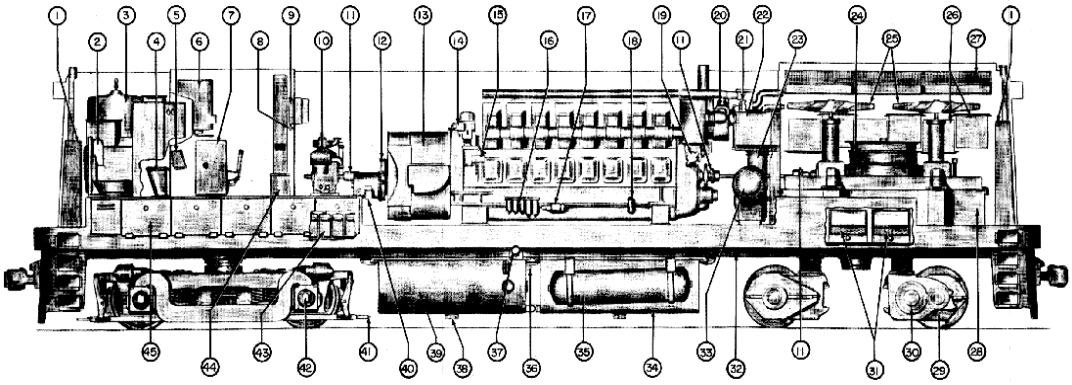

Figure 3.7.a: U25B freight locomotive real sketch [90]

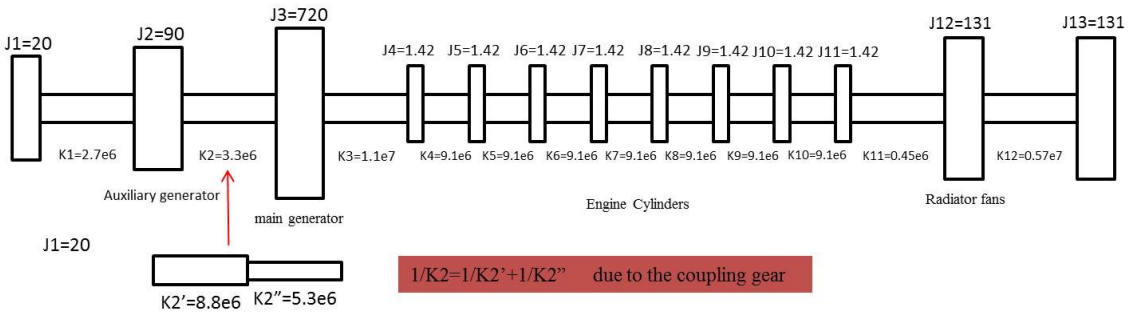

Figure 3.7.b: Torsional modeling of U25B locomotive

3.5 Free torsional vibration analysis of the case study model

The torsional model of the locomotive engine developed in the previous section can be effectively used to extract the natural frequencies and mode shapes.

3.5.1 Natural frequencies (stiffness matrix method)

As we have the simplified model for our case study, we can use the common analysis methods to find the natural frequencies of the locomotive engine in different modes of vibration.

In reciprocating machine installation, the number of stations is generally few in the mathematical model and it is convenient to adopt the classical eigen value analysis approach based on the stiffness matrix to calculate the natural frequencies and different mode shapes [19]. The procedure is briefly described here. Let $\emptyset_i$ denote the angle of twist of ith rotor. The free torsional vibration equations of motion are:

$$
\begin{aligned}
&J_1\ddot{\emptyset}_1 + K_1\emptyset_1 - K_1\emptyset_2 = 0\\
&J_2\ddot{\emptyset}_2 - K_1\emptyset_1 + (K_1 + K_2)\emptyset_2 - K_2\emptyset_3 = 0\\
&J_3\ddot{\emptyset}_3 - K_2\emptyset_2 + (K_2 + K_3)\emptyset_3 - K_3\emptyset_4 = 0\\
&J_4\ddot{\emptyset}_4 - K_3\emptyset_3 + (K_3 + K_4)\emptyset_4 - K_4\emptyset_5 = 0\\
&J_5\ddot{\emptyset}_5 - K_4\emptyset_4 + (K_4 + K_5)\emptyset_5 - K_5\emptyset_6 = 0\\
&J_6\ddot{\emptyset}_6 - K_5\emptyset_5 + (K_5 + K_6)\emptyset_6 - K_6\emptyset_7 = 0\\
&J_7\ddot{\emptyset}_7 - K_6\emptyset_6 + (K_6 + K_7)\emptyset_7 - K_7\emptyset_8 = 0
\end{aligned}
\qquad (3.8)
$$

$$J_8\ddot{\emptyset}_8 - K_7\emptyset_7 + (K_7 + K_8)\emptyset_8 - K_8\emptyset_9 = 0$$

$$J_9\ddot{\emptyset}_9 - K_8\emptyset_8 + (K_8 + K_9)\emptyset_9 - K_9\emptyset_{10} = 0$$

$$J_{10}\ddot{\emptyset}_{10} - K_9\emptyset_9 + (K_9 + K_{10})\emptyset_{10} - K_{10}\emptyset_{11} = 0$$

$$J_{11}\ddot{\emptyset}_{11} - K_{10}\emptyset_{10} + (K_{10} + K_{11})\emptyset_{11} - K_{11}\emptyset_{12} = 0$$

$$J_{12}\ddot{\emptyset}_{12} - K_{11}\emptyset_{11} + (K_{11} + K_{12})\emptyset_{12} - K_{12}\emptyset_{13} = 0$$

$$J_{13}\ddot{\emptyset}_{13} - K_{12}\emptyset_{12} + K_{12}\emptyset_{13} = 0$$

In matrix form the above equations can be written as:

$$[J]\{\ddot{\emptyset}\} + [K]\{\emptyset\} = 0$$

where:

$$[J] = \begin{bmatrix} J_1 & 0 & \cdots & 0 & 0 \\ 0 & J_2 & & 0 & 0 \\ \vdots & & \ddots & \vdots & \\ 0 & 0 & & J_{12} & 0 \\ 0 & 0 & \cdots & 0 & J_{13} \end{bmatrix}$$

$$[K] = \begin{bmatrix} K_1 & -K_1 & 0 & \cdots & 0 \\ -K_1 & (K_1 + K_2) & -K_2 & & 0 \\ 0 & -K_2 & (K_2 + K_3) & & \\ 0 & 0 & & & \vdots \\ \vdots & \vdots & & \ddots & 0 \\ & & & (K_{11} + K_{12}) & -K_{12} \\ 0 & 0 & \ldots\ 0 & -K_{12} & K_{12} \end{bmatrix}$$

In the above matrices, $[J]$ and $[K]$ are the mass and stiffness matrices and $\{\emptyset\}$ is the response vector.

For harmonic vibrations at the natural frequencies we have:

$$\{[K] - \omega^2[J]\}\{\emptyset\} = 0$$

We can see that if we calculate the eigen values of $[K][J]^{-1}$ matrix and take their square roots, we have the natural frequencies of each mode.

In our case study the stiffness and inertia matrices are in the order of 13*13 and here are the final values:

$$[K] = 10^4 \times \begin{pmatrix} 270 & -270 & 0 & 0 & 0 & 0 & 0 & 0 & 0 & 0 & 0 & 0 & 0 \\ -270 & 600 & -330 & 0 & 0 & 0 & 0 & 0 & 0 & 0 & 0 & 0 & 0 \\ 0 & -330 & 440 & -110 & 0 & 0 & 0 & 0 & 0 & 0 & 0 & 0 & 0 \\ 0 & 0 & -110 & 1020 & -910 & 0 & 0 & 0 & 0 & 0 & 0 & 0 & 0 \\ 0 & 0 & 0 & -910 & 1820 & -910 & 0 & 0 & 0 & 0 & 0 & 0 & 0 \\ 0 & 0 & 0 & 0 & -910 & 1820 & -910 & 0 & 0 & 0 & 0 & 0 & 0 \\ 0 & 0 & 0 & 0 & 0 & -910 & 1820 & -910 & 0 & 0 & 0 & 0 & 0 \\ 0 & 0 & 0 & 0 & 0 & 0 & -910 & 1820 & -910 & 0 & 0 & 0 & 0 \\ 0 & 0 & 0 & 0 & 0 & 0 & 0 & -910 & 1820 & -910 & 0 & 0 & 0 \\ 0 & 0 & 0 & 0 & 0 & 0 & 0 & 0 & -910 & 1820 & -910 & 0 & 0 \\ 0 & 0 & 0 & 0 & 0 & 0 & 0 & 0 & 0 & -910 & 955 & -45 & 0 \\ 0 & 0 & 0 & 0 & 0 & 0 & 0 & 0 & 0 & 0 & -45 & 5745 & -57 \\ 0 & 0 & 0 & 0 & 0 & 0 & 0 & 0 & 0 & 0 & 0 & -57 & 57 \end{pmatrix}$$

It can be seen that the stiffness matrix is a narrow banded matrix and inertial matrix is a diagonal matrix:

$$[J] = \begin{pmatrix} 20 & 0 & 0 & 0 & 0 & 0 & 0 & 0 & 0 & 0 & 0 & 0 & 0 \\ 0 & 90 & 0 & 0 & 0 & 0 & 0 & 0 & 0 & 0 & 0 & 0 & 0 \\ 0 & 0 & 750 & 0 & 0 & 0 & 0 & 0 & 0 & 0 & 0 & 0 & 0 \\ 0 & 0 & 0 & 1.42 & 0 & 0 & 0 & 0 & 0 & 0 & 0 & 0 & 0 \\ 0 & 0 & 0 & 0 & 1.42 & 0 & 0 & 0 & 0 & 0 & 0 & 0 & 0 \\ 0 & 0 & 0 & 0 & 0 & 1.42 & 0 & 0 & 0 & 0 & 0 & 0 & 0 \\ 0 & 0 & 0 & 0 & 0 & 0 & 1.42 & 0 & 0 & 0 & 0 & 0 & 0 \\ 0 & 0 & 0 & 0 & 0 & 0 & 0 & 1.42 & 0 & 0 & 0 & 0 & 0 \\ 0 & 0 & 0 & 0 & 0 & 0 & 0 & 0 & 1.42 & 0 & 0 & 0 & 0 \\ 0 & 0 & 0 & 0 & 0 & 0 & 0 & 0 & 0 & 1.42 & 0 & 0 & 0 \\ 0 & 0 & 0 & 0 & 0 & 0 & 0 & 0 & 0 & 0 & 1.42 & 0 & 0 \\ 0 & 0 & 0 & 0 & 0 & 0 & 0 & 0 & 0 & 0 & 0 & 131 & 0 \\ 0 & 0 & 0 & 0 & 0 & 0 & 0 & 0 & 0 & 0 & 0 & 0 & 131 \end{pmatrix}$$

Using Matlab to calculate the eigen values of $[K][J]^{-1}$ we can find the natural frequencies of the model. This modeling will give us the thirteen natural frequencies.

Here are the results for ω_n (RPM) derived from Matlab programming:

ans =

47429
44710
40299
34376
27190
19080
10591
3976
3357
1733
944
0
322

The natural frequencies are expressed in RPM. As it can be realized the natural frequencies above 2000 RPM do not contribute significantly to the system response as the engine under study has the he maximum speed of 2000 (RPM). Therefore, here the first four natural frequencies as provided in Table 3.2 are considered for this case study.

Table 3.2: Natural frequencies or critical speeds of locomotive crankshaft

Mode shape #	Natural frequency (RPM)
1st	0
2nd	322
3rd	944
4th	1733

3.5.2 Sketching corresponding mode shapes

For finding the mode shape at each natural frequency we should find the eigen vectors of $[K][J]^{-1}$matrix. This will give us the mode shape diagrams of case study locomotive at different critical speeds.

We can use the Matlab program to find the Eigen vectors from the frequency matrix and here are the results:

v =

-0.7721	-0.0334	0.2774	-0.2110
-0.5838	-0.0310	0.2774	-0.2093
0.0947	-0.0207	0.2774	-0.2013
0.0890	0.1426	0.2774	-0.0275
0.0879	0.1621	0.2774	-0.0065
0.0863	0.1814	0.2774	0.0145
0.0842	0.2004	0.2774	0.0355
0.0818	0.2191	0.2774	0.0566

0.0789	0.2374	0.2774	0.0775
0.0756	0.2554	0.2774	0.0985
0.0719	0.2730	0.2774	0.1195
-0.0101	0.6207	0.2774	0.5430
0.0015	-0.4985	0.2774	0.7354

Each column in matrix above is associated with each natural frequency. Column 3 is for the 1st mode, column 4 is for the 2nd mode, column 2 is for the 3rd mode, and column 1 is for the 4th mode, respectively. As our system is semi definite, one of the natural frequencies is zero and obviously this corresponds to the rigid mode.

To see results more clearly, it would be better to normalize the results with values between 0 and 1. The sketch of displacements for the inertia disks representing each components of the locomotive have been shown in Figure 3.8 to Figure 3.11 for each mode shapes.

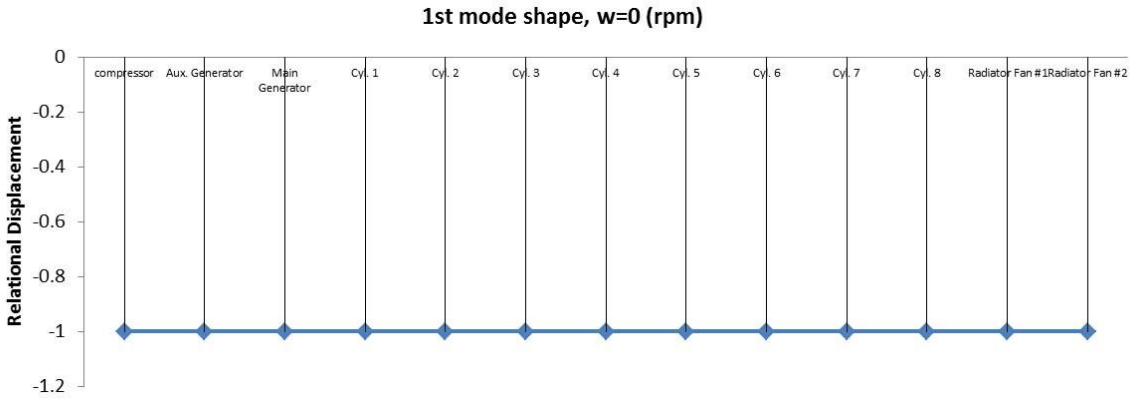

Figure 3.8: First mode shape of the crankshaft model (rigid mode)

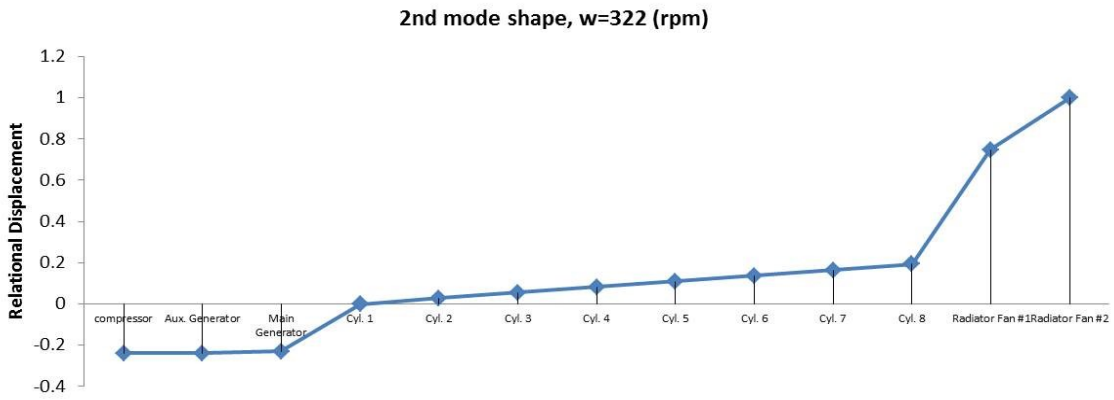

Figure 3.9: Second mode shape of the crankshaft model

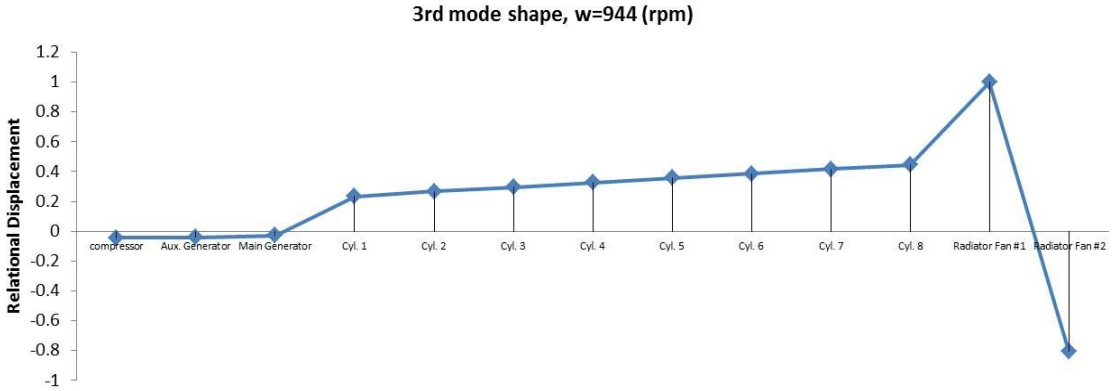

Figure 3.10: Third mode shape of the crankshaft model

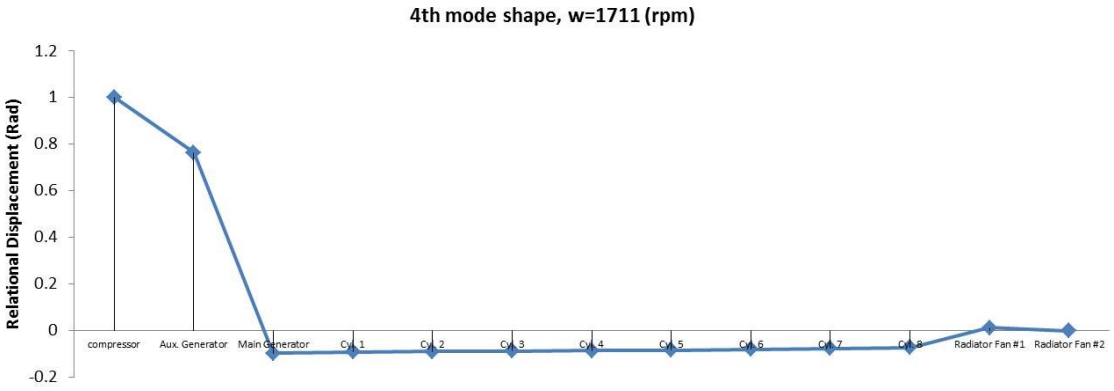

Figure 3.11: Fourth mode shape of the crankshaft model

3.6 Verifying the results

To examine whether torsional vibration is meaningful with reasonable errors which are negligible, it would be better to check the results based on the characteristics of the case study locomotive in other references. Taylor in [88] provides the sketch of first mode critical speed of ordinary engines with different arrangement. Although these amounts are experimental and very rough and depend on various conditions and arrangement of engine, it can be a criterion to judge the accuracy of the method described in this modeling. Figure 3.12 shows the first mode natural frequencies of an isolated torsional system consisting of a crankshaft with a flywheel at one end that has a relatively large amount of inertia.

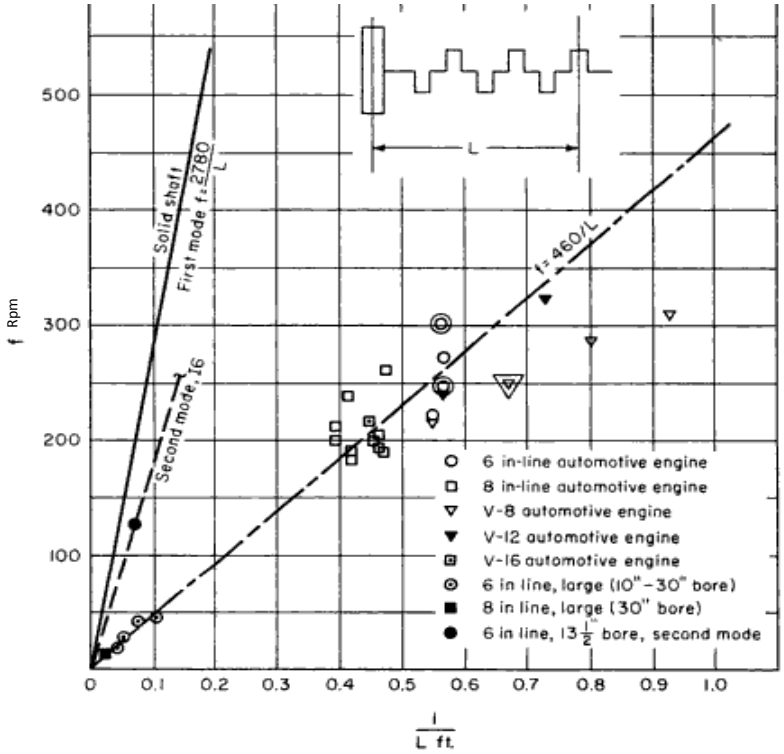

Figure 3.12: First mode torsional frequency of crankshaft with flywheel at one end. Where the actual value of L was not known, it was taken as b(1.1N)for inline engines and as b(0.55N+0.5) for V engines, where b is the bore in feet and N is the number of cylinders. [88]

For exactly similar designs, frequency in any mode is proportional to 1/L [91]. This figure gives the data on the first mode torsional frequency of crankshafts isolated from the external driven system and carrying a heavy flywheel at one end. In spite of large differences in detail design, this natural frequency shows the paramount influence of shaft length on the torsional natural frequency. This figure can be used for a rough prediction of first order critical speed.

One of the curve fit lines in the figure is for a solid shaft, which is our case. To find the fundamental natural frequency of an engine, we have to calculate the effective length of its crankshaft ($L \ \ m$) in the horizontal coordinate system. Based on the information, this value depended on piston bore in meter (b) and the number of cylinders (N).

For the V-type engines the following calculation should be done to find the case effective length:

$$L = 3.281b(0.55N + 0.5) \qquad \text{Effective length for V-type engines}$$
$$L = 0.75(0.55 \times 16 + 0.5) = 6.975 \ \ ft \qquad \text{U25B-GE freight locomotive} \qquad (3.9)$$
$$\frac{1}{L} = 0.143$$

Having the reverse of effective length from Eq. (3.9) and referring to the figure we can find that the experimental natural frequency (critical resonance speed) is about 390 (rpm) for the first mode solid shaft. This is comparable to the simulation result for the first model which is found to be 322 (rpm). Considering the difference in modeling of the engine in this approach and the way it has been done in this study, such as non-existence of flywheel which is replaced by the generator instead, and also existence of other parts

(such as fans and compressors) coupled to the crankshaft, the developed model can reasonably predict the first natural frequency.

There are some other references where the natural frequencies of similar diesel engines are obtained experimentally such as [92] where the fundamental natural frequency calculated is around 400 (rpm) for a V20 diesel engine

3.7 Conclusions

In this chapter the torsional modeling of a common V-type locomotive engine crankshaft has been conducted based on some valid simplifications and approximate methods. Real sample locomotive data for the case study U25B-GE locomotive, especially parts dimensions such as radii, widths and lengths etc. are difficult to obtain. In addition to the available technical manual of the locomotive, in this study some approximate but acceptable assumptions have been done based on existing information and data based on handbooks such as [20]. These estimations have been done with the help of the standards to minimize the inaccuracy of the modeling of the case study locomotive crankshaft. All of these have been applied as a case study on a real diesel-electric locomotive engine and the natural frequencies and mode shapes of the engine have been obtained based on the inertia disk-rotor modeling using stiffness matrix method.

Based on the applicable range of speed of the locomotive it has been found that only first four natural frequencies of the system are effective during the operation of engine. Also based on the mode shapes the critical inertia disk at each resonance frequency can be detected which is an important criteria for designing the absorber for the system as discussed in chapter 5.

Finally results have been verified based on the previous works in this area.

Chapter 4. Derivation of Excitation Force on Crankshaft due to Gas Pressure of in Engine Cylinder

4.1 Introduction

In chapter 3 we discussed the modeling of an engine with its crankshaft from the torsional vibration point of view. However, in reciprocating system the situation is more complex because the system is subjected to forced vibrations where the sources of excitation are due to crankshaft dynamical behavior and in-cylinder gas pressure variations. The part of excitation which is related to the dynamic inertia of the crankshaft itself based on its geometry has been discussed before in the previous chapter. However, the most important part of the excitation is actually because of firing in the cylinder as well as the firing order in a multi cylinder engine which will be discussed in this chapter.

4.2 In-Cylinder pressure curve of the case study

A typical in-cylinder pressure curve should normally be provided by the engine manufacturers based on the characteristics of their design experimentally. Based on standards this should be obtained by running the engine at 75% of the full load condition [11]. However the theory behind simulating the in-cylinder pressure curve and modeling can be discussed by using the theory of Fluid Mechanics along with some characteristics of the engines.

The in-cylinder pressure P is the superposition of the compression-expansion and combustion pressures. From the well-known polytrophic process of Eq. (4.1) the compression/expansion contribution can easily be estimated as:

$$PV^{\gamma} = constant \tag{4.1}$$

The volume V depends on mechanical geometry and crankshaft position. The constant γ is the polytrophic index of the fluid (a fuel/air mixture). Its value is typically between 1.3 and 1.4. However, modeling of combustion contribution is related to different factors. Therefore for more simplicity the phenomenological approach will be widely used which lead to different non-dimensional models. These models are based on predicting the *Rate of Heat Released* (RoHR) with predefined functions. One of the most famous functions is called Wiebe's function. As several stages of pre-mixture and mixing-controlled phases exist during the combustion process several Wiebe's functions are adding together to reproduce RoHR closely. Figure 4.1 shows typical RoHRs with the use of a single Wiebe's function. Four parameters are necessary for defining correct form of function [43]:

- The ignition delay
- The combustion duration
- The combustion efficiency
- And a Wiebe's function shape parameter (m_v)

The relationship between the in-cylinder pressure and heat is through the well known thermodynamic relation between heat Q, pressure P and volume V:

$$dQ = c_p \frac{P}{c_p - c_v} dV + c_v \frac{V}{c_p - c_v} dP \tag{4.2}$$

where c_p is heat capacity of the fluid at constant pressure and c_v is the heat capacity at constant volume.

These parameters will be set by curve-fitting the experimental measurements for in-cylinder pressure at 75% of the full load running condition.

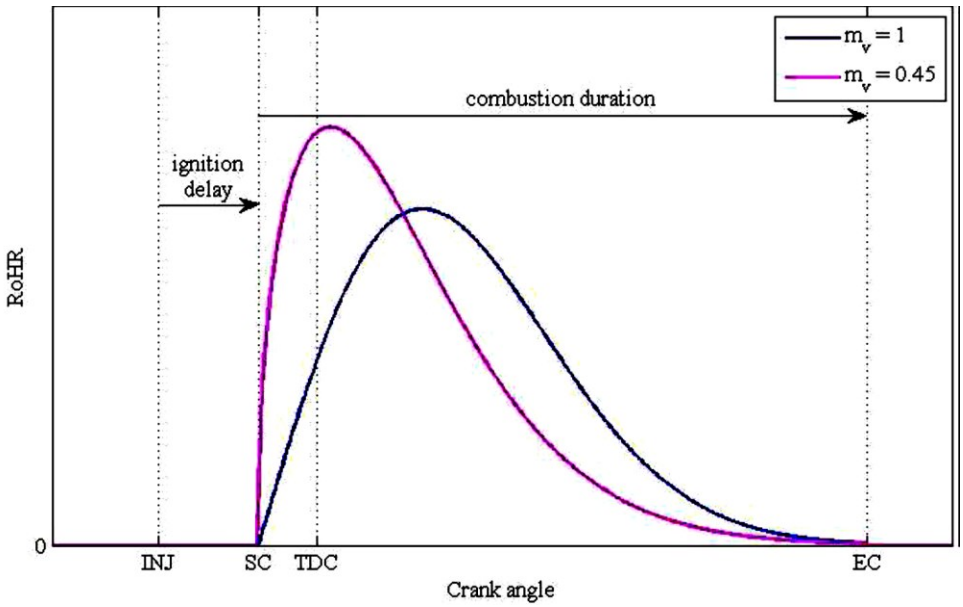

Figure 4.1: Rate of Heat Released (RoHR) modeling parameters during combustion with a Wiebe's function. INJ is injection timing, SC is start of combustion, TDC is Top Dead Center and EC is End of Combustion. [43]

The curve-fitting parameters for a diesel engine will lead to the Wiebe's function parameters as shown in Table 4.1:

Table 4.1: Wiebe's function parameters

Ignition delay (°)	19
Combustion duration (°)	115
Combustion efficiency	0.95
Wiebe's function shape parameter	0.45

Based on these parameters and equation (4.2) we can find analytically and experimentally the in-cylinder pressure curve in terms of the crank angle. For the case of a 4-stroke V-type diesel engine of a locomotive with 16 cylinders these curves are as shown in Figure 4.2.

It can be seen that the experimental and calculated results agree with each other closely.

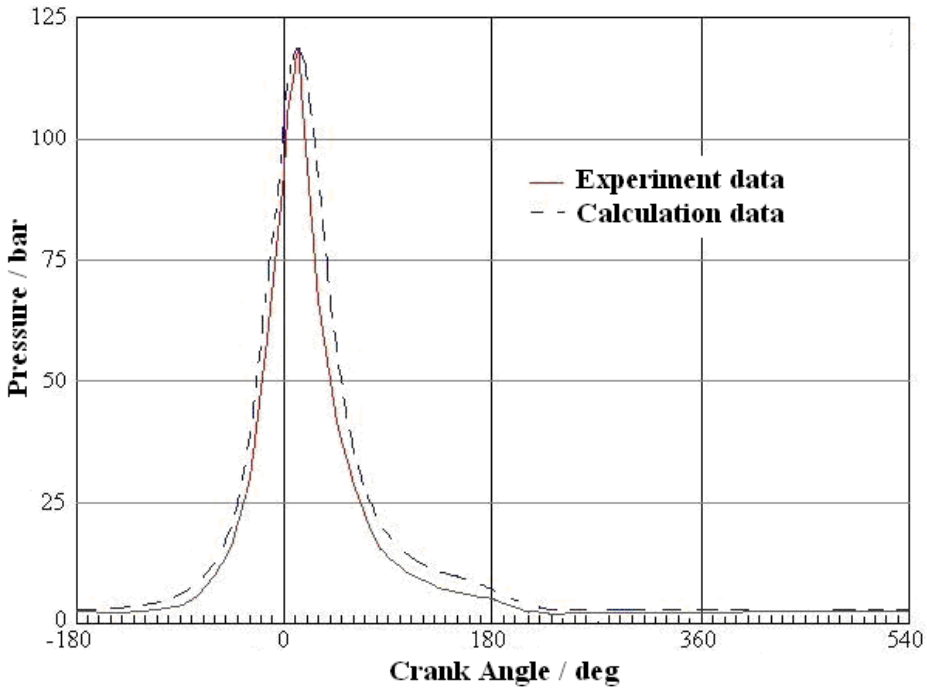

Figure 4.2: In-cylinder pressure change curve [93]

This curve will be repeated with a period of two-cycles (720°) in 4-stroke engines and it will be the basis for derivation of harmonic excitation force in the upcoming sections.

4.3 Extraction of equivalent harmonic curve of gas pressure using curve fitting

As we saw in the previous section the in-cylinder pressure curve for a diesel engine is a periodic function with the behavior in one period shown in Figure 4.2. However, for vibrational analysis of a crankshaft with this curve as its basic source of excitation, it is necessary to find this pressure curve in a harmonic format.

The Fourier series will be used to describe the harmonic components of a periodic function. Fourier series provides us with the summation of sinusoidal terms (in general like equation (4.3)) in a way that by good approximation will fit the original periodic shape. The rate of accuracy depends on how many terms are considered for each series (the value of j). However, normally the first few terms will give us sufficient accuracy.

$$f(x) = a_0 + \sum_{j=1}^{\infty} a_j \cos(j\omega t) + \sum_{j=1}^{\infty} c\sin(j\omega t) \tag{4.3}$$

The curve fitting tool in Matlab software will provide the facility for extracting the Fourier series representation of any curve which is given to the system as input.

The curve fitting has been done in Matlab for the in-cylinder pressure curve of Figure 4.2. The number of terms of Fourier series have been set as 8 and in Figure 4.3 the result can be seen where the output are the coefficients of the Fourier series (a_j and b_j) for the first eight terms.

The output curve is P(θ°) which gives the pressure in terms of the rotational angle in degree unit. To find the equation in time domain in radians, we should put x*w=(180/π)w*ωt, where ω is in (rad/s), t is time in (sec) and x and w are the curve

fitting constants. Finally, the Fourier series for a 4-stroke V-type diesel engine of a locomotive with 16 cylinders is as follows:

$$\begin{aligned} P(t) = {} & 16.06 + 24.47\cos(0.61\omega t) + 4.98\sin(0.61\omega t) + 18.9\cos(2*0.61\omega t) + \\ & 5.44\sin(2*0.61\omega t) + 15.36\cos(3*0.61\omega t) + 4.99\sin(3*0.61\omega t) + \\ & 11.81\cos(4*0.61\omega t) + 4.99\sin(4*0.61\omega t) + 8.78\cos(5*0.61\omega t) + \\ & 4.51\sin(5*0.61\omega t) + 6.66\cos(6*0.61\omega t) + 3.86\sin(6*0.61\omega t) + \\ & 4.67\cos(7*0.61\omega t) + 3.3\sin(7*0.61\omega t) + 3.21\cos(8*0.61\omega t) + \\ & 3.37\sin(8*0.61\omega t) \end{aligned} \tag{4.4}$$

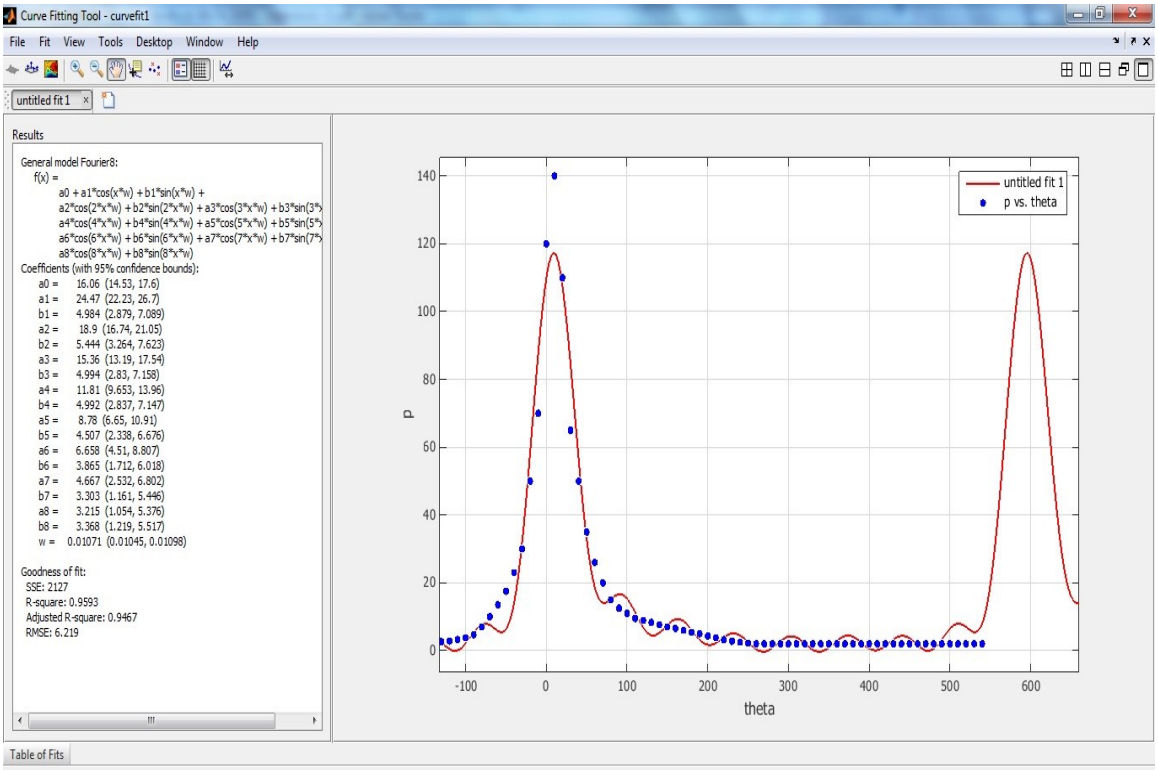

Figure 4.3: The Fourier series curve fitting result for in-cylinder pressure curve with Matlab

4.4 Derivation of final excitation torque due to reciprocating mechanism of case study engine

In the previous section the harmonic in-cylinder pressure curve due to combustion has been obtained. Using this curve, we can find the final excitation torque acting on crankshaft for torsional vibration analysis. A simplified expression of this torque has been presented in Harris Handbook of Vibration and shown in Eq. (4.5) [11]. The geometry characteristics of the crankshaft and in-cylinder pressure are the effective parameters in this equation.

$$T(t) = ARP(t)\left[\sin(\omega t) + \frac{\sin(2\omega t)}{2\lambda}\right] \tag{4.5}$$

where A, R and ω are piston section, crank radius and excitation frequency (rad/s), respectively. The constant λ is the ratio between connecting rod length and the crank radius. P(t) is also calculated in Eq. (4.4).

Considering the U25B-GE freight locomotive data from Appendix IV the geometrical parameters can be calculated as follows:

Piston section: $\mathrm{A} = \frac{\pi}{4}(\mathrm{d}^2) = \frac{\pi}{4}(0.229^2)\ \ m^2$

Crank radius: 0.203/2 = 0.1015 m

$$\lambda = \frac{l}{R} = \frac{0.6}{0.1015} = 5.911 \tag{4.6}$$

Considering the calculated data, excitation torque on the case study locomotive has been derived. Figure 4.4 shows the resulting excitation torque of Eq. (4.5) for the locomotive.

However, this excitation is related to the effect of combustion for just one piston-cylinder. The locomotive has a V-type engine with 16 cylinder coupling two by two to each other in left and right bank on 8 positions. The only difference for each cylinder excitation curve is that there is a phase difference between them. This difference depends on the firing cycle and order of the engine.

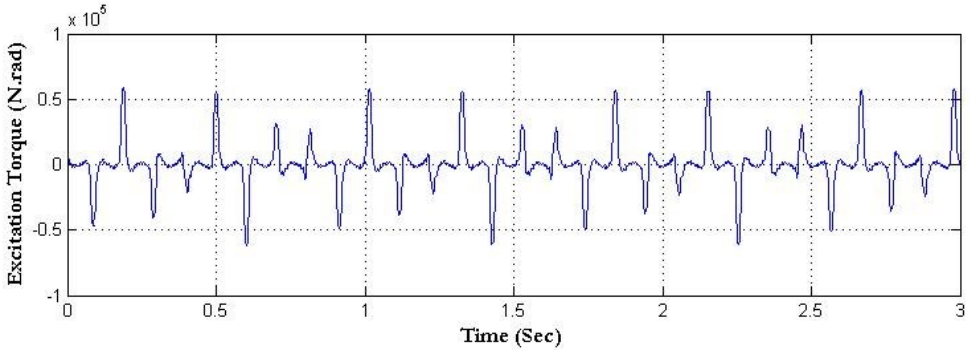

Figure 4.4: The derived excitation torque curve on crankshaft of the U25B-GE locomotive

As the sample locomotive has the 4-stroke engine, each cylinder fires once in every two rotations of the crankshaft and hence the range of firing cycle is 4π. It has 16 cylinders and hence the lag between the firing of each cylinder is $\pi/4$. On the other hand the firing order of locomotive based on the manual data is 1R-1L, 3R-3L, 7R-7L, 4R-4L, 8R-8L, 6R-6L, 2R-2L, 5R-5L. It means that first the cylinder on right bank of position 1 will fire and subsequently the left bank cylinder of the same position will fire with a $\pi/4$ lag, then the cylinders of position 3 will fire and so on. We should consider the phase lag of each cylinder and replace ωt in equation of T(t) and P(t) with $\omega t+lag$. Sample of the excitation torque of cylinders in position of 3 and 4 is shown in Figure 4.5.

All of these phase lags should be considered for each of the cylinders specifically during the modeling. This package of excitations will be considered in next chapter for obtaining the vibration response of the locomotive crankshaft under the excitation and effect of pendulum absorber. The complete equations of all cylinders and related Matlab coding and Simulink block diagrams are given in Appendix V.

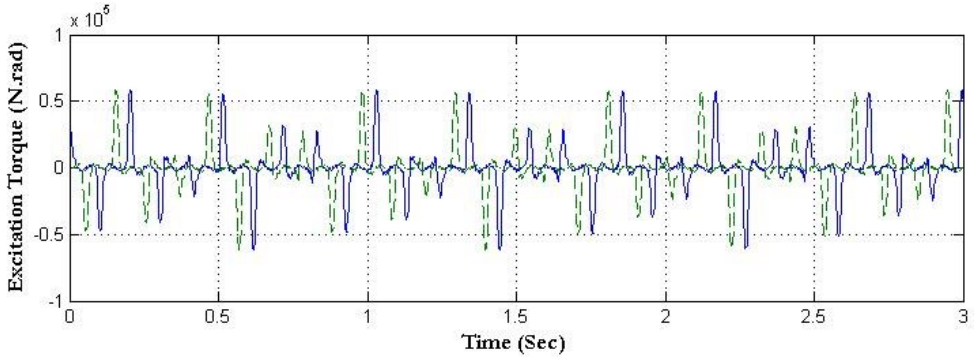

Figure 4.5: The lag in excitation torque curves on crankshaft applying by different cylinders for the U25B-GE locomotive

4.5 Conclusions

In this chapter we tried to simulate the combustion mechanism in reciprocating engine considering in-cylinder pressure in a harmonic way with Matlab/Simulink software. Using this harmonic excitation, we can analyse the torsional vibration behavior of the crankshaft. Considering the geometry data and characteristics of the U25B-GE freight locomotive engine the excitation torque has been derived in harmonic form using Fourier series.

It can be seen from the Figure 4.4 that the torque changes from negative to positive during the excitation cycle. It seems logical as during the firing cycle the expansion and compression apply the actuation or resistive torque on the crankshaft.

These excitation equations will be used in next chapter for forced vibration analysis of the case study locomotive.

Chapter 5. Torsional Vibration Reduction of Locomotive Crankshaft using Tuned CPVA

5.1 Introduction

In this chapter we investigate the capability of the centrifugal pendulum vibration absorber (CPVA) to attenuate the vibration in locomotive crankshaft based on its tuning factor discussed in chapter two. For this purpose, the torsional vibration model of the case study locomotive which has been developed in chapter three will be used. Finally as this locomotive is equipped with V-Type diesel engine, the excitation force applying on the crankshaft is similar to the excitation torque derived in Chapter four.

The vibration response of the crankshaft under derived excitation toque will be obtained in time and frequency domains and proper tuning strategy will be suggested for attenuation of the vibration in crankshaft.

5.2 Application of tuned CPVA on the complete case study engine set with excitation

In chapter three the mode shapes of vibration for the locomotive crankshaft at different natural frequencies have been obtained using the stiffness matrix of the torsional model.

For the U25B-GE freight locomotive which is equipped with diesel engine 7FDL16 the full running speed of the crankshaft is 1000 rpm (refer to Appendix IV), it can be seen that the third resonance frequency is 944 rpm. This contiguity of the resonance frequency and the running speed is crucial for the performance of the engine as it causes the increase of amplitude of vibration at the running speed.

Designing an absorber for this critical speed will help to attenuate the amplitude of vibration.

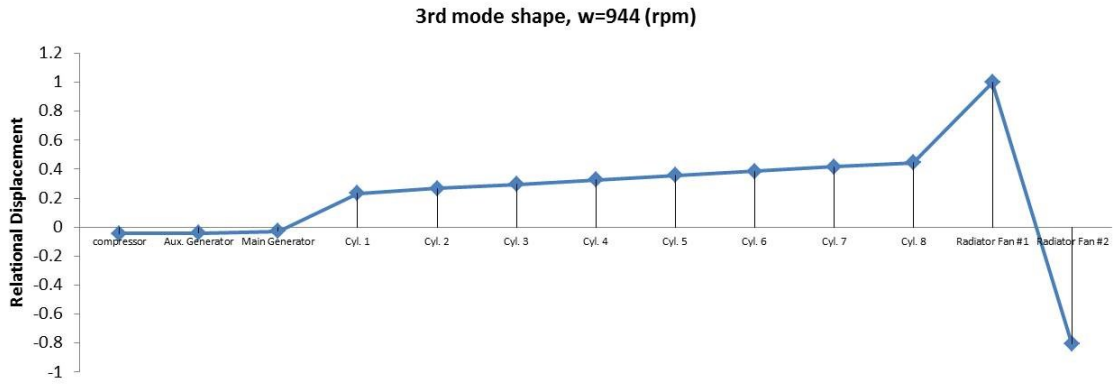

Figure 5.1: Normalized 3rd mode shape of the sample locomotive torsional model

The third normalized mode shape associated with natural frequency w=944 (rpm) is shown in Figure 5.1. As can be seen, the inertia disk J12 which represents the fan radiator #1 has the highest relational amplitude among others. Thus naturally, the best position to attach the CPVA is on the inertia disk #12 or on the crankshaft at the edge of this disk connected to the shaft.

Considering this design approach, the simplified torsional model of the crankshaft together with the CPVA is shown in Figure 5.2. In this figure, the disk inertias represent the different parts of locomotive engine coupled to the crankshaft for which the detailed calculations were done in chapter 3. The red arrows and the number on their top actually provide the firing order in all eight V-type cylinders in their position. According to sample locomotive manual (Appendix IV) the firing order is 1R-1L , 3R-3L , 7R-7L, 4L-4R , 8R-8L , 6R-6L , 2R-2L , 5R-5L, where L and R means the Cylinder of left and right bank, respectively, in each position. The dynamic model of the pendulum absorber is the

same as shown in chapter two, section 2.3, where the design parameters are the pendulum length (r) and pendulum mass (m).

This model will be the basis for deriving the governing equations of motion and tuning of absorber in subsequent sections.

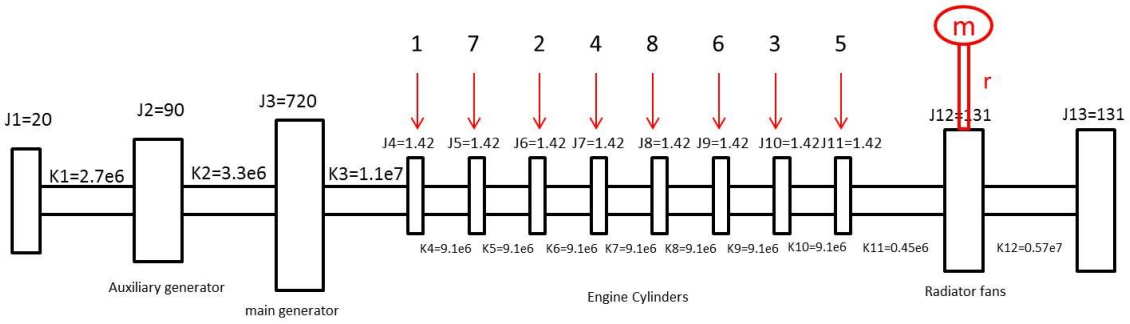

Figure 5.2: The torsional modeling of U25B-GE locomotive crankshaft with application of CPVA

5.3 Derivation of equations of motion using Lagrange's equations

The crankshaft torsional vibration modeling of the locomotive together with targeted position CPVA has been derived in previous section. Now, using this model we can find the equations of motion from Lagrange's equation. The first step is to find the kinetic energy and potential energy of the system. Unlike the single degree of freedom model discussed in Chapter two, here we have multi degrees of freedom system. Therefore, in addition to the terms of the pendulum absorber and the disk on which it has been connected (J12), the kinetic and potential energy of other inertia disks and shafts should be included. Considering this, the kinetic energies (T) and potential energy (U) of the model shown in Figure 5.2 can be described as:

$$T = \frac{1}{2} J_1 \dot{\theta}_1{}^2 + \frac{1}{2} J_2 \dot{\theta}_2{}^2 + \frac{1}{2} J_3 \dot{\theta}_3{}^2 + \frac{1}{2} J_4 \dot{\theta}_4{}^2 + \frac{1}{2} J_5 \dot{\theta}_5{}^2 + \frac{1}{2} J_6 \dot{\theta}_6{}^2$$
$$+ \frac{1}{2} J_7 \dot{\theta}_7{}^2 + \frac{1}{2} J_8 \dot{\theta}_8{}^2 + \frac{1}{2} J_9 \dot{\theta}_9{}^2 + \frac{1}{2} J_{10} \dot{\theta}_{10}{}^2 + \frac{1}{2} J_{11} \dot{\theta}_{11}{}^2 + \frac{1}{2} J_{12} \dot{\theta}_{12}{}^2$$
$$+ \frac{1}{2} m[R^2 \dot{\theta}_{12}{}^2 + r^2 (\dot{\varphi} + \dot{\theta}_{12})^2 + 2Rr \left(\dot{\theta}_{12}{}^2 + \dot{\varphi}\dot{\theta}_{12}\right) \cos\varphi] +$$
$$+ \frac{1}{2} J_{13} \dot{\theta}_{13}{}^2$$

$$where: \ \theta_i = \Omega t + \psi_i \tag{5.1}$$

$$U = \frac{1}{2} K_1 (\psi_1 - \psi_2)^2 + \frac{1}{2} K_2 (\psi_2 - \psi_3)^2 + \frac{1}{2} K_3 (\psi_3 - \psi_4)^2$$
$$+ \frac{1}{2} K_4 (\psi_4 - \psi_5)^2 + \frac{1}{2} K_5 (\psi_5 - \psi_6)^2 + \frac{1}{2} K_6 (\psi_6 - \psi_7)^2$$
$$+ \frac{1}{2} K_7 (\psi_7 - \psi_8)^2 + \frac{1}{2} K_8 (\psi_8 - \psi_9)^2 + \frac{1}{2} K_9 (\psi_9 - \psi_{10})^2$$
$$+ \frac{1}{2} K_{10} (\psi_{10} - \psi_{11})^2 + \frac{1}{2} K_{11} (\psi_{11} - \psi_{12})^2 + \frac{1}{2} K_{12} (\psi_{12} - \psi_{13})^2$$

In Eq. (5.1), ψ_i is the vibratory part of rotating disk number i, φ is the vibration of pendulum and Ω in the rotational speed of the shaft , m, r and R are pendulum mass, pendulum length and radius of disk #12 or the radius of the position where the pendulum is connected.

Using Lagrange's equation, the equations of motion for each disk will be derived as below:

$$
\begin{aligned}
&J_1\ddot{\psi}_1 + K_1\psi_1 - K_1\psi_2 = 0\\
&J_2\ddot{\psi}_2 - K_1\psi_1 + (K_1{+}K_2)\psi_2 - K_2\psi_3 = 0\\
&J_3\ddot{\psi}_3 - K_2\psi_2 + (K_2{+}K_3)\psi_3 - K_3\psi_4 = 0\\
&J_4\ddot{\psi}_4 - K_3\psi_3 + (K_3{+}K_4)\psi_4 - K_4\psi_5 = T_1(t)\\
&J_5\ddot{\psi}_5 - K_4\psi_4 + (K_4{+}K_5)\psi_5 - K_5\psi_6 = T_7(t)\\
&J_6\ddot{\psi}_6 - K_5\psi_5 + (K_5{+}K_6)\psi_6 - K_6\psi_7 = T_2(t)\\
&J_7\ddot{\psi}_7 - K_6\psi_6 + (K_6{+}K_7)\psi_7 - K_7\psi_8 = T_4(t)\\
&J_8\ddot{\psi}_8 - K_7\psi_7 + (K_7{+}K_8)\psi_8 - K_8\psi_9 = T_8(t)\\
&J_9\ddot{\psi}_9 - K_8\psi_8 + (K_8{+}K_9)\psi_9 - K_9\psi_{10} = T_6(t)\\
&J_{10}\ddot{\psi}_{10} - K_9\psi_9 + (K_9{+}K_{10})\psi_9 - K_{10}\psi_{11} = T_3(t)\\
&J_{11}\ddot{\psi}_{11} - K_{10}\psi_{10} + (K_{10}{+}K_{11})\psi_{10} - K_{11}\psi_{12} = T_5(t)\\
&(J_{12} + mR^2 + mr^2 + 2mRr\cos\varphi)\ddot{\psi}_{12} + (mr^2 + mRr\cos\varphi)\ddot{\varphi}\\
&\quad -2mRr\dot{\varphi}\sin\varphi\left(\Omega + \dot{\psi}_{12}\right) - mRr\dot{\varphi}^2\sin\varphi + (K_{11}{+}K_{12})\psi_{12}\\
&\quad -K_{11}\psi_{11} - K_{12}\psi_{13} = 0\\
&J_{13}\ddot{\psi}_{13} + K_{12}\psi_{12} - K_{12}\psi_{13} = 0\\
&r\ddot{\varphi} + (r + R\cos\varphi)\ddot{\psi} + R\sin\varphi\,(\Omega + \dot{\psi})^2 = 0 \qquad \text{(equation of motion for pendulum)}
\end{aligned}
\tag{5.2}
$$

Each of the equation in Eq. (5.2) is the governing equation of motion for every inertia disk J_i for i=1 to 13 and the last equation relates to the centrifugal pendulum absorber. $T_i(t)$s' are the excitation torque which is applied at the position where 8 cylinders of the engine exist. And their number shows their order of firing. These excitation torques can

be calculated from the Eq. (4.5) considering their phase lag based on firing order where the P(t) has been calculated in Eq. (4.4) for the case study locomotive.[1]

5.4 Response of the complete system with/without CPVA using Matlab/Simulink modeling

The equations of motion have been derived in the previous section. Using these equations of motion, the application of tuned CPVA can be studied, and the amount of attenuation in vibration amplitude under the simulated torque excitation can be discussed.

For extracting the time domain response, the modeling with Matlab\Simulink software has been done, and the block diagram and coding are given in Appendix VI.

The result for the case without CPVA at the critical speed of Ω=944 (rpm), is shown in Figure 5.3. It can be seen that the system experiences resonance and the amplitude of vibration violently increases during operation.

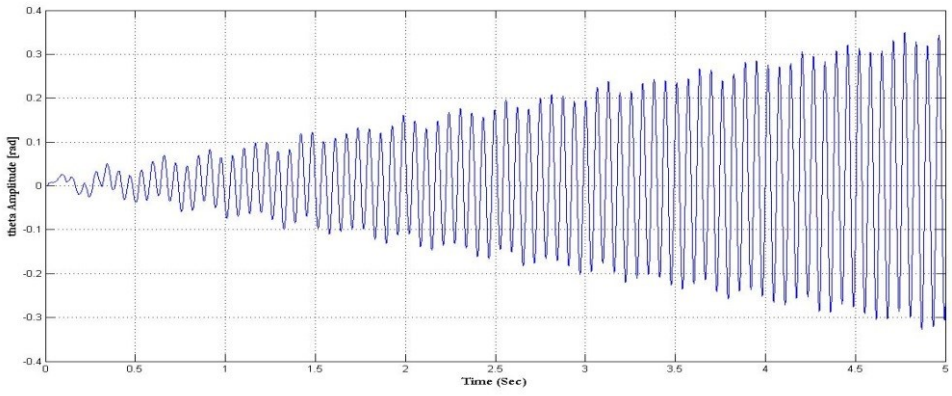

Figure 5.3: Time domain response of disk #12 in U25B-GE locomotive torsional system without CPVA excited on its natural frequency where Ω=944 (rpm).

[1] To be sure that the calculation and driving the equations of the motion have been done correctly, the Matlab parametric codes of Lagrange's equation have been written. Giving the kinetic energy and potential energy of any mechanism as input, the final equation of motions as the output of the program are provided. The coding and the results exist in Appendix I-2.

This is obviously undesirable and forms the basis for using CPVA to control the vibration. As discussed in Chapter two, the tuning factor depends on the relationship between the rotational speed (Ω) of the crankshaft and the excitation frequency. In the case study locomotive, as we have the 4-stroke engine the rotational speed of the shaft (Ω) is twice the excitation frequency (ω) from the cylinders, because for each cylinder firing cycle the crankshaft rotates 720° or two cycles in a 4-stroke engine. So the equation (5.3) will give us the relationship between the position radius (R) and pendulum length (r) as follows:

$$\omega = \Omega\sqrt{\frac{R}{r}} \quad , \quad \Omega = 2\omega$$
$$r = 4R \tag{5.3}$$

It means that the length of the pendulum should be four times the radius of the position where it is connected. Because of the dimensional limitation for engine, the logical choice for the connection position is on the minimum possible radius, which means exactly at the point where the crankshaft touches the disk #12. Thus the radius of the position will be approximately equal to the radius of the crankshaft in the locomotive. Based on the locomotive manual in Appendix IV , radius of crankshaft (here *R*) is equal to 0.2 m and thus for tuning purposes the length of the pendulum should be 0.8 m in the modeling.

The pendulum mass (*m*) has been assumed to be 2.5 kg which is in the range of standard values for centrifugal pendulum absorber mass.

Considering the tuning factors and incorporating them in the model with the same excitation force, the result in the time domain is shown in Figure 5.4. It can be seen that the use of CPVA has significant effect on reducing the vibration amplitude of the critical disk.

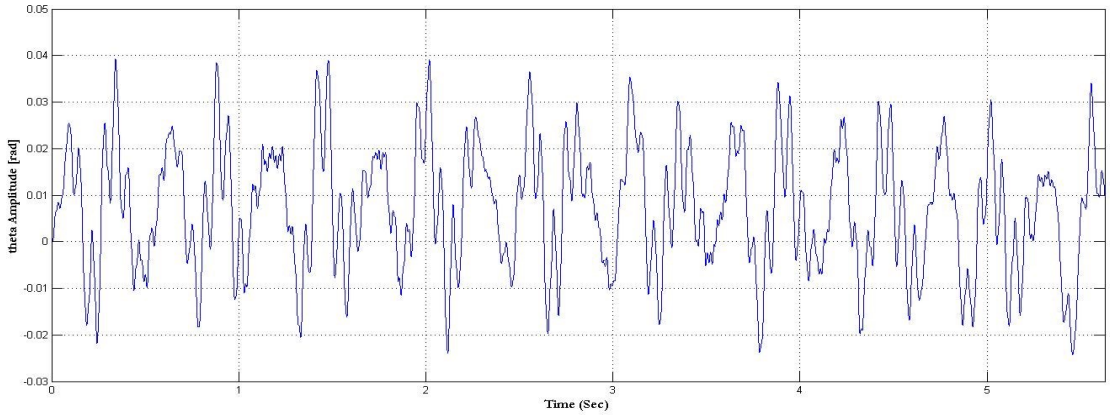

Figure 5.4: Time domain response of disk #12 in U25B-GE locomotive torsional model with CPVA tuned (r=4R) excited on its natural frequency.

As can realized from Figure 5.4, for the case with CPVA, the maximum amount of vibration amplitude is roughly 0.04 (rad) while as it can be seen from Figure 5.3, the amplitude reaches to the value of 0.35 (rad) just after the first 5 seconds without CPVA due to the resonance.

The importance of tuning can be observed when we investigate the un-tuned results. For example, Figure 5.6 shows the un-tuned results in which the length of pendulum (r) is considered to be three times R.

It can be seen that the amount of attenuation has been reduced to the maximum amplitude of about 0.1 (rad) and the CPVA is not as effective as in the tuned condition.

The result also shows that as the un-tuned absorber becomes ineffective, the beating phenomenon happens. When the forcing frequency is close to, but not exactly equal to the natural frequency of any system, a phenomenon known as beating may occur. The characteristic of a beating phenomenon is shown in Figure 5.5. The Eq. (5.4) shows the relationship between the forcing frequency (ω), natural frequency (ω_n) and beating frequency (ε).

$$\omega_n - \omega = 2\varepsilon \tag{5.4}$$

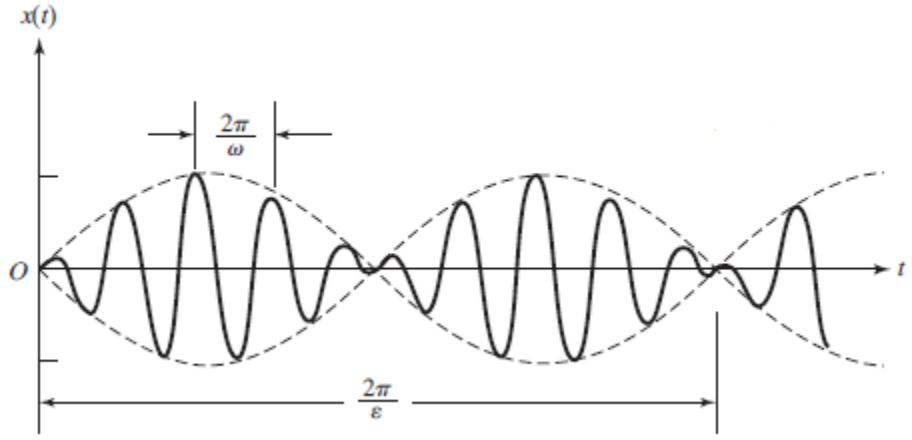

Figure 5.5: Phenomenon of beats [94]

In Figure 5.6, we can see that the beating period is approximately 9.4 seconds, therefore the beating frequency is 0.11 Hz, and forcing frequency is 944 RPM or 15.73 Hz. Hence, from the Eq. (5.4) the natural frequency would be 15.95 Hz or 957 RPM.

The reason for changing of the system natural frequency is due to the mass of the absorber added to the system which slightly increases its value. Basically if we excite the

system at 944 RPM, as it is very close to natural frequency (957 RPM), the beating can occur.

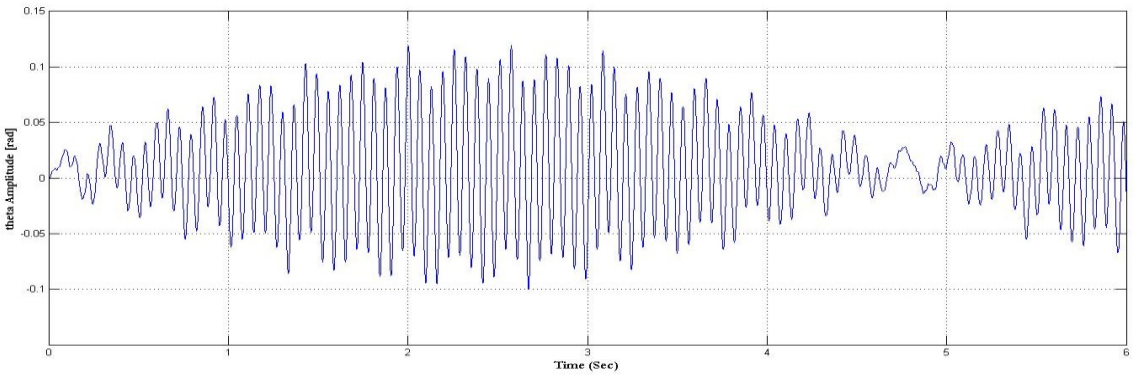

Figure 5.6: Time domain response of disk #12 in U25B-GE locomotive torsional model with CPVA un-tuned (r=3R) excited on its natural frequency.

The response behavior is the same when the length of pendulum (r) is considered to be more than the proposed tuned length. For example the result for the case of r=5R is shown in Figure 5.7.

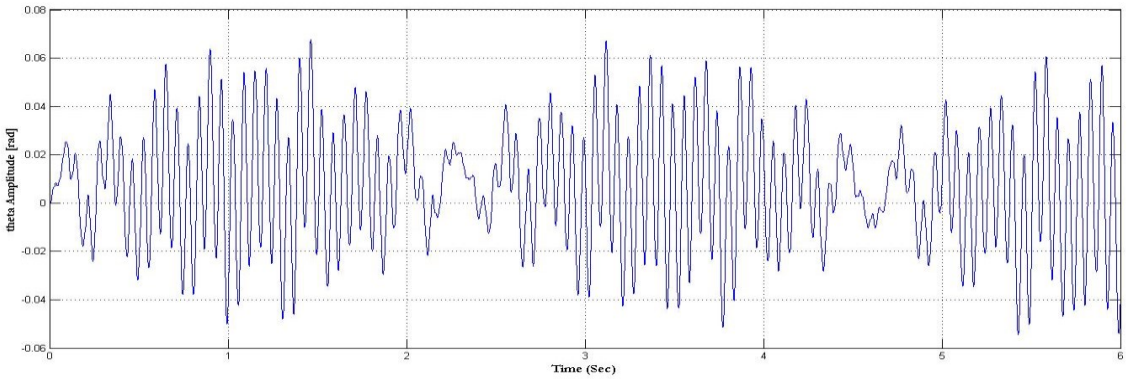

Figure 5.7: Time domain response of disk #12 in U25B-GE locomotive torsional model with CPVA un-tuned (r=5R) excited on its natural frequency.

It can be seen from this figure that the amount of maximum vibration amplitude for disk number 12 will be in the range of maximum 0.07 (rad) and again the reduction in vibration amplitude is not as much as under the tuned condition.

Similar to Figure 5.6, the beating phenomenon happens, and while the beating period is about 4.6 seconds the beating frequency is 0.22 Hz. Hence, the natural frequency would be 16.17 Hz or 970 RPM.

The effective mass of absorber is the reason for shifting the natural frequency. As the forcing frequency (944 RPM) is close to the natural frequency (970 RPM) the beating phenomenon occurs. However, these two values are farther from each other in comparison to the previous arrangement. The beating amplitude of vibration decreases significantly.

5.5 Frequency response of the system with/without tuned CPVA

To better realize the effect of CPVA, the response of the system with and without CPVA has been transferred into the frequency domain.

The approach is similar to that in Chapter two for simple two DOFs system in which Fast Fourier Transform (FFT) has been applied to the time-domain response in Matlab environment. By giving the time domain response of the system as input to this program (coding exist in Appendix III), the output is the frequency spectrum of the locomotive crankshaft system.

To see clearly the resonance frequencies which are our concern, the free vibration response of the system has been given as input by applying an initial displacement of 0.1 to one of the inertia disks.

Figure 5.8 shows the frequency spectrum response of the model without CPVA.

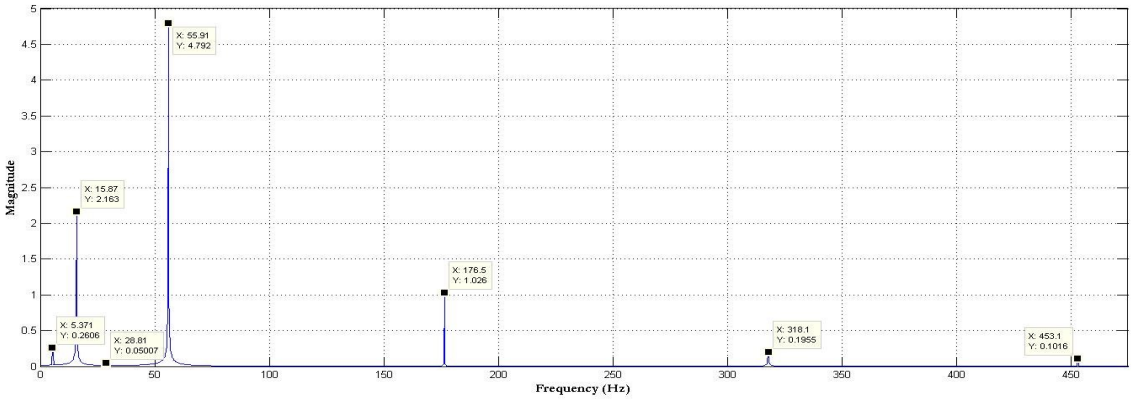

Figure 5.8: Frequency response of U25B-GE locomotive crankshaft modeling, without CPVA

As the model is the 13 DOFs system, normally it should have 13 resonance frequencies, and some of them can be seen in this figure. However, the resonance or natural frequencies which are in the range of the operating engine speed (less than 16 Hz) are our concern.

The Figure 5.9 shows the zooming in the more applicable region of frequencies where we have the resonance frequencies of 5.37 Hz and 15.87 Hz.

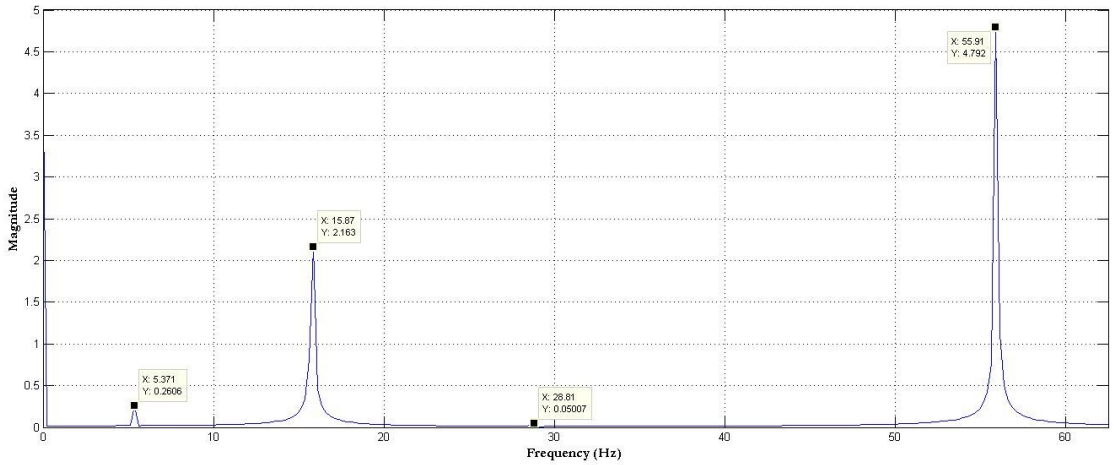

Figure 5.9: The applicable area for Frequency Response of U25B-GE locomotive crankshaft modeling, without CPVA

Considering the existing resonance frequencies, the targeted resonance frequency is close to the running frequency of our model. Therefore, $\omega_{n2} = 15.87 \ \ Hz$ is the frequency where the CPVA is designed to attenuate the amplitude of vibration.

After applying the tuned CPVA with the length (r) equal to four times the position radius (R) as we have a 4-stroke engine and mass of 2.5 kg, the result of the frequency response is shown in Figure 5.10. The absorber normally splits the targeted resonance frequency into two new frequencies in such a way that it attenuates the magnitude of vibration at the specified frequency.

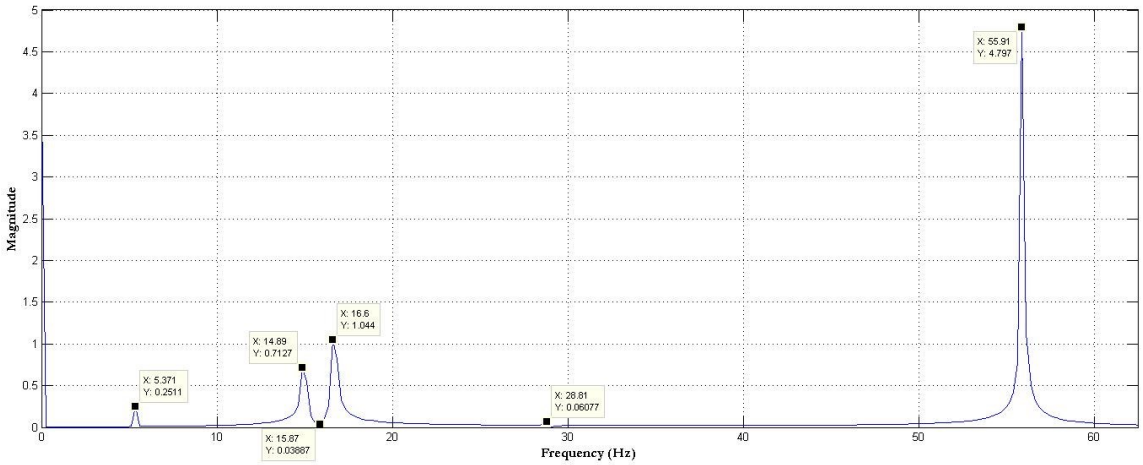

Figure 5.10: Frequency response U25B-GE locomotive crankshaft modeling, with CPVA, tuned (r=4R)

It can be seen that the targeted frequency (15.87 Hz) has been shifted to two new frequencies of 14.89 Hz and 16.6 Hz and magnitude of vibration has been dropped down from 2.163 to 0.039 at the targeted frequency and the magnitude at the new frequencies are 0.713 and 1.044. It should be noted that these values of magnitude will relate to the maximum amplitude of vibration in time domain response through dividing them by half of Numbers of the FFT points (NFFT) chosen in program. This value depends on the length of the signal on which FFT is applied on that. However, it clearly shows the relation between amplitudes in different frequencies.

The importance of tuning can be observed by putting un-tuned data as input to the program. This has been done for the value of r=3R and r=5R for which the results are shown in Figure 5.11 and Figure 5.12, respectively.

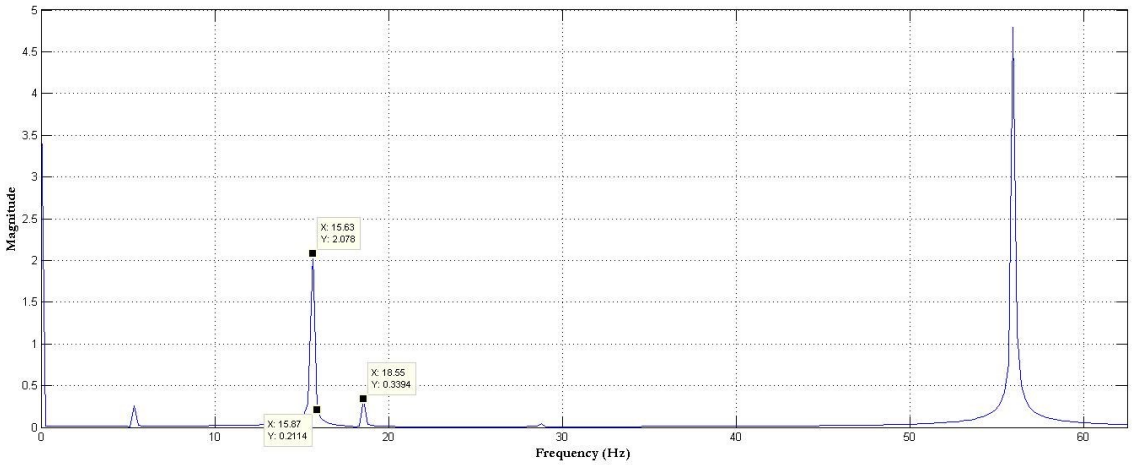

Figure 5.11: Frequency response U25B-GE locomotive crankshaft modeling, with CPVA, un-tuned (r=3R)

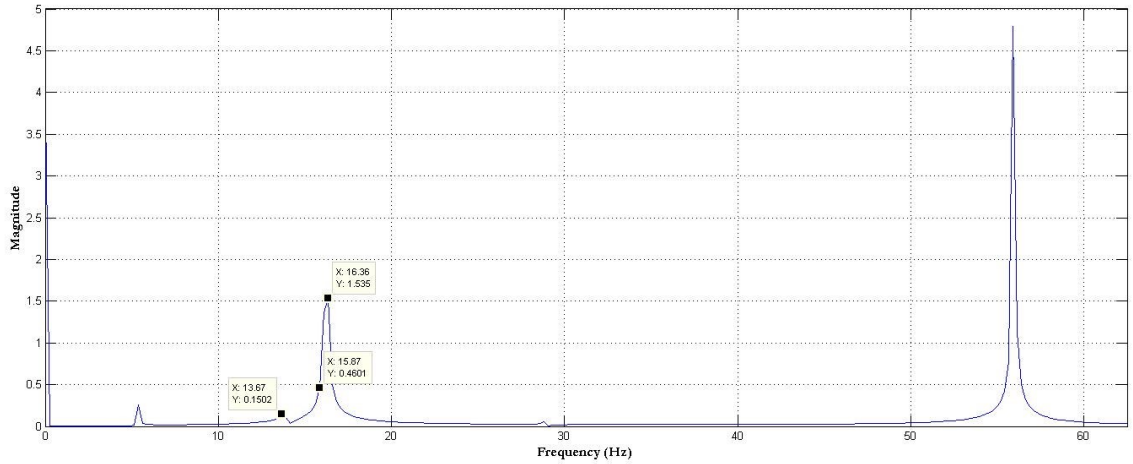

Figure 5.12: Frequency response U25B-GE locomotive crankshaft modeling, with CPVA, un-tuned (r=5R)

It can be seen that by putting pendulum length (r) less than tuned value ($3R$ instead of 4R), although the natural frequency has been shifted the magnitude value is 0.211 on the targeted frequency ($\omega_{n2} = 15.87$ Hz) and it is much higher than that of the tuned setting with magnitude of 0.039.

Also by keeping the pendulum length (r) more than the tuned value ($5R$ instead of $4R$), the magnitude on the targeted frequency ($\omega_{n2} = 15.87^{Hz}$) is 0.46 and is again much higher than that for the tuned condition.

The changes in the pendulum mass will lead to the results shown in Figure 5.13 and Figure 5.14, where former figure is the frequency response when the pendulum mass is set as 1 kg instead of 2.5 kg and the latter is for the mass of m equal 7.5 kg.

In the case of m equal to 1 kg it can be seen that the shifted frequencies became 15.38 Hz and 16.36 Hz. Whereas when the m is 2.5 kg the shifted frequencies were 14.89 Hz and 16.6 Hz.

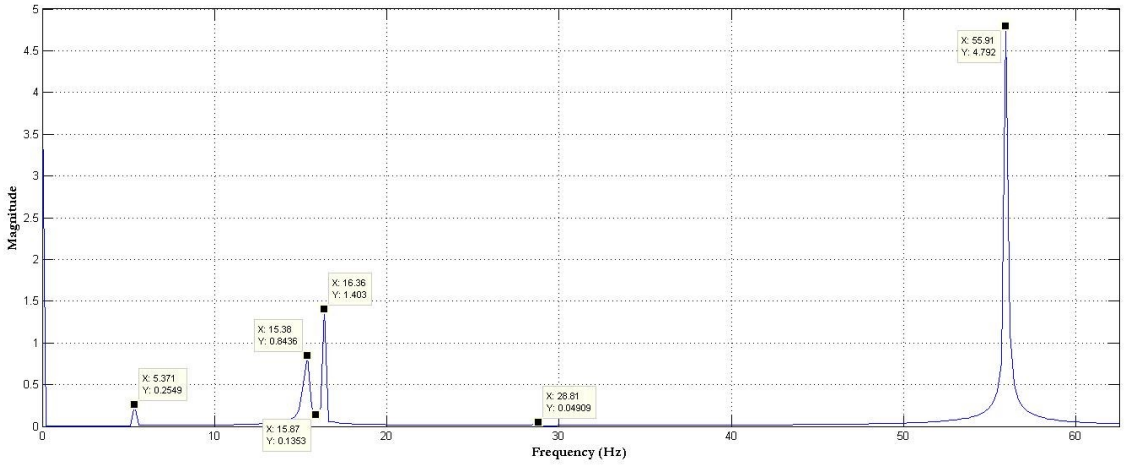

Figure 5.13: Frequency response U25B-GE locomotive crankshaft modeling, with CPVA, tuned (r=4R), m=1 (kg)

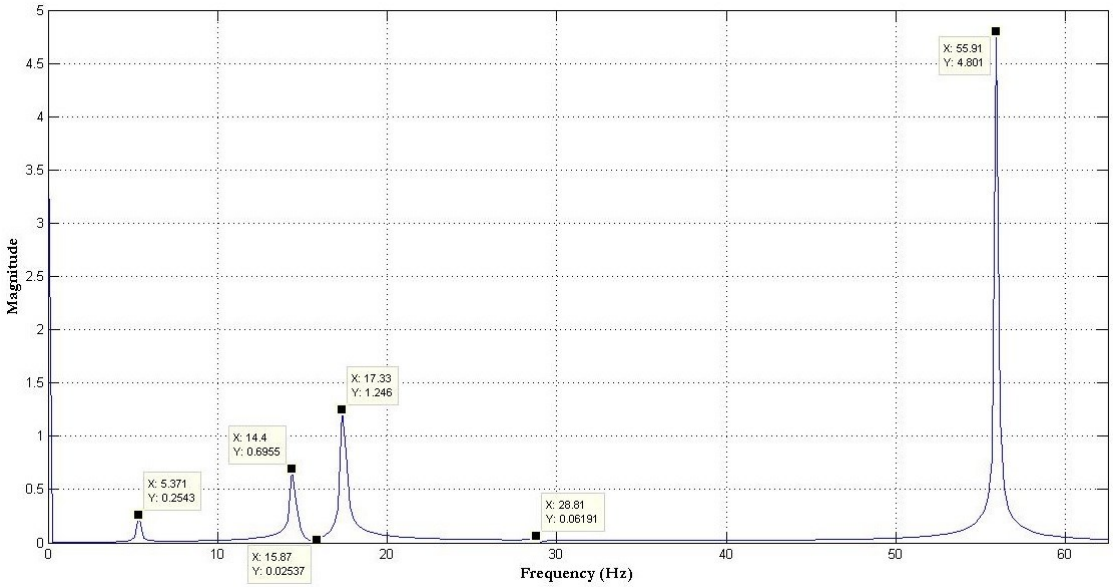

Figure 5.14: Frequency response U25B-GE locomotive crankshaft modeling, with CPVA, tuned (r=4R), m=7.5 (kg)

On the other hand, when the pendulum mass is set as 7.5 kg the split frequencies were at 14.4 Hz and 17.33 Hz. These values show that by increasing the value of the pendulum mass (m) the shifting amount for the two new frequencies will be increased and by decreasing the 'm' this split range also became smaller.

These results can be confirmed by considering the general characteristics of all absorbers which is mentioned in reference [94]. By attaching an auxiliary mass m_2 to a machine with mass m_1 and stiffness of K_1 through a spring with stiffness K_2, the resulting two-degrees of freedom system can be considered as general mass absorber system. This model is subjected to a simple harmonic excitation of $F_0 \sin \omega t$ as shown in Figure 5.15. The tuning for this simple system corresponds to the natural frequency of the main system equal to the natural frequency of the absorber and forcing frequency ω.

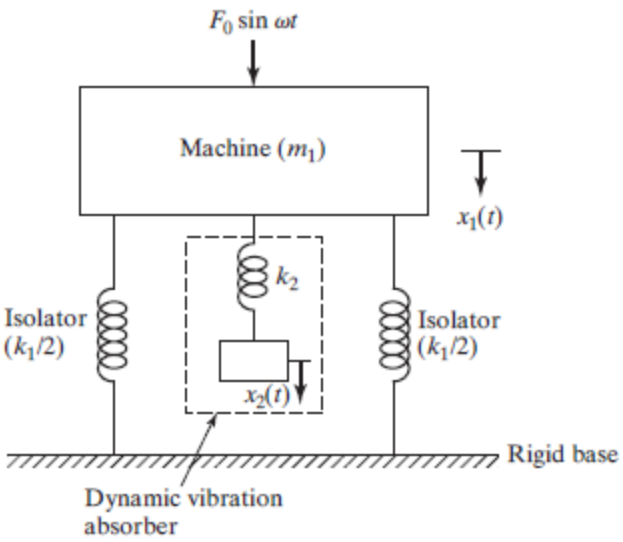

Figure 5.15: Un-damped dynamic vibration absorber [94]

Considering the tuning order, the two new shifted frequencies in the frequency response has been shown in Figure 5.16 as Ω_1 and Ω_2.

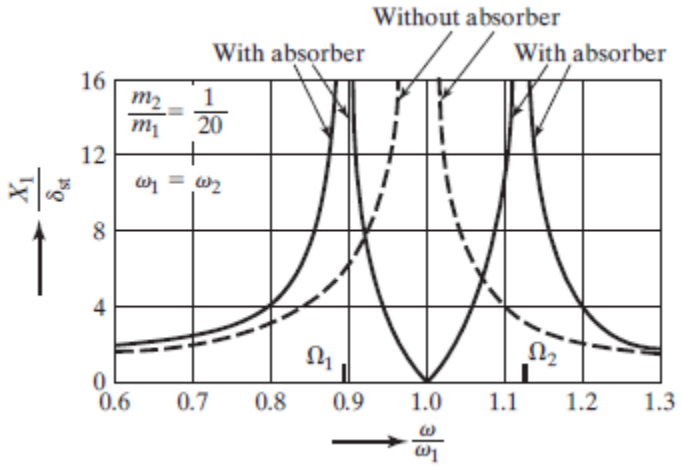

Figure 5.16: Effect of un-damped vibration absorber on the response of machine [94]

In this well-known reference after analytical calculation and finding the relationship between different parameters, the variation of Ω_1/ω_2 and Ω_2/ω_2 in proportional to the

ratio of m_2/m_1 in three different values of frequency ratio ω_2/ω_1 which has been shown in Figure 5.17. The solid line in this figure shows the tuned situation where natural frequencies of absorber (ω_2) and machine (ω_1) are the same.

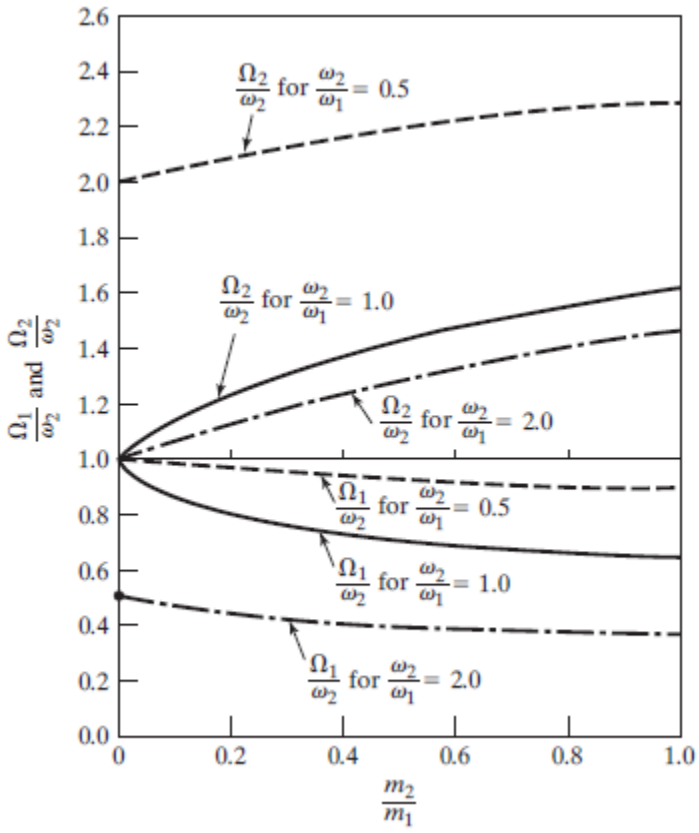

Figure 5.17: Variation of Ω_1 and Ω_2 with respect to the mass ratio m_2/m_1 [94]

It can be seen that the difference between Ω_1 and Ω_2 decreases as the mass ratio m_2/m_1 decreases and increases with increasing mass ratio. Normally, the main system mass (here machine mass m_1) remains constant. But one of the parameters for designing a suitable absorber is its mass.

Referring to the Figure 5.13 and Figure 5.14, this figure confirms our result for the centrifugal pendulum absorber, whereby increase of pendulum mass (m) has increased the difference between the shifted frequencies and vice versa.

5.6 Conclusions

In this chapter we investigated the use of centrifugal pendulum absorber for reducing the torsional vibration of a real V-type engine locomotive, which is excited by harmonic forcing function due to the fluctuating torque of reciprocating mechanism.

The targeted frequency was the resonance frequency which was close to the operating running speed of the locomotive. Based on the torsional analysis done in chapter three the critical inertia disk in the mode shape has been chosen for locating the CPVA. The positive damping effect of CPVA on tuned setting is observed. The application of tuned CPVA moderates the infinite resonance phenomenon in the model and limits the amplitude of vibration under 0.04 (rad) while under excitation without CPVA the amplitude oversteps this value just after 0.5 second of operation.

The importance of tuning has been observed by putting two un-tuned settings on the system. It is seen that by 25% under-tuning (decreasing the value of pendulum length 25%) the effectiveness of the CPVA decreases by 66%. On the other hand, by 25% over-tuning (increasing the value of pendulum length 25%), again effectiveness of the CPVA decreases by almost 43%. Also in both situations, we observed a beating phenomenon. Therefore, although the situation in over-tuning is better in comparison to the under-tuning, they are not as effective as the tuned setting.

The frequency responses show that the value of the splitting frequencies created as the result of CPVA application tuned at the resonance frequency can be set by changing the value of pendulum mass (m). The rule is similar to the ordinary linear absorbers. By increasing m, the split distance becomes larger and by decreasing m, the split distance becomes narrower.

Chapter 6. Contributions, Conclusions and Future recommendations

6.1 Major contributions

The present study comprises the following:

- Observing the effect of tuning and un-tuning setting for the CPVA in a 2-DOF modeling on suppression of vibration under resonance situation.
- Studying the importance of changing pendulum parameters, such as the length and mass based on their positive or adverse effect on suppression ability of the CPVA
- Developing an advanced torsional vibration modeling of crankshaft for a V-type diesel engine of a real locomotive, considering the various coupling parts such as main and auxiliary generator, air compressor and radiator fans.
- Extracting a more accurate combustion excitation force equation (covering up to the 8^{th} order) for a real reciprocating diesel engine using the numerical curve fitting procedure for minimizing the error values.
- Study the possibility of using circular path CPVA for attenuating the torsional vibration in a crankshaft modeling of a real V-type engine of locomotive, which is excited by simulated harmonic fluctuating torque, and observing the effect of changing CPVA parameters on reducing the vibration response.

6.2 Major conclusions

The major conclusions drawn from this thesis study can be summarized as below:

- Considering the effect of different values for CPVA parameters in tuned and un-tuned setting, it can be concluded that the weakest performance happens when the pendulum length is less than tuned value. The weaker performance happened in setting pendulum length larger than the tuned value and the optimum performance can be reached exactly by putting the pendulum length equal to the tuned value.
- In torsional vibration modeling of a locomotive crankshaft, the largest inertia would be that of the main generator which actually provides electric energy to the traction motors, and other ranks in order would be related to radiator fans, auxiliary generator and air compressor, respectively.
- It is observed that normally in most of the locomotive diesel engines where their speed of rotation is limited to 2000 rpm or lower, the first three or four natural frequencies is in the range of operation and the concerns should be focused more on them not to be too close to the speed of operation of the engine.
- After deriving the excitation curve from the reciprocating mechanism in a real diesel engine of a locomotive with the accuracy of up to 8^{th} order, it can be seen that for the order of more than 5 the amplitude of in-cylinder pressure are negligible in comparison to the first four orders.
- The suggestion of putting circular tuned CPVA on the position of critical inertia disk of the locomotive crankshaft torsional model in the targeted mode shape will decrease significantly the amplitude of vibration.

- In comparison to the tuned setting, the over-tuning (increase of pendulum length form the tuned length) is weaker in reducing vibration and the weakest performance happens in the under-tuning (decrease of pendulum length form the tuned length) setting for M-DOF torsional model.
- The change of mass of CPVA does not affect the attenuation of vibration significantly. It will just change the splitting value in the natural frequencies response. Therefore the nonlinear CPVA behavior from the prospect of absorber mass is same as ordinary linear absorber. And by changing the pendulum mass we can set the value of the two new created natural frequencies based on our requirements.

6.3 Suggested future works

Some Additional studies can be done to extend the present analysis further as listed in the following:

1. The analytical results could be validate through experimental tests.
2. Studying the attenuation with cycloid and epicycloid paths for CPVA application, on the M-DOF torsional system such as diesel engines and a parametric study of CPVA performance.
3. Developing a semi-active control scheme using a MR damper along with CPVA to form a Hybrid damper in order to enhance the damping action under unpredictable excitation conditions.

4. Taking into account the weight of the crankshaft main journal and working on modeling of whirling and bending vibration of V-type diesel engine crankshaft of locomotive.
5. Investigating the possible unbalance phenomenon and causes in locomotive engines based on the response of rotors.
6. Considering more parts of locomotive power transmission mechanisms and coupled instruments which were neglected in this project due to their less important role. For example, considering locomotive governor, air pumps etc. in the modeling of the crankshaft.
7. After careful analysis of the crankshaft model and ensuring the accuracy of derived results, the vibration response could be automatically minimized using a control scheme
8. Studying the stability or instability effect, advantages and disadvantages of using multiple CPVAs for attenuating the vibration in a range of speeds and excitation orders.

References

[1] A. Preumont, Vibration control of active structures: An introduction, Kluwer Academic Publishers, 1997.

[2] S. J. Dyke, B. F. Spencer, M. K. Sain, and J. D. Carlson, "Modeling and control of magnetorheological dampers for seismic response reduction,"*Smart Materials and Structures,* vol. 5, p. 565–575, 1996.

[3] Kim, S. B. Choi, W. K., "Vibration control of a semi-active suspension featuring electrorheological fluid dampers," *Journal of Sound and Vibration,* vol. 234, p. 537–546, 2000.

[4] B. C. Nakra, "Vibration control in machines and structures using viscoelastic damping," *Journal of Sound and Vibration,* vol. 211, p. 449–465, 1998.

[5] H. Frahm, "A device for damping vibrations of bodies". US Patent Patent 989958, 1911.

[6] J. P. D. Hartog, Mechanical vibrations. (4th edition), Dover books on engineering, 1985.

[7] W. T. Thomson, Theory of vibration with applications (4th edition), New Jersy: CRC press, 1996.

[8] G. Genta, Vibration dynamics and control, Springer US, 2009.

[9] J. R. C. Brenner, "A practical treatise on engine crankshaft torsional vibration control," in *Society of Automotive Engineers Inc. (West Coast Int'l Meeting)*, Portland, Oregon, 1979.

[10] L. R. C. Lily, Diesel engine reference book, London: Butterworth & Co. publishers Ltd, 1984.

[11] Piersol, Allen G.; Paez, Thomas L., "Torsional vibration in reciprocating and rotating machinery," in *Harris' Shock and vibration Handbook (Sixth Edition)*, Mc Graw Hill, p. 37-12, 2010.

[12] Troy Feese P.E., Charles Hill, "Guidelines for preventing torsional vibration problems in reciprocating machinery," in *Gas Machinery Conference*, San Antonio, Texas, 2002.

[13] S. Industries, "Torsional vibration dampers, Simpson int'l (uk) ltd.," [Online]. Available: http://www.simpindeu.com/aspects/. [Accessed Jan 12, 2001].

[14] "Engineering service bulletin #272," Superior Ltd., May 1997.

[15] Das A.S., Dutt J.K., Ray K., "Active control of coupled flexural torsional vibration in a flexible rotor bearing system using electromagnetic actuator, "*International Journal of NonLinear Mechanics,* vol. 46, no. 9, pp. 1093-1109, 2011.

[16] Stoykov S., Ribeiro P., "Nonlinear free vibrations of beams in space due to internal resonance," *Journal of Sound and Vibration,* vol. 330, no. 19, pp. 574-595, 2011.

[17] Patel T. H., Zuo M. J., Darpe A. K., "Vibration response of coupled rotor systems with crack and misalignment,"*Journal of Mechanical Engineering Science,* vol. 225, no. 3, p. 700–713, 2011.

[18] W. Wilson, Practical solutions of torsinal vibration problems (1), New York: John Wiley & Sons Inc., 1956.

[19] J.S.Rao, Rotor dynamics, , Third Edition, chapter 3, New Age International, 1996.

[20] E. J. Nestorides, A Handbook on torsional vibration (Reissue edition), Cambridge University Press, Aug 11, 2011.

[21] J. Maurice L. Adams, Rotating machinery vibration from analysis to troubleshooting, New York: Marcel Dekker, Inc., 2001.

[22] C. Xykis, S. Seidlitz, "Torsional analysis of a single cylinder gasoline engine," in *Society of Automotive Engineers Technical Paper Series, International Off-Highway and Powerplant Congress and Exposition*, Milwaukee, USA, 1990.

[23] K. Shimoyamada, S. Iwamoto, T. Kodama, Y. Honda, K. Wakabayashi, "A numerical simulation method for vibration waveforms of high-speed diesel engine crankshaft system," *Society of Automotive Engineers Transactions,* vol. 100, no. 3, pp. 933-953, 1991.

[24] A.A. Smaili, M.P. Khetawat, "Dynamic modeling of automotive engine crankshafts," *Mechanism and Machine Theory,* vol. 29, no. 7, pp. 995-1006, 1994.

[25] Y. Kang, G.J. Sheen, M.H. Tseng, S.H. Tu, H.W. Chiang, "Modal analyses and experiments for engine crankshafts," *Journal of Sound and vibration,* vol. 214, no. 3, pp. 413-430, 1998.

[26] J. Yang, L. Pu, Z. Wang, Y. Zhou and X. Yan, "Fault detection in a diesel engine by analysing," *Mechanical Systems and Signal Processing,* vol. 15, pp. 549-564, 2001.

[27] D. Taraza, N. Henein, W. Bryzik, "The frequency analysis of the crankshaft's speed variation: a reliable tool for the diesel engine diagnosis," *Journal of Engineering for Gas Turbines and power,* vol. 123, pp. 428-432, 2001.

[28] Wladislav Mitianiec, Konrad Buczek, "Torsional vibration analysis of crankshaft in heavy duty six cylinder inline engine," in *Automobiles and internal combustion engines congress*, Warsaw, 2008.

[29] P. Charles, L. Lidstone, F. Gu, and A.D. Ball, "Research into flywheel torsional speed variation for large diesel engine applications," in *In Proceedings of COMADEM*, Faro, Portugal, 2007.

[30] M. Desbazeille, R.B. Randall, F. Guillet, M. El Badaoui, C. Hoisnard, "Identification of the crankshaft torsional properties of a large diesel engine from a single point measurement of angular speed," in *3rd International Conference on Integrity, Reliability and Failure*, Porto, Portugal, 2009.

[31] Z.M. Bulatovic, M.S. Stavljanin, M.V. Tomic, D.M. Knezevic, S.Lj. Biocanin, "Measurement and analysis of angular velocity variations of twelve-cylinder diesel engine crankshaft," *Mechanical Systems and Signal Processing,* vol. 25, pp. 3043-3061, 2011.

[32] P. Charlesa, Jyoti K. Sinha, F. Gu, L. Lidstone, A.D. Ball, "Detecting the crankshaft torsional vibration of diesel engines for combustion related diagnosis," *Journal of Sound and Vibration,* vol. 321, pp. 1171-1185, 2009.

[33] Neda Nickmehr, Lars Eriksson, Jan Aslund, "Methodology for modeling, parameter estimation, and validation of powertrain torsional vibration," in *research environment for Control, Autonomy and Decision-making in Complex Systems*, Linkoping, Sweden, 2012.

[34] E. Brusa, C. Delprete, G. Genta, "Torsional vibration of crankshafts: effects of non-constant moments of inertia," *Journal of Sound and Vibration,* vol. 205, no. 2, pp. 135-150, 1997.

[35] Nguyen Van Khang, Nguyen Phong Dien, Hoang Manh Cuong, "Parametric torsional vibration of mechanical drive systems with non-uniform transmission mechanisms," *Technical Mechanic,* vol. 28, no. 3-4, pp. 310-323, 2008.

[36] H. Ying, Y. Shouping, Z. Fujun, Z. Changlu, L. Qiang, W. Haiyan, "Non-linear torsional vibration characteristics of an internal combustion engine crankshaft assembly," *Chinese Journal Of Mechanical Engineering,* vol. 25, 2012.

[37] S. Doughty, "Fundamental of IC engine torsional vibration," in *Energy-source technlogy confernece and exhibition*, New Orleans, Luisiana, 1988.

[38] R. G., "Estimate of indicated torque from crnakshaft speed fluctiations: a model for the dynamics of the IC engine," *IEEE transactions on vehicular technology,* vol. 38, no. 3, pp. 168-179, 1989.

[39] Jacob P.J, Gu F., "Non-parametric models in the monitoring of engine performance and condition Part I," *Journal of Automobile Engineering (Part D),* vol. 213, pp. 73-81, 1999.

[40] Cho H., Song H., Lee J. and Kauh S., "Simulation of a transient torque response for engine performance in a spark ignition engine," *Journal of Automobile Engineering (Part D),* vol. 215, pp. 127-140, 2001.

[41] Jeong T., Singh R., "Analytical method of decoupling the automotive engine torque roll axis," *Journal of sound and vibration,* vol. 234, no. 1, pp. 85-114, 2000.

[42] A. S. Mendes, P. S. Meirelles and D. E. Zampieri, "Analysis of torsional vibration in internal combustion engines: Modelling and experimental validation,"*Journal of Multi-body Dynamics,* vol. 222, no. 2, pp. 155-178, 2008.

[43] M. Desbazeille, R.B. Randall, F. Guillet, M. El Badaoui, C. Hoisnard, "Identification of the Crankshaft Torsional Properties of a Large Diesel Engine from a Single Point Measurment of Angular Speed," in *3rd International Conference on Integrity, Reliability and Failure*, Porto/Portugal, July 2009.

[44] R. Wang, "A study of vibration isolation of engine mount system,"Concordia University, Montreal, Quebec, Canada, 2005.

[45] E. S. Taylor, "Eliminating crack shaft vibration in radial aircraft engines," *Transactions of the Society of Aeronautical Engineers,* vol. 38, pp. 81-87, 1936.

[46] J.P.DenHartog, "Tuned pendulums as torsional vibration eliminators,"in *Stephen Timoshenko 60th Anniversary*, pp.17-26, 1938.

[47] D. E. Newland, "Nonlinear aspects of the performance of centrifugal pendulum vibration absorbers," *Journal Engineering for Industry, Transaction of the ASME,*

vol. 86, pp. 257-263, 1964.

[48] S.B. Bailey, C.H.Bulleid, "The dynamic absorber and its application to multi-throw crankshafts,," *Proceedings of the Institution of Mechanical Engineers,* vol. 145, no. 1, p. 73–82, 1941.

[49] Wei Li, Tieshi Gao, Yongkui Cui, Wanfu Guo and Wenku Shi, "Study and simulation of isolation performance of torsional vibration of dmf-cs with centrfugal pendulu-type absorber," in *Proceedings of the FISITA 2012 World Automotive Congress*, Berlin, 2013.

[50] H. Jose, "On the passive control of vibrations with viscoelastic dynamic absorbers of ordinary and pendulum types," *Journal of the Franklin Institute,* vol. 347, pp. 102-115, 2010.

[51] M. Sharif-Bakhitar, S. W. Shaw, "The dynamic response of a centrifugal pendulum vibration absorber with motion-limiting stops,," *Journal of Sound and Vibration,* vol. 126, pp. 221-235, 1988.

[52] Shaw, M. Sharif-Bakhtiar and S. W., "Effects of nonlinearities and damping on the dynamic response of a centrifugal pendulum vibration absorber," *Journal of Vibration and Acoustics, Transaction of the ASME,* vol. 114, pp. 305-311, 1992.

[53] D. L. Cronin, "Shake reduction in an automobile engine by means of crankshaft-mounted pendulums," *Mechanism and Machine Theory,* vol. 27, no. 5, pp. 517-533, 1992.

[54] M.A.Wachs, "The main rotor bifilar absorbe rand its effect on helicopter reliability/maintainability," in *SAE Technical Paper*, 1973.

[55] M. Hamouda, H.Nabil, G.A.Pierce, "Helicopter vibration suppression using simple pendulum absorbers on the rotor blade," *Journal of the American Helicopter Society,* vol. 29, no. 3, p. 19–29, 1984.

[56] Imao Magasaka, Yukio Ishida, Takayuki Koyoma, Naoki Fujimatsu, "Vibration suppression of a helicopter usinh pendulum absorbers: first elastic mode of a blade," *Journal of system design and dynamics,* vol. 4, no. 6, pp. 1148-1154, 2010.

[57] P. M. Swank, "Dynamic absorbers for modern powertrains,2011,1-1554," in *SAE Technical Paper*, 2011.

[58] Chengzhi Shi, Robert G.Parker, "Modal properties and stability of centrifugal

pendulum vibration absorber systems with equally spaced,identical absorbers," *Journal of Sound and Vibration,* vol. 331, pp. 4807-4824, 2012.

[59] Shang-Teh Wu, Yu-Rong Chen, Se-Si Wang, "Two-degree-of-freedom rotational-pendulum vibration absorbers," *Journal of Sound and Vibration,* vol. 330, pp. 1052-1064, 2011.

[60] J. Madden, "Constant frequency bifilar vibration absorber". US patent Patent 4218187, 1980.

[61] H. H. Denman, "Tautochronic Bifilar Pendulum Torsion Absorbers for Reciprocating Engines," *Journal of Sound and Vibration,* vol. 159, no. 2, p. 251–277, 1992.

[62] S. W. Shaw, P. M. Schmitz, and A. G. Haddow, "Dynamics of tautochronic pendulum vibration absorbers : Theory and experiment," *Journal of Computational and Nonlinear Dynamics,* vol. 1, pp. 283-293, 2006.

[63] A. Wedin, "Reduction of vibrations in engines using centrifugal pendulum vibration absorbers," Master's Thesis in the Master's programme Automotive Engineering, Chalmers University, 2011.

[64] C. P. Chao, C. T. Lee, S.W. Shaw, "Non-unison dynamics of multiple centrifugal pendulum vibration absorbers," *Journal of Sound and Vibration,* vol. 204, pp. 769-794, 1997.

[65] Shaw, A. S. Alsuwaiyan and S. W., "Performance and dynamic stability of general path centrifugal pendulum vibration absorbers," *Journal of Sound and Vibration,* vol. 252, pp. 791-815, 2002.

[66] T. M. Nester, A. G. Haddow, and S. W. Shaw, "Experimental investigation of a system with nearly identical centrifugal pendulum vibration absorbers," in *Proceedings of the ASME 19th Biennal Conference on Mechanical Vibration and Noise*, Chicago, Ilinois, 2003.

[67] Pierre, S. W. Shaw and C., "The dynamic response of tuned impact absorbers for rotating flexible structures," *Journal of Computational and Nonlinear Dynamics,* vol. 1, pp. 13-24, 2006.

[68] Y. Ishida, T. Inoue, T. Kagaw, M. Ueda, "Nonlinear analysis of a torsional vibration of a rotor with centrifugal pendulum vibration absorbers and its suppression," *Japan*

Society of Mechanical Engineers, vol. C71, pp. 2431-2438, 2005.

[69] Bram Demeulenaere, Pieter Spaepen, Joris De Schutter, "Input torque balancing using a cam-based centrifugal pendulum: design procedure and example," *Journal of Sound and Vibration,* vol. 283, pp. 1-20, 2005.

[70] J. Ehyaei, Majid M.Moghaddam, "Dynamic response and stability analysis of an unbalanced flexible rotating shaft equipped with n automatic ball-balancers," *Journal of Sound and Vibration,* vol. 321, pp. 554-571, 2009.

[71] Tyler M. Nester, Peter M. Schmitz, Alan G. Haddow, and Steven W. Shaw, "Experimental observations of centrifugal pendulum vibration absorbers," in *The 10th International Symposium on Transport Phenomena and Dynamics of Rotating Machinery*, Honolulu, Hawaii, 2004.

[72] Tyler M. Nester, Alan G. Haddow and Steven W. Shaw, John E. Brevick, Victor J. Borowski, "Vibration reduction in a variable displacement engine using pendulum absorbers," in *SAE International*, Michigan, 2003.

[73] Karsten Stahl, Hermann Pflaum, Georg Johann Meingabner, habil. Heinz Ulbrich, Johannes Mayer, "Planetary Centrifugal Pendulum Absorber (PCPA)-new type of centrifugal pendulum absorber for applications in highly downsized hybrid and range extender combustion engines," in *Conference on Future Automotive Technology*, Lienkamp, 2013.

[74] J. Mayet n, H.Ulbrich, "Tautochronic centrifugal pendulum vibration absorbers General design and analysis," *Journal of Sound and Vibration,* vol. 333, pp. 711-729, 2014.

[75] Chi-Hsiung Liang, Pi-cheng Tung, "The active vibration control of a centrifugal pendulum vibration absorber using a CK-propagation neural network," *International Journal of innovative computing information and control,* vol. 9, no. 4, pp. 1573-1592, 2013.

[76] D.E.Newland, "Nonlinear aspects of the performance of centrifugal pendulumn vibration absorbers.," *ASME Journal of Engineering for Industry,* pp. 257-263, 1964.

[77] J. Madden, "Constant frequency bifilar vibration absorber". United State Patent 4218187, 1980.

[78] V.J.Borowski, H.H Denman, D.L Cronin, S. Shaw, J.P Hanisko , L.T.Brooks,D.A Milulec, W.B. Crum, and M.P Anderson, "Reducing vibration of reciprocating

engines with crankshaft pendulum vibration absorbers.," in *SAE Technical Paper Series 911876*, The engineering Society for advanced Mobility Land, Sea, Air and Space, 1991.

[79] G. Genta, Vibration dynamics and control, New York: Springer, 2009.

[80] B. Balachandran, Magrab, Edward B., Vibrations, Toronto: Cengage Learning Publishment, 2009.

[81] Thomson, William T; Dahleh, Marie Dillon, Theory of vibration with applications (5th edition), Prentice-Hall, Inc., 1998.

[82] J. H. Armstrong, The railroad, what it is, what it does, Simmons Boardman Books Inc., 1993.

[83] Copyright railway technical web pages, 13 Feb 2014. [Online]. Available: http://www.railway-technical.com/about.shtml. [Accessed 24 March 2014].

[84] British railways diesel traction manual for enginemen, British Transport Commission, 1962.

[85] D. Gibbons, British rail equipment drawings from railnews 'stockspot', Ian Allan Ltd., 1986.

[86] D. Gibbons, British rail equipment: no. 2, drawings from railnews 'stockspot', London: Ian Allan Publishing, 1990.

[87] B. Solomon, The american diesel locomotive, Osceola, WI: MBI Publishing Company, 2000.

[88] C. F. Taylor, The internal combustion engine in theory and practice: vol. 2, MIT Press, 1985.

[89] N. I. Limited, Writer, Generator technical data sheet, model HCI1634G. [Performance]. Stamford Co., 2004.

[90] G. E. company, "GE-U25B freight locomotive service manual," Documents GEK-18151G, 1980.

[91] C. F. Taylor, "chapter 2," in The internal combustion engine in theory and practice: vol. 1, MIT Press, 1985.

[92] M. Desbazeille a, R.B.Randall, F.Guillet, M.ElBadaoui, C.Hoisnard, "Model-based diagnosis of large diesel engines based on angular speed variations of the crankshaft," *Mechanical Systems and Signal Processing,* vol. 24, p. 1529–1541, 2010.

[93] Minghai Li, Juan wang, Xiaowei Li, shukuan Mou, "Torsional vibration analysis of 16v240zj diesel engine based on virtual prototype technology," in *WASE International Conference on Information Engineering*, BeiDai, China, 2010.

[94] S. S. Rao, Mechanical vibrations (Fifth Edition), Pearson Education Inc., 2011.

Appendix I

Appendix I-1: (Matlab Coding for Calculation of Lagrange Equation)

(Centrifugal Pendulum absorber on Simple Rotating System)

```
clc
clear all
close all

syms theta1 theta2 theta3 thetap phip Dtheta1 Dtheta2 Dtheta3 Dthetap
Dphip DDtheta1 DDtheta2 DDtheta3 DDthetap DDphip Jp K1 r R m

% kinetic and potential energy for the two DOF Centrifugal Pendulum
Absorber model
% applying lagrange equation:

Vm2 =
(R*Dthetap)^2+(r*(Dthetap+Dphip))^2+2*r*R*(Dthetap^2+Dphip*Dthetap)*cos
(phip);
T = (0.5*Jp*Dthetap^2)+(0.5*m*Vm2);
U = 0.5*K1*(thetap^2);

DVar = [Dtheta1,Dthetap,Dphip,Dtheta2];
Var = [theta1,thetap,phip,theta2];
DDVar = [DDtheta1,DDthetap,DDphip,DDtheta2];
for i=1:1:4
Term1(1,i)= diff(T,DVar(1,i));
end
for i2 = 1:1:length(Var)
    for j=1:1:length(Var)
TermA1(i2,j) = diff(Term1(1,i2),Var(1,j))*DVar(1,j);
TermA2(i2,j) = diff(Term1(1,i2),DVar(1,j))*DDVar(1,j);
    end
TermA(1,i2) = sum(TermA1(i2,1:j))+sum(TermA2(i2,1:j));
end

for j=1:1:4
Term2(1,j)= diff(U,Var(1,j));
end

for k=1:1:4
Term3(1,k)= -diff(T,Var(1,k));
end

E1 = TermA(1,2)+Term2(1,2)+Term3(1,2)
E2 = TermA(1,3)+Term2(1,3)+Term3(1,3)
```

Results:

E1 =

K1*thetap+DDthetap*(Jp+(m*(2*R^2+4*cos(phip)*R*r+2*r^2))/2)+

(DDphip*m*(2*r^2+2*R*cos(phip)*r))/2-Dphip*R*m*r*sin(phip)*(Dphip+ 2*Dthetap)

E2 =

DDthetap*m*(2*r^2+2*R*cos(phip)*r))/2+DDphip*m*r^2+R*m*r*sin(phip)*(Dthetap^

2 + Dphip*Dthetap) - Dphip*Dthetap*R*m*r*sin(phip)

Appendix I-2: (Matlab Coding for Calculation of Lagrange Equation)

(CPVA on Multi Degrees of Freedom Torsional Modeling of U25B-GE Locomotive)

```
clc
clear all
close all

syms theta1 theta2 theta3 theta4 theta5 theta6 theta7 theta8 theta9
theta10 theta11 theta12 phi theta13 ...
     Dtheta1 Dtheta2 Dtheta3 Dtheta4 Dtheta5 Dtheta6 Dtheta7 Dtheta8
Dtheta9 Dtheta10 Dtheta11 Dtheta12 Dphi Dtheta13 ...
     DDtheta1 DDtheta2 DDtheta3 DDtheta4 DDtheta5 DDtheta6 DDtheta7
DDtheta8 DDtheta9 DDtheta10 DDtheta11 DDtheta12  DDtheta13 DDphi ...
     J1 J2 J3 J4 J5 J6 J7 J8 J9 J10 J11 J12 J13 K1 K2 K3 K4 K5 K6 K7 K8
K9 K10 K11 K12 r R m

% kinetic and potential energy for the multi DOF masses of the model
with CPVA (J1, J2, J3, J4, J5, J6, J7, J8, J9, J10, J11, J12, J13) for
% applying lagrange equation:

Vm2 =
(R*Dtheta12)^2+(r*(Dtheta12+Dphi))^2+2*r*R*(Dtheta12^2+Dphi*Dtheta12)*c
os(phi);

T =
(0.5*J1*Dtheta1^2)+(0.5*J2*Dtheta2^2)+(0.5*J3*Dtheta3^2)+(0.5*J4*Dtheta
4^2)+(0.5*J5*Dtheta5^2)+(0.5*J6*Dtheta6^2)+(0.5*J7*Dtheta7^2)+(0.5*J8*D
theta8^2)+(0.5*J9*Dtheta9^2)+(0.5*J10*Dtheta10^2)+(0.5*J11*Dtheta11^2)+
(0.5*J12*Dtheta12^2)+0.5*m*Vm2+(0.5*J13*Dtheta13^2);

U = 0.5*K1*(theta1-theta2)^2+0.5*K2*(theta2-theta3)^2+0.5*K3*(theta3-
theta4)^2+0.5*K4*(theta4-theta5)^2+0.5*K5*(theta5-theta6)^2+
0.5*K6*(theta6-theta7)^2+0.5*K7*(theta7-theta8)^2+
0.5*K8*(theta8-theta9)^2+0.5*K9*(theta9-theta10)^2+
0.5*K10*(theta10-theta11)^2+0.5*K11*(theta11-theta12)^2
+0.5*K12*(theta12-theta13)^2;

DVar =
[Dtheta1,Dtheta2,Dtheta3,Dtheta4,Dtheta5,Dtheta6,Dtheta7,Dtheta8,Dtheta
9,Dtheta10,Dtheta11,Dtheta12,Dphi,Dtheta13];

Var =
[theta1,theta2,theta3,theta4,theta5,theta6,theta7,theta8,theta9,theta10
,theta11,theta12,phi,theta13];

DDVar =
[DDtheta1,DDtheta2,DDtheta3,DDtheta4,DDtheta5,DDtheta6,DDtheta7,DDtheta
8,DDtheta9,DDtheta10,DDtheta11,DDtheta12,DDphi,DDtheta13];

for i=1:1:14
Term1(1,i)= diff(T,DVar(1,i));
end
```

```
for i2 = 1:1:length(Var)
    for j=1:1:length(Var)
TermA1(i2,j) = diff(Term1(1,i2),Var(1,j))*DVar(1,j);
TermA2(i2,j) = diff(Term1(1,i2),DVar(1,j))*DDVar(1,j);
    end
TermA(1,i2) = sum(TermA1(i2,1:j))+sum(TermA2(i2,1:j));
end

for j=1:1:14
Term2(1,j)= diff(U,Var(1,j));
end

for k=1:1:14
Term3(1,k)= -diff(T,Var(1,k));
end

E1 = TermA(1,2)+Term2(1,2)+Term3(1,2)
E2 = TermA(1,3)+Term2(1,3)+Term3(1,3)
E3 = TermA(1,4)+Term2(1,4)+Term3(1,4)
E4 = TermA(1,5)+Term2(1,5)+Term3(1,5)
E5 = TermA(1,6)+Term2(1,6)+Term3(1,6)
E6 = TermA(1,7)+Term2(1,7)+Term3(1,7)
E7 = TermA(1,8)+Term2(1,8)+Term3(1,8)
E8 = TermA(1,9)+Term2(1,9)+Term3(1,9)
E9 = TermA(1,10)+Term2(1,10)+Term3(1,10)
E10 = TermA(1,11)+Term2(1,11)+Term3(1,11)
E11 = TermA(1,12)+Term2(1,12)+Term3(1,12)
E12 = TermA(1,13)+Term2(1,13)+Term3(1,13)
E13 = TermA(1,14)+Term2(1,14)+Term3(1,14)
```

Results:

E1 = (K2*(2*theta2 - 2*theta3))/2 - (K1*(2*theta1 - 2*theta2))/2 + DDtheta2*J2

E2 = (K3*(2*theta3 - 2*theta4))/2 - (K2*(2*theta2 - 2*theta3))/2 + DDtheta3*J3

E3 = (K4*(2*theta4 - 2*theta5))/2 - (K3*(2*theta3 - 2*theta4))/2 + DDtheta4*J4

E4 = (K5*(2*theta5 - 2*theta6))/2 - (K4*(2*theta4 - 2*theta5))/2 + DDtheta5*J5

E5 = (K6*(2*theta6 - 2*theta7))/2 - (K5*(2*theta5 - 2*theta6))/2 + DDtheta6*J6

E6 = (K7*(2*theta7 - 2*theta8))/2 - (K6*(2*theta6 - 2*theta7))/2 + DDtheta7*J7

E7 = (K8*(2*theta8 - 2*theta9))/2 - (K7*(2*theta7 - 2*theta8))/2 + DDtheta8*J8

E8 = (K9*(2*theta9 - 2*theta10))/2 - (K8*(2*theta8 - 2*theta9))/2 + DDtheta9*J9

E9 = (K10*(2*theta10 - 2*theta11))/2 - (K9*(2*theta9 - 2*theta10))/2 + DDtheta10*J10

E10 = (K11*(2*theta11-2*theta12))/2 - (K10*(2*theta10-2*theta11))/2 + DDtheta11*J11

E11= (K12*(2*theta12-2*theta13))/2 - (K11*(2*theta11-2*theta12))/2 + DDtheta12*(J12+(m*(2*R^2+4*cos(phi)*R*r+2*r^2))/2) + (DDphi*m*(2*r^2 + 2*R*cos(phi)*r))/2 - Dphi*R*m*r*sin(phi)*(Dphi + 2*Dtheta12)

E12= (DDtheta12*m*(2*r^2+2*R*cos(phi)*r))/2 + DDphi*m*r^2 + R*m*r*sin(phi)*(Dtheta12^2 + Dphi*Dtheta12) - Dphi*Dtheta12*R*m*r*sin(phi)

E13 = DDtheta13*J13 - (K12*(2*theta12 - 2*theta13))/2

Appendix II

A. (Modeling of Simple one DOF rotary system with Harmonic Excitation in Simulink)

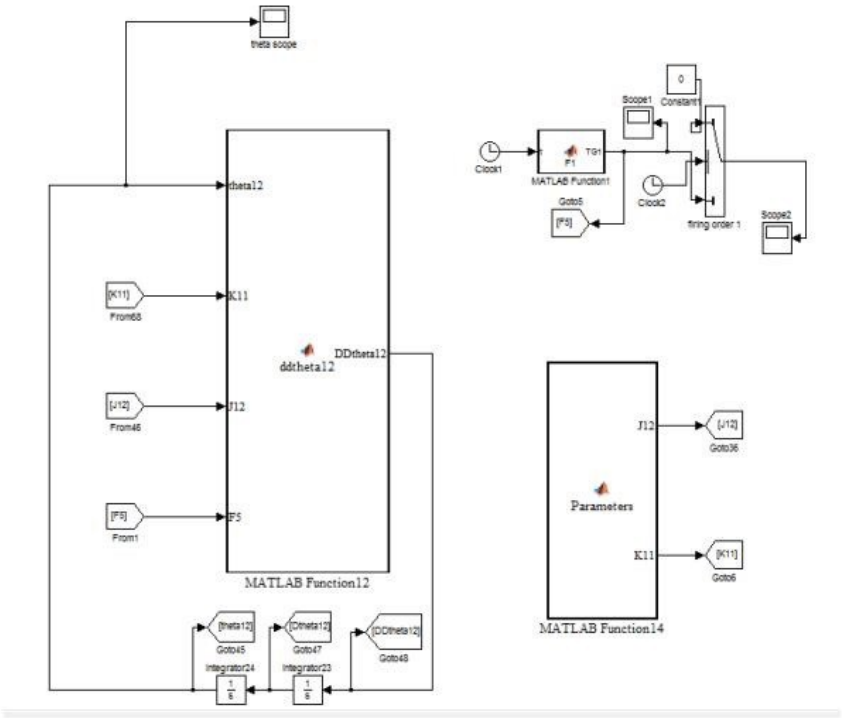


```
function DDtheta12 = ddtheta12(theta12,K11,J12,F5)

DDtheta12 = (F5-K11*theta12)/J12;
```

```
function TG1 = F1(t)

 x = (100)*t ; %crankshaft angle (deg)

TG1 = 50*sin(x);
```

```
function [J12,K11] = Parameters

J12 = 0.1;

K11 = 1000;
```

(B. Modeling of Simple Two DOF rotary system connected to CPVA with Harmonic Excitation in Simulink)

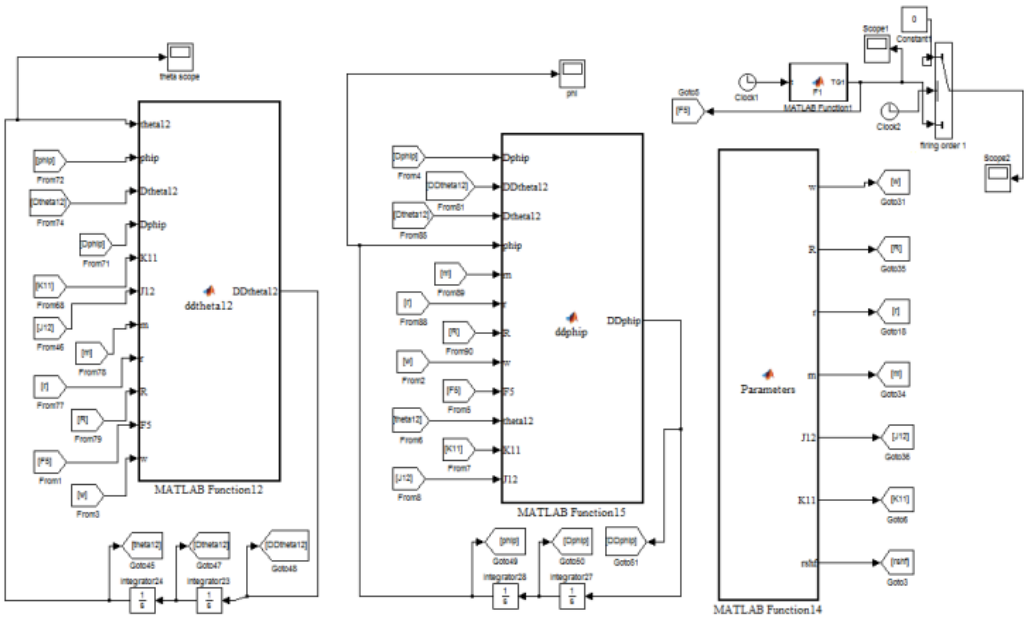


```
function DDtheta12 = ddtheta12(theta12, phip, Dtheta12, Dphip, K11, J12, m, r, R, F5, w)
DDtheta12 =  ((-m*r*R*w^2 + m*R^2*w^2)*phip - K11*theta12 + F5)/(J12);
```

```
function DDphip = ddphip(Dphip,DDtheta12,Dtheta12,phip,m,r,R,w,F5,theta12,K11,J12)
DDphip =  (F5 - K11*theta12 + ((R*w^2)*(J12+m*R^2+m*r^2+2*m*R*r)/(r+R))*phip) /
          (m*r^2 + m*R*r - (J12+m*R^2+m*r^2+2*m*R*r)*(r/(r+R)));
```

```
function TG1 = F1(t)

 x = (100)*t ; %crankshaft angle (deg)
TG1 = 50*sin(x);
```

Appendix III

(The FFT-function programming in Matlab for deriving the frequency response of rotating system)

Input: The time domain response of rotary system

Output: The frequency response of rotary system

```
close all
clear all
clc

% --time vector 2 sec [fs = 1/2 = 1024/2 ] T...time vector step--------
--

fs = 8192; % 683Hz
n_bins = 2^18;

load thetasim
load timesim

figure
subplot(2,1,1)
plot(timesim,thetasim);
% title('Phi Response Horizontal
Plane','FontName','garamond','FontSize',12,'FontWeight','bold')
xlabel('Time
(Sec)','FontName','garamond','FontSize',12,'FontWeight','bold')
ylabel('theta Amplitude
[rad]','FontName','garamond','FontSize',12,'FontWeight','bold')
grid on
%
Y_w = fft(thetasim, n_bins);    % perform fft
bin_width = fs/n_bins;     % determine point spacing in frequency
f = 0:bin_width:(0.5*fs); % create frequency vector

subplot(2,1,2)
plot(f, abs(Y_w(1:0.5*n_bins+1)))
xlabel('Frequency
(Hz)','FontName','garamond','FontSize',12,'FontWeight','bold')
ylabel('Magnitude','FontName','garamond','FontSize',12,'FontWeight','bo
ld')
grid on
```

Appendix IV

Locomotive manual data

MAJOR EQUIPMENT

Diesel Engine . . . . . …….. . . . . . 7FDL16

Main Generator …… . . . GT-598

Traction Motors . . . . . …..…….. . . . . . GE-752

Auxiliary Generator . . …….. . . . . . GY-27

Exciter . . . . . …….….. . . . . . GY-50

Air Compressor (Gardner-Denver) W130

(WABCO) . . . . ……... . . . 3CWDL

Fan &Blower Unit . ……. GDY-40

Air Brake System . . ……. 26L

Wheel Diameter (New)…….....…… . 40 inch

WEIGHTS (Approximate Weights for Lifting Purposes Only)

Complete Locomotive (Fully Serviced) …… . 250, 000 lbs.

One Truck (Complete) . …….……. . 43, 000 lbs.

One Truck Frame . …… 6, 050 lbs.

One Swing Bolster . ……..……. 1, 475 lbs.

One Spring Plank . . . ……. . ……... . . . 390 lbs.

One Motor, Wheel and Axle Assembly ……. . 11, 600 lbs.

Traction Motor (Less Gear Case) . …….……. 7, 000 lbs.

Air Compressor (Dry) . ……..……. . 1, 370 lbs.

One Battery Tray . . . . ……. . . . . 300 lbs.

Engine Hood Assembly (Not Including Radiator Hood) . …… . 4, 000 lbs.

Fan & Blower Unit (Complete with Fans) ……..……. 4, 500 lbs.

Each Radiator Fan . . . . . ……..... . . . 370 lbs

Fan & Blower Unit Drive Shaft and Couplings . . . …. . . …… . . . . . 200 lbs.

Radiator and Frame Assembly . . . …….……...…… . . . . 1, 750 lbs.

Each Radiator Section . . . . . ……..… . . . . . 280 lbs.

Equipment Blower Rotor . . . . . ……... . . . 200 lbs.

En-gine and Generator (Complete) . . ……..……..……. . . . 57, 000 lbs.

Main Generator with Auxiliaries . . ……...…….. . . . 17, 500 lbs.

Auxiliary Generator . . . . ……. . . . . 690 lbs.

Exciter . . . . ……..……... . . 625 lbs.

En-gine (Less Generator) . . . . . ……..….. . . . . 37, 500 lbs.

Engine Component Parts Main Frame (Bare). . . . ……..…….. . . . . 10, 670 lbs.

Crankshaft . . . . . …….. . . . . . 3, 955 lbs.

Turbocharger. . . . . ……... . . . … 1, 330 lbs.

Intercooler (Dry) . . . . . ……..……..... . . . . 480 lbs.

Cylinder Complete . . . . . ……..…….. . . . . 540 lbs.

Piston and Master Rod Assembly . . ……..….. . . 207 lbs.

Piston and Articulating Rod Assembly……..…….. . . 94 lbs.

Oil Pump . . . . . ……..……...…. . . . . 250 lbs.

Water Pump . . . . . ……..……. . . . . 248 lbs.

Control Governor . . ……...……..…… . . 112 lbs.

Governor Drive Assembly . . ……..…… . . . . . 159 lbs.

Oil Pan . . . . . ……...……..……. . . . . 995 lbs.

Free-End Cover . . . . . ……..……... . . . . . 1, 330 lbs.

End Cover (Generator End) . ……..……..…… . . .. . . 89 lbs.

Lube Oil Cooler (Dry) . . . . . ……..……. . .. . . 570 lbs.

Lube Oil Filter Tank (Dry-including 8 elements) . . .. ….. . . . . 600 lbs.

ENGINE SPECIFICATIONS

Model . ……..….. . . 7FDL16

Gross Horsepower . . . . . ……. 2750

Number of Cylinders . . . . . ……. 16

Stroke Cycle . . . . . ……. 4

Cylinder Arrangement . ……... . . . . 450V

Bore . . . . . ……..…… . . .. 9-In.

Stroke . . . . . ……. . . .. 101/2-In.

Compression Ratio . . . ……. . . …. 12.7-1

Idle Speed . . . . . ……. . . . . …. . . . . 400 RPM

Maximum Governed Speed . . . . . ……... . . . . 2000 RPM

Firing Order . …….. . 1R-11, 3R-3L, 7R-7L, 4R-4L, 8R-8L,
6R-6L, 2R-2L, 5R-5L

Turbocharger . . . . . ……. . . . . Single

Engine Dimensions:

Height (Overall Including Stack)……..... . 8 Ft. 10 ¾ In.

Length (Overall Including Generator). 21 Ft….. 8 7/16 In.

Width (Overall) . . . . ……. …….. . . ….... . . 5 Ft. 8 ¼ In.

Weight (Including Generator) . . . …….. ……. . . 57,000 Lbs.

Other data required for modeling:

Piston mass: 10 (kg)

Crank throw: 0.133 (m)

Crankshaft diameter: 0.203 (m)

Connecting rod length: 0.6 (m), Mass: 63 (kg), thickness: 0.09 (m)

Width varying from 0.1 to 0.2 (m)-narrow end connected to piston

Crank web cross section: 0.15 x 0.09

Crank pin diameter: 0.203 (m)

Engine mounted to the crankshaft at 0.146 (m) interval

Auxiliary generator geared ratio: (3:1)

Radiator fans geared ration: (2.5:1)

Appendix V

Matlab/Simulink block diagram and coding of excitation torque modeling for the case study locomotive:

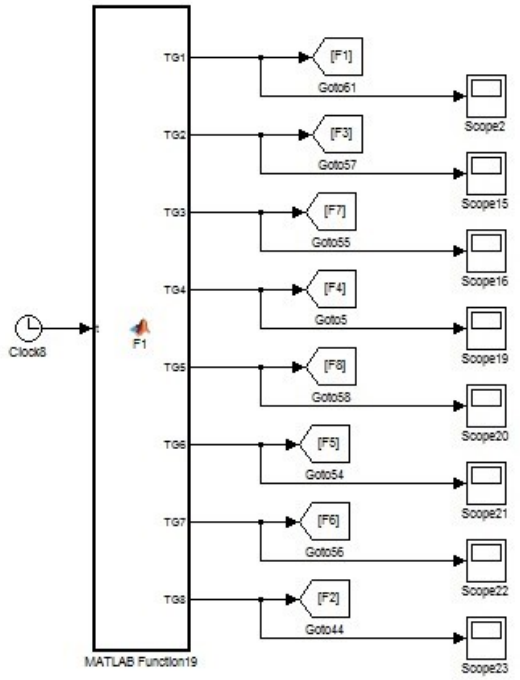


```
function [TG1,TG2,TG3,TG4,TG5,TG6,TG7,TG8] = F1(t)

 %Fourier Series multiplyer derived from Matlan curve fitting tool:
 a0 = 16.08;
 a1 = 24.48;
 b1 = 5.007;
 a2 = 18.91;
 b2 = 5.479;
 a3 = 15.41;
 b3 = 5.042;
 a4 = 11.87;
 b4 = 5.045;
 a5 = 8.872;
 b5 = 4.58;
 a6 = 6.79;
 b6 = 3.954;
 a7 = 4.807;
 b7 = 3.409;
 a8 = 3.35;
 b8 = 3.544;
 x  = (w)*t;         %crankshaft angle (rad)- right bank
 x1 = (w)*t + pi/4; %crankshaft angle (rad)- left bank
 w  =  0.6151;
```

```
%F1:
%Right bank in-cylinder combustion pressure Fourier Series:
PR = a0 + a1*cos(x*w) + b1*sin(x*w) +
a2*cos(2*x*w) + b2*sin(2*x*w) + a3*cos(3*x*w) + b3*sin(3*x*w) +
a4*cos(4*x*w) + b4*sin(4*x*w) + a5*cos(5*x*w) + b5*sin(5*x*w) +
a6*cos(6*x*w) + b6*sin(6*x*w) + a7*cos(7*x*w) + b7*sin(7*x*w) +
a8*cos(8*x*w) + b8*sin(8*x*w);


%Left bank in-cylinder combustion pressure:
PL = a0 + a1*cos(x1*w) + b1*sin(x1*w) +
a2*cos(2*x1*w) + b2*sin(2*x1*w) + a3*cos(3*x1*w) + b3*sin(3*x1*w) +
a4*cos(4*x1*w) + b4*sin(4*x1*w) + a5*cos(5*x1*w) + b5*sin(5*x1*w) +
a6*cos(6*x1*w) + b6*sin(6*x1*w) + a7*cos(7*x1*w) + b7*sin(7*x1*w) +
a8*cos(8*x1*w) + b8*sin(8*x1*w);

S= pi/4*0.229^2; %piston section
R= 0.203/2;      %crank radius
CR=0.6/0.1015;   %connecting rod length/crank radius


% Total excitation torque due to cylinder in position number 1:
TG1 = S*R*10^5*PR*(sin(x)+sin(2*x)/(2*CR)) +
      S*R*10^5*PL*(sin(x1)+sin(2*x1)/(2*CR));



%F3:
PR = a0 + a1*cos((x+pi/2)*w) + b1*sin((x+pi/2)*w) +
a2*cos(2*(x+pi/2)*w) + b2*sin(2*(x+pi/2)*w) + a3*cos(3*(x+pi/2)*w) +
b3*sin(3*(x+pi/2)*w) + a4*cos(4*(x+pi/2)*w) + b4*sin(4*(x+pi/2)*w) +
a5*cos(5*(x+pi/2)*w) + b5*sin(5*(x+pi/2)*w) + a6*cos(6*(x+pi/2)*w) +
b6*sin(6*(x+pi/2)*w) + a7*cos(7*(x+pi/2)*w) + b7*sin(7*(x+pi/2)*w) +
a8*cos(8*(x+pi/2)*w) + b8*sin(8*(x+pi/2)*w);
%right bank cylinder pressure curve furier series

PL = a0 + a1*cos((x1+pi/2)*w) + b1*sin((x1+pi/2)*w) +
a2*cos(2*(x1+pi/2)*w) + b2*sin(2*(x1+pi/2)*w) + a3*cos(3*(x1+pi/2)*w) +
b3*sin(3*(x1+pi/2)*w) + a4*cos(4*(x1+pi/2)*w) + b4*sin(4*(x1+pi/2)*w) +
a5*cos(5*(x1+pi/2)*w) + b5*sin(5*(x1+pi/2)*w) + a6*cos(6*(x1+pi/2)*w) +
b6*sin(6*(x1+pi/2)*w) + a7*cos(7*(x1+pi/2)*w) + b7*sin(7*(x1+pi/2)*w) +
a8*cos(8*(x1+pi/2)*w) + b8*sin(8*(x1+pi/2)*w);
%left bank cylinder pressure curve furier series

TG2 = S*R*10^5*PR*(sin((x+pi/2))+sin(2*(x+pi/2))/(2*CR)) +
S*R*10^5*PL*(sin((x1+pi/2))+sin(2*(x1+pi/2))/(2*CR));



%F7:
PR = a0 + a1*cos((x+pi)*w) + b1*sin((x+pi)*w) + a2*cos(2*(x+pi)*w) +
b2*sin(2*(x+pi)*w) + a3*cos(3*(x+pi)*w) + b3*sin(3*(x+pi)*w) +
a4*cos(4*(x+pi)*w) + b4*sin(4*(x+pi)*w) + a5*cos(5*(x+pi)*w) +
b5*sin(5*(x+pi)*w) + a6*cos(6*(x+pi)*w) + b6*sin(6*(x+pi)*w) +
```

```
a7*cos(7*(x+pi)*w) + b7*sin(7*(x+pi)*w) + a8*cos(8*(x+pi)*w) +
b8*sin(8*(x+pi)*w);
%right bank cylinder pressure curve furier series

PL = a0 + a1*cos((x1+pi)*w) + b1*sin((x1+pi)*w) + a2*cos(2*(x1+pi)*w) +
b2*sin(2*(x1+pi)*w) + a3*cos(3*(x1+pi)*w) + b3*sin(3*(x1+pi)*w) +
a4*cos(4*(x1+pi)*w) + b4*sin(4*(x1+pi)*w) + a5*cos(5*(x1+pi)*w) +
b5*sin(5*(x1+pi)*w) + a6*cos(6*(x1+pi)*w) + b6*sin(6*(x1+pi)*w) +
a7*cos(7*(x1+pi)*w) + b7*sin(7*(x1+pi)*w) + a8*cos(8*(x1+pi)*w) +
b8*sin(8*(x1+pi)*w);
%left bank cylinder pressure curve furier series

TG3 = S*R*10^5*PR*(sin((x+pi))+sin(2*(x+pi))/(2*CR)) +
S*R*10^5*PL*(sin((x1+pi))+sin(2*(x1+pi))/(2*CR));


%F4:
PR = a0 + a1*cos((x+3*pi/2)*w) + b1*sin((x+3*pi/2)*w) +
a2*cos(2*(x+3*pi/2)*w) + b2*sin(2*(x+3*pi/2)*w) +
a3*cos(3*(x+3*pi/2)*w) + b3*sin(3*(x+3*pi/2)*w) +
a4*cos(4*(x+3*pi/2)*w) + b4*sin(4*(x+3*pi/2)*w) +
a5*cos(5*(x+3*pi/2)*w) + b5*sin(5*(x+3*pi/2)*w) +
a6*cos(6*(x+3*pi/2)*w) + b6*sin(6*(x+3*pi/2)*w) +
a7*cos(7*(x+3*pi/2)*w) + b7*sin(7*(x+3*pi/2)*w) +
a8*cos(8*(x+3*pi/2)*w) + b8*sin(8*(x+3*pi/2)*w);
%right bank cylinder pressure curve furier series

PL = a0 + a1*cos((x1+3*pi/2)*w) + b1*sin((x1+3*pi/2)*w) +
a2*cos(2*(x1+3*pi/2)*w) + b2*sin(2*(x1+3*pi/2)*w) +
a3*cos(3*(x1+3*pi/2)*w) + b3*sin(3*(x1+3*pi/2)*w) +
a4*cos(4*(x1+3*pi/2)*w) + b4*sin(4*(x1+3*pi/2)*w) +
a5*cos(5*(x1+3*pi/2)*w) + b5*sin(5*(x1+3*pi/2)*w) +
a6*cos(6*(x1+3*pi/2)*w) + b6*sin(6*(x1+3*pi/2)*w) +
a7*cos(7*(x1+3*pi/2)*w) + b7*sin(7*(x1+3*pi/2)*w) +
a8*cos(8*(x1+3*pi/2)*w) + b8*sin(8*(x1+3*pi/2)*w);
%left bank cylinder pressure curve furier series

TG4 = S*R*10^5*PR*(sin((x+3*pi/2))+sin(2*(x+3*pi/2))/(2*CR)) +
S*R*10^5*PL*(sin((x1+3*pi/2))+sin(2*(x1+3*pi/2))/(2*CR));


%F8:
PR = a0 + a1*cos((x+2*pi)*w) + b1*sin((x+2*pi)*w) +
a2*cos(2*(x+2*pi)*w) + b2*sin(2*(x+2*pi)*w) + a3*cos(3*(x+2*pi)*w) +
b3*sin(3*(x+2*pi)*w) + a4*cos(4*(x+2*pi)*w) + b4*sin(4*(x+2*pi)*w) +
a5*cos(5*(x+2*pi)*w) + b5*sin(5*(x+2*pi)*w) + a6*cos(6*(x+2*pi)*w) +
b6*sin(6*(x+2*pi)*w) + a7*cos(7*(x+2*pi)*w) + b7*sin(7*(x+2*pi)*w) +
a8*cos(8*(x+2*pi)*w) + b8*sin(8*(x+2*pi)*w);
%right bank cylinder pressure curve furier series

PL = a0 + a1*cos((x1+2*pi)*w) + b1*sin((x1+2*pi)*w) +
a2*cos(2*(x1+2*pi)*w) + b2*sin(2*(x1+2*pi)*w) + a3*cos(3*(x1+2*pi)*w) +
b3*sin(3*(x1+2*pi)*w) + a4*cos(4*(x1+2*pi)*w) + b4*sin(4*(x1+2*pi)*w) +
a5*cos(5*(x1+2*pi)*w) + b5*sin(5*(x1+2*pi)*w) + a6*cos(6*(x1+2*pi)*w) +
```

```
b6*sin(6*(x1+2*pi)*w) + a7*cos(7*(x1+2*pi)*w) + b7*sin(7*(x1+2*pi)*w) +
a8*cos(8*(x1+2*pi)*w) + b8*sin(8*(x1+2*pi)*w);
%left bank cylinder pressure curve furier series

TG5 = S*R*10^5*PR*(sin((x+2*pi))+sin(2*(x+2*pi))/(2*CR)) +
S*R*10^5*PL*(sin((x1+2*pi))+sin(2*(x1+2*pi))/(2*CR));


%F5:
PR = a0 + a1*cos((x+7*pi/2)*w) + b1*sin((x+7*pi/2)*w) +
a2*cos(2*(x+7*pi/2)*w) + b2*sin(2*(x+7*pi/2)*w) +
a3*cos(3*(x+7*pi/2)*w) + b3*sin(3*(x+7*pi/2)*w) +
a4*cos(4*(x+7*pi/2)*w) + b4*sin(4*(x+7*pi/2)*w) +
a5*cos(5*(x+7*pi/2)*w) + b5*sin(5*(x+7*pi/2)*w) +
a6*cos(6*(x+7*pi/2)*w) + b6*sin(6*(x+7*pi/2)*w) +
a7*cos(7*(x+7*pi/2)*w) + b7*sin(7*(x+7*pi/2)*w) +
a8*cos(8*(x+7*pi/2)*w) + b8*sin(8*(x+7*pi/2)*w);
%right bank cylinder pressure curve furier series

PL = a0 + a1*cos((x1+7*pi/2)*w) + b1*sin((x1+7*pi/2)*w) +
a2*cos(2*(x1+7*pi/2)*w) + b2*sin(2*(x1+7*pi/2)*w) +
a3*cos(3*(x1+7*pi/2)*w) + b3*sin(3*(x1+7*pi/2)*w) +
a4*cos(4*(x1+7*pi/2)*w) + b4*sin(4*(x1+7*pi/2)*w) +
a5*cos(5*(x1+7*pi/2)*w) + b5*sin(5*(x1+7*pi/2)*w) +
a6*cos(6*(x1+7*pi/2)*w) + b6*sin(6*(x1+7*pi/2)*w) +
a7*cos(7*(x1+7*pi/2)*w) + b7*sin(7*(x1+7*pi/2)*w) +
a8*cos(8*(x1+7*pi/2)*w) + b8*sin(8*(x1+7*pi/2)*w);
%left bank cylinder pressure curve furier series

TG6 = S*R*10^5*PR*(sin((x+7*pi/2))+sin(2*(x+7*pi/2))/(2*CR)) +
S*R*10^5*PL*(sin((x1+7*pi/2))+sin(2*(x1+7*pi/2))/(2*CR));


%F6:
PR = a0 + a1*cos((x+5*pi/2)*w) + b1*sin((x+5*pi/2)*w) +
a2*cos(2*(x+5*pi/2)*w) + b2*sin(2*(x+5*pi/2)*w) +
a3*cos(3*(x+5*pi/2)*w) + b3*sin(3*(x+5*pi/2)*w) +
a4*cos(4*(x+5*pi/2)*w) + b4*sin(4*(x+5*pi/2)*w) +
a5*cos(5*(x+5*pi/2)*w) + b5*sin(5*(x+5*pi/2)*w) +
a6*cos(6*(x+5*pi/2)*w) + b6*sin(6*(x+5*pi/2)*w) +
a7*cos(7*(x+5*pi/2)*w) + b7*sin(7*(x+5*pi/2)*w) +
a8*cos(8*(x+5*pi/2)*w) + b8*sin(8*(x+5*pi/2)*w);
%right bank cylinder pressure curve furier series

PL = a0 + a1*cos((x1+5*pi/2)*w) + b1*sin((x1+5*pi/2)*w) +
a2*cos(2*(x1+5*pi/2)*w) + b2*sin(2*(x1+5*pi/2)*w) +
a3*cos(3*(x1+5*pi/2)*w) + b3*sin(3*(x1+5*pi/2)*w) +
a4*cos(4*(x1+5*pi/2)*w) + b4*sin(4*(x1+5*pi/2)*w) +
a5*cos(5*(x1+5*pi/2)*w) + b5*sin(5*(x1+5*pi/2)*w) +
a6*cos(6*(x1+5*pi/2)*w) + b6*sin(6*(x1+5*pi/2)*w) +
a7*cos(7*(x1+5*pi/2)*w) + b7*sin(7*(x1+5*pi/2)*w) +
a8*cos(8*(x1+5*pi/2)*w) + b8*sin(8*(x1+5*pi/2)*w);
%left bank cylinder pressure curve furier series
```

```
TG7 = S*R*10^5*PR*(sin((x+5*pi/2))+sin(2*(x+5*pi/2))/(2*CR)) +
S*R*10^5*PL*(sin((x1+5*pi/2))+sin(2*(x1+5*pi/2))/(2*CR));


%F2:
PR = a0 + a1*cos((x+6*pi/2)*w) + b1*sin((x+6*pi/2)*w) +
a2*cos(2*(x+6*pi/2)*w) + b2*sin(2*(x+6*pi/2)*w) +
a3*cos(3*(x+6*pi/2)*w) + b3*sin(3*(x+6*pi/2)*w) +
a4*cos(4*(x+6*pi/2)*w) + b4*sin(4*(x+6*pi/2)*w) +
a5*cos(5*(x+6*pi/2)*w) + b5*sin(5*(x+6*pi/2)*w) +
a6*cos(6*(x+6*pi/2)*w) + b6*sin(6*(x+6*pi/2)*w) +
a7*cos(7*(x+6*pi/2)*w) + b7*sin(7*(x+6*pi/2)*w) +
a8*cos(8*(x+6*pi/2)*w) + b8*sin(8*(x+6*pi/2)*w);
%right bank cylinder pressure curve furier series

PL = a0 + a1*cos((x1+6*pi/2)*w) + b1*sin((x1+6*pi/2)*w) +
a2*cos(2*(x1+6*pi/2)*w) + b2*sin(2*(x1+6*pi/2)*w) +
a3*cos(3*(x1+6*pi/2)*w) + b3*sin(3*(x1+6*pi/2)*w) +
a4*cos(4*(x1+6*pi/2)*w) + b4*sin(4*(x1+6*pi/2)*w) +
a5*cos(5*(x1+6*pi/2)*w) + b5*sin(5*(x1+6*pi/2)*w) +
a6*cos(6*(x1+6*pi/2)*w) + b6*sin(6*(x1+6*pi/2)*w) +
a7*cos(7*(x1+6*pi/2)*w) + b7*sin(7*(x1+6*pi/2)*w) +
a8*cos(8*(x1+6*pi/2)*w) + b8*sin(8*(x1+6*pi/2)*w);
%left bank cylinder pressure curve furier series


TG8 = S*R*10^5*PR*(sin((x+6*pi/2))+sin(2*(x+6*pi/2))/(2*CR)) +
S*R*10^5*PL*(sin((x1+6*pi/2))+sin(2*(x1+6*pi/2))/(2*CR));
```

Appendix VI

Modeling of torsional vibration for U25B-GE locomotive diesel engine in Matlab/Simulink software with simulated in-cylinder pressure excitation force.

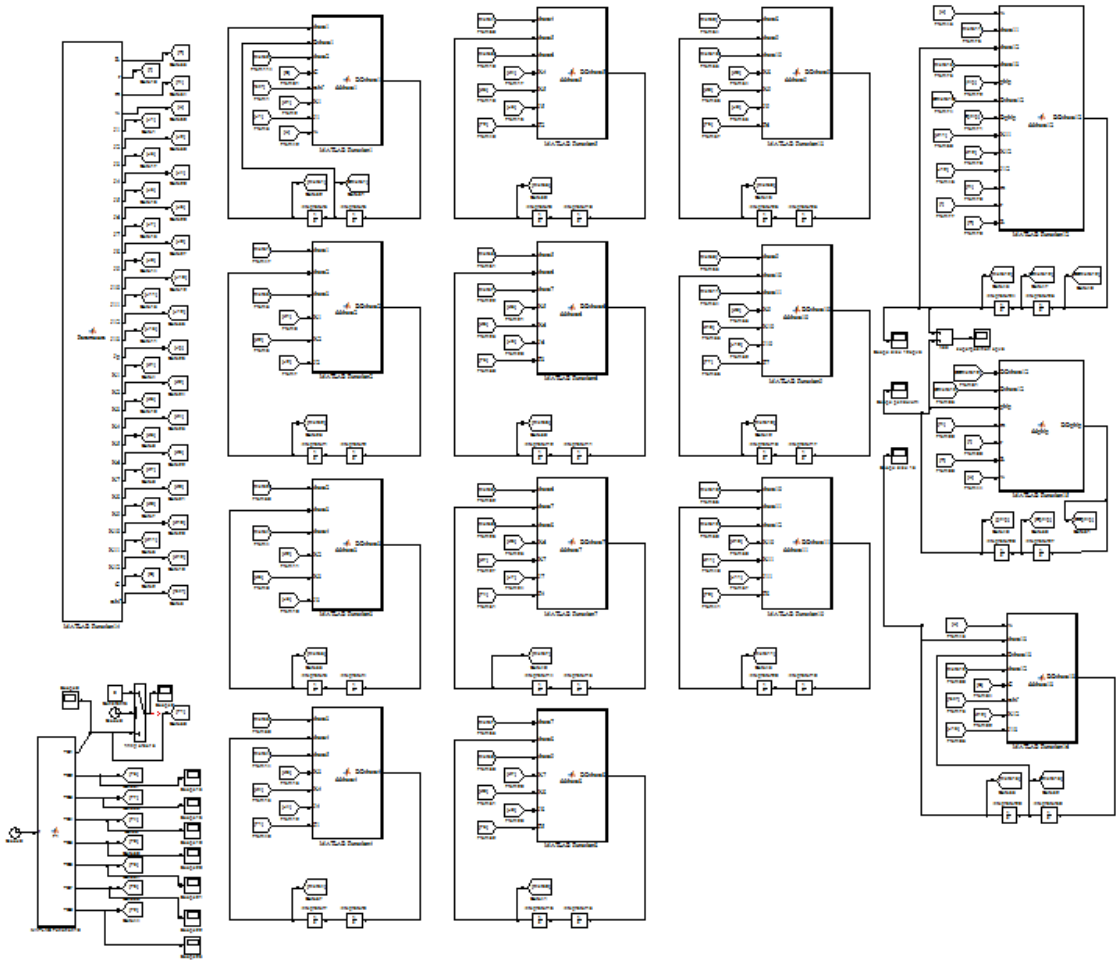

Sample Embeded functions:

Equation of motion for Inertia Disk #4:

```
function DDtheta4 = ddtheta4(theta3,theta4,theta5,K3,K4,J4,F1)
DDtheta4 = -((K3+K4)*theta4 - K3*theta3 - K4*theta5 - F1)/J4;
```

Block Diagram (Inertia disk #4):

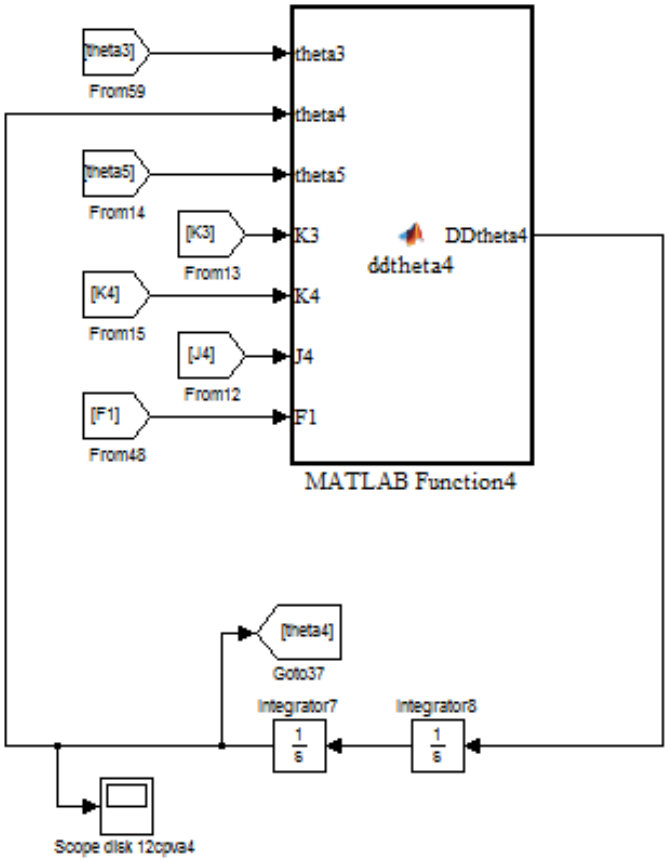

Equation of motion for Inertia Disk #12:

```
function DDtheta12 = ddtheta12(w, theta11, theta12, theta13, phip,…
                               Dtheta12, Dphip, K11, K12, J12, m, r, R)
DDtheta12 =  -((-m*r*R*sin(phip)*(w+Dtheta12) -
                 m*R^2*sin(phip)*cos(phip)*(w+Dtheta12) -
                 2*m*r*R*Dphip*sin(phip))*(w+Dtheta12) -
                 m*r*R*Dphip^2*sin(phip) + (K11+K12)*theta12 -
                 K11*theta11 - K12*theta13)/(J12+m*R^2*(1-
                 cos(phip)^2));
```

Block Diagram (Inertia disk #12):